

NORTHWESTERN UNIVERSITY

**Mitochondrial Complex III Is Necessary For Endothelial
Cell Proliferation During Angiogenesis**

A DISSERTATION

SUBMITTED TO THE GRADUATE SCHOOL
IN PARTIAL FULFILLMENT OF THE REQUIREMENTS

for the degree

DOCTOR OF PHILOSOPHY

Field of Driskill Graduate Training Program of Life Sciences

By

Lauren P. Diebold

EVANSTON, ILLINOIS

DECEMBER 2018

ABSTRACT

Mitochondrial Complex III Is Necessary For Endothelial Cell Proliferation During Angiogenesis

Lauren P. Diebold

Endothelial cells (ECs) require glycolysis for proliferation and migration during angiogenesis; however, the necessity for the mitochondrial respiratory chain during angiogenesis is not known. In this study, we report that inhibition of respiratory chain complex III impairs proliferation, but not migration of ECs *in vitro* by decreasing the NAD⁺/NADH ratio. To determine whether mitochondrial respiration is necessary for angiogenesis *in vivo*, we conditionally ablated a subunit of the respiratory chain complex III (QPC) in ECs. Loss of QPC decreased respiration, resulting in diminished EC proliferation, and impairment in retinal and tumor angiogenesis. Loss of QPC did not decrease genes associated with anabolism or nucleotides levels in ECs, but diminished amino acid levels. Our findings indicate that mitochondrial respiration is necessary for angiogenesis, and that the primary role of mitochondria in ECs is to serve as biosynthetic organelles for cell proliferation.

ACKNOWLEDGMENTS

I would like to express my sincere gratitude to everyone who has been there to support me during my graduate training. First and foremost, I would like to thank my mentor, Nav Chandel. His enthusiasm and scientific curiosity have always motivated me to strive to be the best scientist I could be. I feel very grateful to have had the opportunity to be a part of Nav's Lab, as he has created a tremendously supportive and positive work environment. Above anything, Nav has taught me to be a critical scientific thinker and has truly gone above and beyond to help guide me through every stage of my project. I would also like to thank all of my labmates throughout the years who have supported me both scientifically and personally. Sam, Colleen, Inma, Hyewon, Jim, Luzi, Josh, Greg, Lizzie, Manan, Ari, Leah, Lucas, AJ, Elena, you all have made my experience in the Chandel lab a tremendously fun experience. Thank you all for your scientific expertise, commiserating failed experiments and celebrating the rare successful ones, and for all the laughs we shared every day. I would especially like to thank Sam Weinberg for all of his scientific advice throughout the years; my paper wouldn't have been the same without it. I thank my thesis committee, Scott Budinger, Susan Quaggin, and Robert Lavker for their commitment, excellent advice, and support at every stage of my thesis project. For all the countless hours I spent in the flow cytometry core, I would like to express my gratitude for Suchitra and Paul for assisting me with my plethora of questions and technical troubles. Peng Gao in the metabolomics core, I thank for all the time he spent tirelessly analyzing my many samples that needed to be processed ASAP. I would also like to thank our collaborators Guillermo Oliver and Hyea Jin Gil, for their endothelial expertise. And finally, I would like to thank everyone in the pulmonary department and the CMBD training grant for their financial support. There have been countless more members of the Northwestern team whom I have not

named that have offered me support over the years, and I am grateful for every bit of help I received.

I would also like to express my gratitude for those who have supported me in my personal life throughout my graduate career. I would especially like to thank my parents for always being there for me. They have never once expressed a hint of doubt in my abilities and never fail to tell others and me how proud they are. Thank you so much for supporting me in every way and for your never-ending love and constant encouragement. Thank you to my two best friends, Kim and Melissa, whom I have known since I was 5 years old and are like sisters to me. Thank you for getting so excited about my accomplishments and milestones throughout my graduate years, and for keeping me sane by distracting me from the stresses of my PhD. And finally, I would especially like to thank my boyfriend, Buzz. Thank you for listening to me drone on about my experiments (even when you had no idea what I was talking about), for all the times you told me I was doing a great job when I cried because I didn't think I could get everything done, and for sharing in my excitement every time I reached another milestone. I couldn't have done it without your love and never-ending encouragement.

LIST OF ABBREVIATIONS

α KG	Alpha-ketoglutarate
2DG	2-deoxy-D-glucose
2HG	L-2-hydroxyglutarate
5mC	5-methylcytosine
ADP	Adenosine 5'-diphosphate
Angpt2	angiopoitin-2
Anti	Antimycin A
AnV	AnnexinV
AOX	Alternative oxidase from <i>Ciona intestinalis</i>
Asn	Asparagine
Asp	Aspartate
ATP	Adenosine 5'-triphosphate
BSA	Bovine serum albumin
Casp3	Cleaved caspase 3
CCCP	carbonyl cyanide m-chlorophenyl hydrazine
Chd5	Cadherin 5
Col IV	Collagen type IV
CPT1/2	Carnitine palmitoyltransferase 1/2
CPT1A	Carnitine palmitoyltransferase 1A
Ct	Control
DAPI	4',6-Diamidino-2-phenylindole dihydrochloride
Dll4	Delta-like 4
EC	Endothelial cell
ECAR	Extracellular acidification rate
ETC	Electron transport chain
EV	Empty vector
FABP	Fatty acid binding protein
FABP4	Fatty acid binding protein 4
FACS	Fluorescence-activated cell sorting
FAD	Oxidized flavin adenine dinucleotide
FADH ₂	Reduced flavin adenine dinucleotide
FAO	Fatty acid oxidation
FASN	Fatty acid synthase
FBS	Fetal bovine serum
FDR	False discovery rate
GAPDH	Glyceraldehyde 3-phosphate dehydrogenase
GFP	Green fluorescent protein
GLS	Glutaminase

GLUD	Glutamate dehydrogenase
GLUT1	Glucose transporter 1
GOT1/2	Aspartate aminotransferase 1/2
H ⁺	Hydrogen ion
H ₂ O ₂	Hydrogen peroxide
HATS	Histone acetyl transferases
Hey1	Hairy/enhancer-of-split related with YRPW motif protein 1
HK2	Hexokinase 2
HPLC-MS/MS	High-Performance Liquid Chromatography and High-Resolution Mass Spectrometry and Tandem Mass Spectrometry
HSCs	Hematopoietic stem cells
HUVECs	Human umbilical vein endothelial cells
IB4	Isolectin-B4
KDM	JmJC domain-containing histone lysine demethylases
KO	Knock out
LbNOX	NADH oxidase from <i>Lactobacillus brevis</i>
LDH	Lactate dehydrogenase
MC	Methylcellulose
Me-Asp	Methyl aspartate
MFI	Median fluorescence intensity
MMC	Mitomycin C
MP	Methyl pyruvate
mROS	Mitochondrial reactive oxygen species
MT	MitoTracker
NAD ⁺	Nicotinamide adenine dinucleotide, oxidized
NADH	Nicotinamide adenine dinucleotide, reduced
NES	Normalized enrichment score
Nrp1	Neuropilin-1
Nrp2	Neuropilin-2
NS	Not significant
O ₂	Oxygen
O ₂ •	Superoxide
OAA	oxaloacetate
OCR	Oxygen consumption
OCT	Optimal cutting temperature
OH•	Hydroxyl radical
OxPhos	Oxidative phosphorylation
PBS	Phosphate buffered saline
PC	Pyruvate carboxylase
PDH	Pyruvate dehydrogenase

PFKFB3	6-phosphofructo-2-kinase/fructose-2,6-bisphosphate
pH3	Phospho-histone 3
PHGDH	Phosphoglycerate Dehydrogenase
PI	Propidium iodide
Pier	Piericidin
PKM2	Pyruvate kinase M2
PMSF	phenylmethane sulfonyl fluoride
Q	Oxidized ubiquinone
QH ₂	Reduced ubiquinone
QPC	Ubiquinol binding protein
qRT-PCR	Quantitative reverse transcription polymerase chain reaction
RFP	Red fluorescent protein
RNAseq	RNA sequencing
ROS	Reactive oxygen species
ROS	Reactive oxygen species
RT	Room temperature
SEM	Standard error of the mean
SHMT2	Serine Hydroxymethyltransferase 2
TCA	Tricarboxylic acid
TEK	TEK receptor tyrosine kinase (aka Tie2)
TET	Ten-eleven translocation
TMRE	Tetramethylrhodamine ethyl ester perchlorate
UPR	Unfolded protein response
<i>Uqcrcq</i>	Ubiquinol-Cytochrome C Reductase Complex III Subunit VII (QPC)
VE-cadherin	Vascular endothelial cadherin
VEGF	Vascular endothelial growth factor
VEGFA	Vascular endothelial growth factor A
VEGFR	Vascular endothelial growth factor receptor
WT	Wild type

TABLE OF CONTENTS

ABSTRACT	2
ACKNOWLEDGMENTS	3
LIST OF ABBREVIATIONS	5
TABLE OF CONTENTS	8
LIST OF FIGURES	11
1. CHAPTER 1: INTRODUCTION	14
1.1 Mitochondrial biology	14
<i>1.1.1 Mitochondrial ATP generation</i>	14
<i>1.1.2 Mitochondria are biosynthetic organelles</i>	18
<i>1.1.3 Mitochondria as signaling organelles</i>	24
1.2 Endothelial Cells	29
<i>1.2.1 Angiogenesis</i>	29
<i>1.2.2 Endothelial cell metabolism</i>	34
2. CHAPTER 2: MATERIALS AND METHODS	40
2.1 Cell Culture and Drug Treatment	40
2.2 Oxygen Consumption and Extracellular Acidification Rate Measurements	41
<i>2.2.1 In vitro OCR:</i>	41
<i>2.2.2 In vivo OCR:</i>	41
2.3 HUVEC Proliferation And Viability Assays	42
<i>2.3.1 Proliferation:</i>	42
<i>2.3.2 Viability:</i>	42
2.4 Measurement of HUVEC mitochondrial membrane potential and content.....	43
2.5 Quantitative RT-PCR and western blot analysis	44
<i>2.5.1 qRT-PCR:</i>	44
<i>2.5.2 Western blot:</i>	44
2.6 HUVEC Sprouting Assay	45
<i>2.6.1 Methylcellulose stock:</i>	45

	9
2.6.2 <i>Sprouting Assay:</i>	45
2.7 HUVEC Scratch-Wound Cell Migration Assay	46
2.8 Lentiviral constructs.....	46
2.8.1 <i>Virus Production:</i>	46
2.8.2 <i>HUVEC viral transduction:</i>	47
2.9 Mice and Tamoxifen Administration.....	47
2.9.1 <i>Mice:</i>	47
2.9.2 <i>Tamoxifen Administration:</i>	48
2.10 Postnatal retinal angiogenesis assay	48
2.11 Isolation of endothelial cells from mouse lungs	49
2.11.1 <i>Preparation of single cells lung homogenates:</i>	49
2.11.2 <i>Isolation of lung ECs for RNAseq:</i>	49
2.11.3 <i>Isolation of lung ECs for metabolomics:</i>	50
2.12 Histological analysis	50
2.12.1 <i>Tumor Histology:</i>	50
2.12.2 <i>Lung histology:</i>	50
2.13 Antibodies, flow cytometry and cell sorting.....	51
2.13.1 <i>Antibodies:</i>	51
2.13.2 <i>Flow cytometry and cell sorting:</i>	52
2.14 Microscopy and image analysis.....	52
2.15 Metabolite analysis	52
2.15.1 <i>In vitro cell collection for metabolomics:</i>	52
2.15.2 <i>In vivo cell collection for metabolomics:</i>	53
2.15.3 <i>Metabolite sample preparation and analysis</i>	53
2.15.4 <i>Measurement of NAD⁺ and NADH metabolites:</i>	54
2.16 RNA sequencing analysis	55
2.17 Tumor angiogenesis assay	56
2.18 Mass spectrometry to identify histone modifications	56

3. CHAPTER 3: MITOCHONDRIAL COMPLEX III IS NECESSARY FOR	
 ENDOTHELIAL CELL PROLIFERATION DURING ANGIOGENESIS.....	58
3.1 Significance.....	58
3.2 Results.....	60
3.2.1 <i>Mitochondrial complex III is required for endothelial cell proliferation</i>	
<i>in vitro</i>	60
3.2.2 <i>Mitochondrial complex III in HUVECs maintains NAD⁺/NADH ratio,</i>	
<i>necessary for endothelial cell proliferation</i>	68
3.2.3 <i>Inhibiting mitochondrial complex III respiration in HUVECs does not broadly</i>	
<i>disrupt histone modifications</i>	80
3.2.4 <i>Mitochondrial complex III respiration in ECs is required for post-natal retinal</i>	
<i>angiogenesis</i>	83
3.2.5 <i>Mitochondrial complex III function in ECs is necessary for post-natal</i>	
<i>developmental angiogenesis</i>	90
3.2.6 <i>Loss of mitochondrial complex III function in ECs increases anabolic-</i>	
<i>associated gene expression</i>	97
3.2.7 <i>Mitochondrial complex III in ECs is necessary to maintain amino acid</i>	
<i>levels in vivo</i>	103
3.2.8 <i>Mitochondrial complex III function in ECs is required for tumor</i>	
<i>angiogenesis</i>	106
3.3 Discussion.....	109
4. CHAPTER 4: CONCLUSIONS AND FUTURE DIRECTIONS.....	114
5. CHAPTER 5: REFERENCES.....	118
6. CURRICULUM VIATE.....	128

LIST OF FIGURES

Figure 1.1.1.1	Diagram of the electron transport chain and oxidative phosphorylation	17
Figure 1.1.2.1	The mitochondrial tricarboxylic acid (TCA) cycle	23
Figure 1.2.1.1	Tip and stalk cell specification during sprouting angiogenesis.....	33
Figure 3.2.1.1	Antimycin treated HUVECs lose oxygen consumption and perform maximum glycolysis	62
Figure 3.2.1.2	Antimycin A treated HUVECs do not increase cell death or apoptosis.....	63
Figure 3.2.1.3	Antimycin A treated HUVECs have increased mitochondrial membrane potential and content.....	64
Figure 3.2.1.4	Complex III function in HUVECs is not required for sprouting or migration....	65
Figure 3.2.1.5	Complex III deficient HUVECs fail to proliferate	66
Figure 3.2.1.6	Mitochondrial complex I is required for endothelial cell proliferation <i>in vitro</i> ..	67
Figure 3.2.2.1	Mitochondrial complex III is required to maintain aspartate levels.....	69
Figure 3.2.2.2	AOX rescues OCR, NAD ⁺ /NADH, and proliferation in antimycin A treated HUVECs	70
Figure 3.2.2.3	AOX rescues TCA cycle metabolites and aspartate levels in antimycin A treated HUVECs	71
Figure 3.2.2.4	LbNOX rescues OCR, NAD ⁺ /NADH, and proliferation in antimycin A treated HUVECs	74
Figure 3.2.2.5	Antimycin A treated HUVECs accumulate succinate and partially maintain aspartate levels	75
Figure 3.2.2.6	Methyl Pyruvate maintains proliferation and aspartate levels in antimycin A treated HUVECs	76
Figure 3.2.2.7	Methyl pyruvate does not restore NAD ⁺ /NADH in antimycin A treated HUVECs	77
Figure 3.2.2.8	Aspartate, methyl aspartate, or asparagine are not sufficient to support proliferation in antimycin treated HUVECs	79
Figure 3.2.3.1	Respiration deficient HUVECs have decreased 2HG, and increased 2HG:αKG, Succinate:αKG, and Fumarate:αKG	81

	12
Figure 3.2.3.2 Inhibiting mitochondrial complex III respiration in HUVECs does not broadly disrupt histone modifications.....	82
Figure 3.2.4.1 Illustration of the strategy utilized to generate Uqcrq floxed and excised alleles.	85
Figure 3.2.4.2 Verification of Cre recombinase activity in QPC KO ECs.....	86
Figure 3.2.4.3 Mitochondrial complex III respiration in ECs is required for post-natal retinal angiogenesis.....	87
Figure 3.2.4.4 Complex III is required for EC proliferation, but not migration during post natal retinal angiogenesis.....	88
Figure 3.2.4.5 Diminished vascularity in QPC-KO retinas is not due to increased EC death or vessel pruning.....	89
Figure 3.2.5.1 Mitochondrial complex III in ECs is required for survival.....	92
Figure 3.2.5.2 QPC-KO lung ECs lose mitochondrial electron transport chain function.....	93
Figure 3.2.5.3 QPC-KO mice have decreased lung EC cellularity.....	94
Figure 3.2.5.4 Schematic of flow cytometric gating strategy from homogenized P15 lung tissue.....	95
Figure 3.2.5.5 QPC-KO lung ECs have diminished proliferative capacity.....	96
Figure 3.2.6.1 Loss of mitochondrial complex III function in ECs increases anabolic-associated gene expression.....	99
Figure 3.2.6.2 QPC-KO lung ECs display increased expression of ribosomal, metabolic and oxphos genes.....	100
Figure 3.2.6.3 Angiogenic genes are largely unchanged in QPC-KO lung ECs.....	101
Figure 3.2.6.4 Metabolic, but not angiogenic genes are altered at the protein level in QPC-KO ECs.....	102
Figure 3.2.7.1 Mitochondrial complex III in ECs is necessary to maintain amino acid levels <i>in vivo</i>	104
Figure 3.2.7.2 Loss of mitochondrial complex III in ECs does not alter 2HG levels.....	105
Figure 3.2.8.1 Mitochondrial complex III respiration in ECs is required for tumor angiogenesis.....	107

Figure 3.2.8.2 Mitochondrial complex III in ECs is necessary to maintain tumor vascularity
and EC proliferation..... 108

1. CHAPTER 1: INTRODUCTION

1.1 Mitochondrial biology

Mitochondria, most commonly known as the “powerhouse” of the cell due to their primary role in generating cellular ATP, are complex organelles¹. Mitochondria are thought to have evolved from α -proteobacteria, which entered into an endosymbiotic relationship with host archaea early during evolution². This ancient fusion generated the first eukaryotic cells containing mitochondria as essential cellular organelles³. The original benefit of this relationship is still debated, however it is now well established that modern mitochondria serve three major functions in eukaryotic cells: (1) they produce large amounts of ATP used to fuel a myriad of energy demanding cellular reactions, (2) they serve as biosynthetic organelles which generate metabolites for macromolecule biosynthesis, and (3) mitochondria are signaling organelles, producing reactive oxygen species (ROS) and other metabolites that are critical for cellular signaling.

1.1.1 Mitochondrial ATP generation

Mitochondria are able to produce energy in the form of ATP in a process known as oxidative phosphorylation (OxPhos) (see Figure 1.1.1.1 below). OxPhos is carried out in the inner membrane of the mitochondria by a series protein complexes known as the electron transport chain (ETC). The ETC consists of NADH-dehydrogenase (complex I), succinate dehydrogenase (complex II), cytochrome c oxidoreductase (complex III), cytochrome c oxidase (complex IV), as well as ubiquinone and cytochrome c⁴. Electrons feed into the ETC via the reducing equivalents NADH and FADH₂ to complexes I and II respectively. NADH derived from glycolysis and the tricarboxylic acid (TCA) cycle are oxidized to NAD⁺ by complex I,

transferring 2 electrons to the first complex of the ETC. Additionally, complex II converts succinate to fumarate, a process that is coupled to the oxidation of FADH_2 to FAD , which donates two electrons to complex II. Both complexes I and II transfer their electrons to an electron carrier protein called ubiquinone (Q), reducing it to QH_2 . Q is a mobile molecule, which is able to travel through the membrane to deliver electrons to complex III. These electrons subsequently move through complex III in a process known as the Q cycle⁵. Importantly, complex III reactive oxygen species (ROS) are generated during the Q cycle, which have been shown to be critical for cellular signaling (discussed in detail in section 1.1.3 below). Complex III then facilitates the transfer of electrons to another mobile electron carrier, cytochrome c, which subsequently passes electrons on to complex IV. Ultimately, complex IV delivers these electrons to the final electron donor of the ETC, molecular oxygen (O_2). O_2 is split, and accepts protons from the matrix to form water⁵. It is this final process that is referred to as “oxygen consumption”, which is measured as a readout for ETC function.

Importantly, the abovementioned transport of electrons through the ETC facilitates the pumping of protons from the matrix of the mitochondria into the intermembrane space by complexes I, III and IV. This pumping produces a proton gradient, with a higher concentration of protons (H^+) in the intermembrane space compared to the matrix. This proton gradient is also referred to as proton-motive force, or membrane potential. Proton buildup in the intermembrane space allows the flow of H^+ ions down the concentration gradient through the hydrophobic membrane tunnel ATP synthase (aka complex V), which finally catalyzes the reaction of ADP to ATP⁶. Notably, the mitochondrial ETC is the most efficient mechanism of ATP production, generating

approximately 32 molecules of ATP per molecule of glucose consumed, versus only 2 ATP generated from glycolysis⁷.

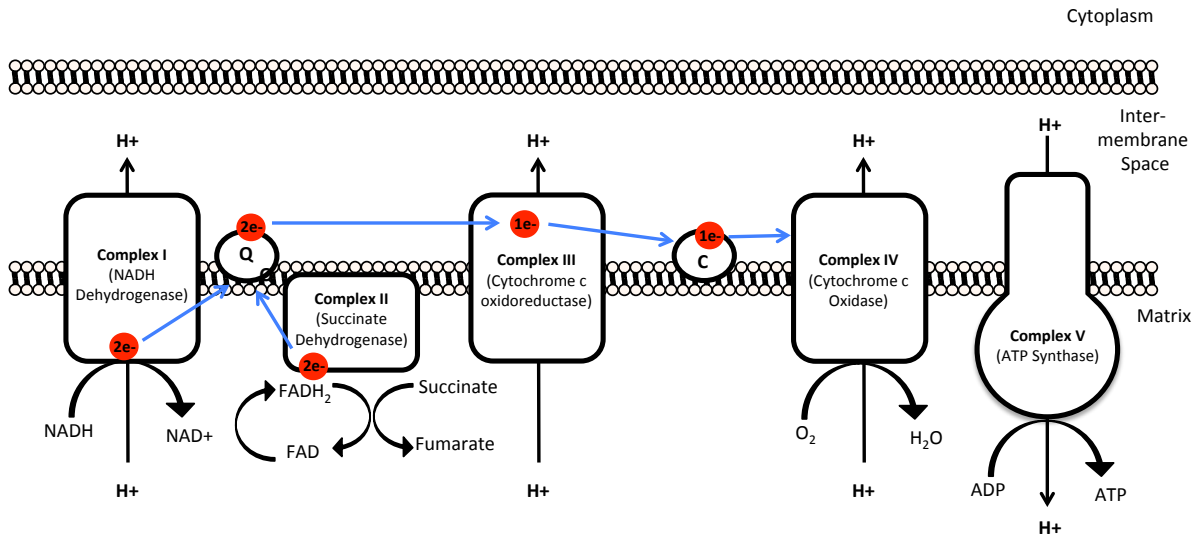


Figure 1.1.1.1 Diagram of the electron transport chain and oxidative phosphorylation

1.1.2 Mitochondria are biosynthetic organelles

While nonproliferating cells (i.e. quiescent or differentiated cells) have relatively little metabolic demand, proliferating cells massively increase anabolic pathways in order to generate the materials required to double their biomass and produce two individual daughter cells. Therefore, proliferating cells reprogram their metabolism to uptake the necessary nutrients to fuel this increased demand^{8,9}. Glucose is the most widely available nutrient in the human body, and proliferating cells consume this carbohydrate readily. In the 1920s, Otto Warburg observed this phenomenon, and recognized that rapidly proliferating cells (i.e. cancer cells) produce copious amounts of lactate, a byproduct of aerobic glycolysis¹⁰. It was initially believed that the processes of aerobic glycolysis and oxidative phosphorylation function much like a cellular switch (when one increases, the other decreases)¹¹. It is for this reason that Warburg concluded that cancer cells must have defective mitochondrial metabolism, a theory that was held for some time. Now, studies show that the vast majority of cancer cells have functional mitochondrial metabolism, which is necessary for cancer cell proliferation¹²⁻¹⁵. While glycolysis alone has subsidiary pathways that generate metabolic intermediates to generate macromolecules required for cell growth, it is not sufficient to meet the metabolic demands for proliferation. The additional metabolic pathways necessary are carried out within the mitochondria and begin with the TCA cycle¹⁶.

The tricarboxylic acid (TCA) cycle:

Through the process of glycolysis, glucose is broken down into pyruvate, which has several known cellular fates including conversion into lactate by the enzyme lactate dehydrogenase (LDH). However, the more predominant fate of glycolytic pyruvate is oxidation by the pyruvate

dehydrogenase (PDH) enzyme into acetyl-CoA, which can enter the TCA cycle within the mitochondria¹⁶. Acetyl-CoA reacts with oxaloacetate to form citrate, the first reaction in the TCA cycle. This cycle continues, forming isocitrate, alpha-ketoglutarate (α KG), succinate, fumarate, malate, and then finally oxaloacetate once again, completing this cyclic chain of reactions. Interestingly, several of the TCA cycle enzymatic reactions are coupled to the reduction of NAD⁺ to NADH (isocitrate to α KG, α KG to succinate, and malate to oxaloacetate) or reduction of FADH₂ to FAD (succinate to fumarate). This property intimately links the TCA cycle to the ETC, which uses the resulting reduced NADH and FADH₂ as electron donors for complexes I and II respectively (discussed in detail in section 1.1.1 above). In addition to generating ETC electron donors, several of the TCA cycle intermediates serve as precursors for critical cellular macromolecules including lipids, amino acids and nucleotides, making the mitochondria a major biosynthetic hub¹⁶. See Figure 1.1.2.1.

Lipid synthesis:

Proliferating cells require increased lipid generation for the production cellular membranes. The majority of cellular membranes are comprised of phospholipids, including phosphatidylcholine and phosphatidylethanolamine, as well as other lipids, such as spingolipids and sterols¹⁷. Many of these lipids contain fatty acids which can be generated in the mitochondria in a process called de novo fatty acid synthesis¹⁷. This process begins when citrate is siphoned out of the TCA cycle and is transported out of the mitochondria where it is cleaved by ATP citrate lyase to generate acetyl-CoA and oxaloacetate¹⁸. Acetyl-CoA in the cytosol is the precursor for fatty acids (Figure 1.1.2.1). The resulting acetyl-CoA is carboxylated by acetyl-CoA carboxylase to generate malonyl-coA. Acetyl-CoA is condensed with malonyl-coA in the cytosol by fatty acid

synthase (FASN) to yield long-chain fatty acids¹⁸. Loss of FASN *in vitro* and *in vivo* lead to diminished cell proliferation and cell cycle arrest, indicating that fatty acid synthesis is necessary for cell growth¹⁹⁻²¹.

Amino acid synthesis:

Of the 20 amino acids cells use to generate proteins, eleven are nonessential or conditionally essential (i.e. not obtained from the diet) and must be synthesized within cells. While two amino acids are synthesized during glycolysis (serine and glycine), the remaining nine are generated from TCA cycle intermediates in the mitochondria. The TCA cycle intermediate α KG is central for generating multiple of these amino acids, including arginine, alanine, and aspartate.

Additionally, aspartate can be converted to asparagine by the enzyme asparagine synthase, while the reverse reaction is catalyzed by asparaginase. Another key TCA cycle precursor to aspartate synthesis is oxaloacetate, which is siphoned out of the TCA cycle and converted to aspartate utilizing the aspartate aminotransferases GOT1 and GOT2^{22,23} (Figure 1.1.2.1).

Aspartate is necessary for cell proliferation:

As mentioned above, aspartate is produced from the TCA cycle intermediate oxaloacetate, and is coupled to the conversion of α KG to glutamate, intimately linking aspartate production to mitochondrial TCA cycle activity. This bidirectional reaction is catalyzed by GOT1 in the cytosol, and GOT2 in the mitochondria. Recent studies have shown that aspartate is both necessary and sufficient to support proliferation of most cancer cells upon ETC inhibition (recall that ETC inhibition also leads to forward TCA cycle impairment due to reduced capacity to overturn NADH)^{24,25}. Through the use of a CRISPR-based genetic screen Birsoy et. al. found

that that upon loss of ETC function, cells utilize GOT1 to generate aspartate, highlighting that aspartate synthesis is an essential role of the ETC and mitochondrial TCA cycle during proliferation²⁴. Sullivan et. al. support these findings, showing that upon ETC inhibition with various pharmacological inhibitors, aspartate is able to, at least partially, restore proliferation in several different cancer cells lines, as well as in complex III null 143B CytB cells²⁵. It is important to note that proliferation of not all cancer cells is rescued by aspartate after ETC inhibition, which is likely due to differences in aspartate uptake^{26,27}. Importantly, the key role of aspartate for cellular proliferation has been studied in cancer cells, however whether aspartate is necessary and sufficient for proliferation of non-tumor cells remains largely uncharacterized.

Aspartate supports amino acid and nucleotide synthesis:

As mentioned above, aspartate is central for several key reactions involving the generation and interconversion of other amino acids. For example, aspartate and glutamine are precursors for asparagine and glutamate, a cytosolic reaction catalyzed by asparagine synthetase, which is critical for the cells ability to utilize glutamine as fuel to replenish the TCA cycle²³.

Additionally, aspartate contributes carbons and nitrogen to the backbone to the pyrimidine ring during pyrimidine nucleotide synthesis. In this reaction, aspartate reacts with carbomoyl phosphate to generate the pyrimidine base, orotate, from which all other mature pyrimidine nucleotides are synthesized. Finally, aspartate donates a nitrogen to the purine base IMP, a key step in purine nucleotide biogenesis²³.

Pyrimidine nucleotide synthesis is supported by DHODH:

Independent of aspartate metabolism, the mitochondrial ETC is required for pyrimidine nucleotide biosynthesis. As mentioned above, aspartate donates a large portion of the pyrimidine ring backbone to generate orotate. However, an intermediate step converts dihydroorotate (DHO) to orotate, which is catalyzed by the enzyme dihydroorotate dehydrogenase (DHODH).

Importantly, DHODH resides in the inner membrane of the mitochondria, in close proximity to the ETC. It is here where DHODH catalyzes the conversion of DHO to orotate and donates an electron to the Q pool in the process. This electron donation is critical for this reaction to proceed; therefore inhibition of the ETC simultaneously inhibits DHODH. Consequently, respiratory deficient cancer cells are auxotrophic for pyrimidines (i.e. uridine) ^{14,25,28}.

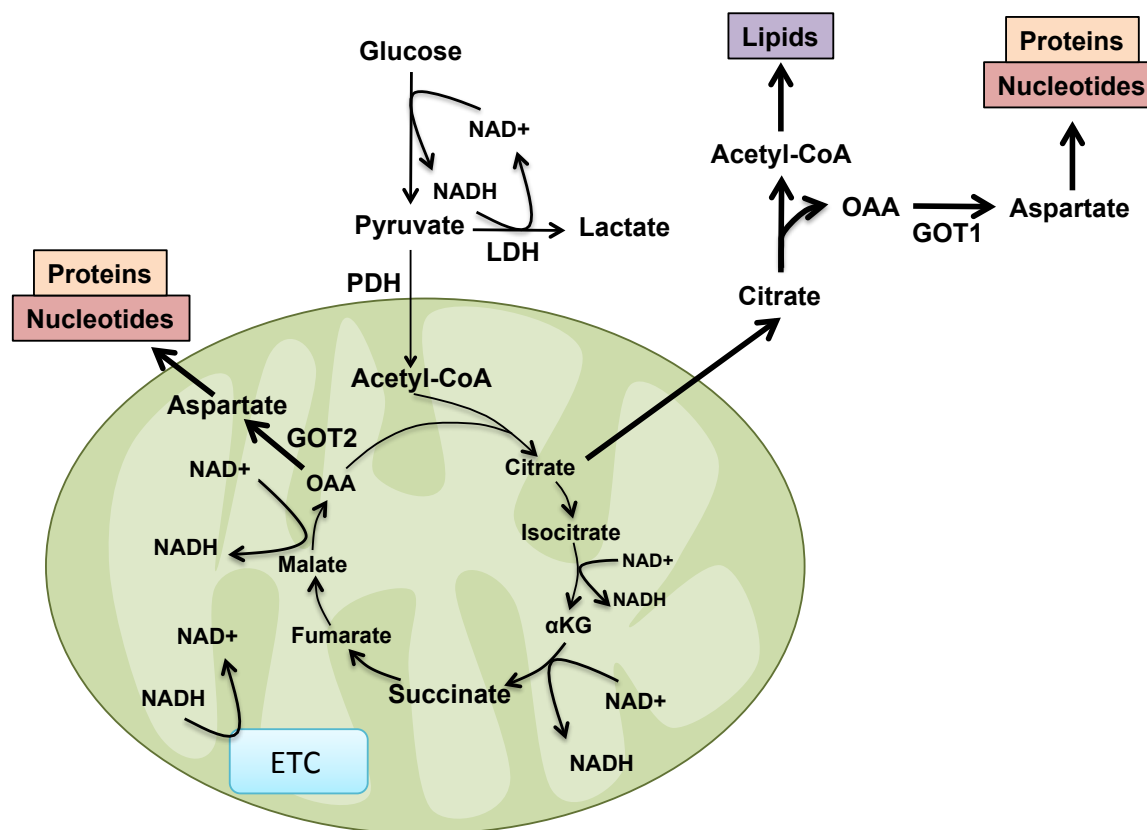


Figure 1.1.2.1 The mitochondrial tricarboxylic acid (TCA) cycle

Glucose generates pyruvate, which either is converted to lactate by lactate dehydrogenase (LDH), or to acetyl-CoA by pyruvate dehydrogenase (PDH). Acetyl-CoA combines with oxaloacetate (OAA) to generate citrate. The TCA cycle intermediate citrate is exported from the mitochondria, where it is converted to acetyl-CoA and OAA. Cytosolic acetyl-CoA is used for lipid synthesis. OAA can be converted to Aspartate by aspartate aminotransferases GOT1 in the cytosol and GOT2 in the mitochondria, which is necessary for protein and nucleotide synthesis. The electron transport chain (ETC) oxidizes NADH to NAD⁺, while several reactions in the TCA cycle are coupled to the reduction of NAD⁺ to NADH.

1.1.3 Mitochondria as signaling organelles

Being such critical organelles for cellular energy and biomass production, it is imperative that mitochondria evolved mechanisms to communicate with the rest of the cell. There are two main types of communication that exist between mitochondria and the cell: anterograde and retrograde signaling. Anterograde signaling involves the cell communicating with the mitochondria to control their function. Mitochondria are considered semi-autonomous organelles; they retain some of their own DNA that encodes for mitochondrial proteins, however replication, transcription and translation of mitochondrial DNA are regulated by the nucleus²⁹. Besides gene regulation, the cell can transduce signals to the mitochondria via calcium. In the presence of high concentrations of cytosolic calcium, calcium is rapidly sequestered into the mitochondria, which can activate TCA cycle enzymes to drive increased oxidative phosphorylation³⁰. Retrograde signaling (signaling from the mitochondria to the rest of the cell) was first recognized when it was found that mitochondria release cytochrome c in order to initiate apoptosis³¹. Presently, several different mechanisms of retrograde signaling are appreciated, including mitochondrial release of reactive oxygen species (mROS) and various metabolites to control cellular functions.

Release of mitochondrial reactive oxygen species controls cellular functions:

Reactive oxygen species (ROS) are formed by the chemical reduction of O₂, and include superoxide (O₂•), hydrogen peroxide (H₂O₂), and the hydroxyl radical (OH•)^{32,33}. Historically, ROS were thought to function solely as damaging molecules, as they were found to be associated with oxidative stress, inducing pathology by indiscriminately damaging lipids, proteins and DNA. Importantly, in the past two decades, it has become evident that ROS can act as intracellular signaling molecules (i.e. redox biology), contributing to signaling pathways to

control numerous physiological and pathological cell processes³⁴. Notably, the mitochondria are a major source of ROS within a cell, and as a byproduct of oxidative phosphorylation, produce $O_2\bullet$ from the one-electron reduction of oxygen³⁵. There are at least ten sites within the mitochondria where $O_2\bullet$ is generated, most notably from complexes I, II and III of the mitochondrial electron transport chain (ETC)^{36,37}. While complexes I and II exclusively create $O_2\bullet$ in the mitochondrial matrix, complex III produces $O_2\bullet$ in both the matrix and intermembrane space^{38,39}. The $O_2\bullet$ generated by complexes I and II in the matrix is rapidly converted to H_2O_2 by mitochondrial superoxide dismutase protein 2 (SOD2)⁴⁰. On the other hand, $O_2\bullet$ made by complex III in the intermembrane space, travels through voltage-dependent ion channels (VDACs) in the outer mitochondrial membrane and into the cytosol, where it can be converted into H_2O_2 by cytosolic SOD1⁴¹. Complex III-generated ROS is of particular interest in the field of ROS signaling, as it theoretically has an easier route to the cytosol, where it can participate in cellular signaling events⁴².

H_2O_2 is the primary form of ROS utilized for intracellular signaling. The most characterized manner in which H_2O_2 signals is through reversible cysteine oxidation. H_2O_2 selectively reacts with critical cysteine residues within redox-sensitive proteins, modifying the target protein's activity or conformation in order to alter signal transduction^{43,44}. Specifically, H_2O_2 modifies proteins by oxidizing low pKa cysteine residues, providing a level of selectivity^{45,46}. The low pKa allows the thiol group (SH) of the cysteine to exist as an un-protonated thiolate (S^-) under physiological pH, permitting it to be oxidized to form sulfenic acid (SO^-)^{45,46}. SO^- only exists as an intermediate residue, as it is commonly incorporated into disulfide (S-S) or sulfenic amide (S-N) bonds^{45,46}. Reversible thiol oxidation (S^- to SO^-) by H_2O_2 is estimated to occur in the nM

range, however, higher levels of peroxide can induce further oxidation of sulfenic acid (SO^\cdot) to sulfinic (SO_2^-) or sulfonic (SO_3^-) acid⁴⁷. The oxidation of thiol residues is tightly regulated by glutaredoxin (GRX), sulfiredoxin (SRX) and thioredoxin (TRX), which use the oxidation of NADPH to NADP⁺ to reduce modified proteins back to their original state⁴⁵.

Over the past two decades, studies have drastically shifted our understanding of ROS. No longer viewed solely as damaging agents, ROS, especially those produced by the mitochondria, are now becoming increasingly appreciated for their integral role in cellular signaling. We support a model where very low mROS levels promote normal cell homeostasis, while precise increases in mROS are required for cellular proliferation and adaptation to stress. Unfortunately, cancers cells take advantage of normal cell processes in order to drive tumor growth; thus, heightened levels of mROS are used to induce pro-tumorigenic signaling. In general, ROS at very high levels no longer act as signaling molecules, but rather overtly damage proteins, lipids and DNA, which normally results in senescence or cell death. Although, much progress has been made, the specific molecular targets of mROS remain largely unknown. Going forward, it will be important to identify these targets, not only to give us a stronger understanding of the role of mROS in normal cellular functions, but also perhaps to better utilize mROS modulation in the treatment of proliferative diseases such as cancer.

Mitochondrial metabolites dictate cellular functions:

In addition to mROS, mitochondria release metabolites into the cytosol in order to alter nuclear gene regulation. Citrate from the TCA cycle is transferred into the cytosol via the citrate shuttle, and is readily converted into acetyl-CoA by ATP citrate lyase⁴⁸. Importantly, acetyl-CoA is the

substrate for histone acetylation transferases (HATS) which acetylate histones, a post-translational modification that regulates gene expression⁴⁹. Consequently, decreased acetyl-CoA levels due to inhibition of the mitochondrial ETC has been associated with diminished histone acetylation^{14,50}.

Another mechanism by which mitochondria regulate epigenetics is through histone demethylation. The family of nearly 30 JmjC domain-containing histone demethylases and 3 ten-eleven translocation (TET) 5-methylcytosine (5mC) hydroxylases are alpha-ketoglutarate (α KG) dependent⁵¹. The reaction catalyzed by the abovementioned demethylase enzymes are coupled to the decarboxylation of α KG to succinate, therefore these reactions are sensitive to the concentration of these mitochondrial metabolites. Recall that complex II of the ETC (succinate dehydrogenase) converts succinate to fumarate. Inhibition of the ETC leads to an accumulation of succinate, as the conversion of succinate to fumarate cannot proceed. Likewise, an accumulation of succinate compared to α KG means that the decarboxylation of α KG to succinate is no longer favorable, and consequently, histone demethylation is diminished causing overall hyper-methylation. Accordingly, mutations in mitochondrial enzymes that lead to the accumulation of succinate or fumarate inhibit histone demethylases by acting as competitive inhibitors, leading to a genome-wide increase in histone methylation⁵².

Another known TCA cycle metabolite that acts as a competitive inhibitor of histone demethylases is 2-hydroxyglutarate (2HG)⁵³. The D enantiomer of this molecule (D-2HG) is a well-characterized oncometabolite generated from mutant isocitrate dehydrogenase 1/2 (IDH1 or IDH2). These enzymes normally generate α KG from isocitrate, however when mutated generate

D-2HG instead of α KG. IDH1/2 mutations occur commonly in glioblastoma and acute myeloid leukemia, and are accompanied by the accumulation of high concentrations of D-2HG and increased histone methylation⁵⁴⁻⁵⁶. Under normal conditions, the L enantiomer of 2HG (L-2HG) is produced from α KG by the promiscuous enzymatic activity of malate dehydrogenase (MDH) and lactate dehydrogenase (LDH)^{57,58}. Interestingly, both MDH and LDH conversion of α KG to L-2HG are coupled to the oxidation of NADH to NAD⁺, so it can be postulated that under cellular conditions with elevated NADH compared to NAD (e.g. ETC inhibition) cells would generate higher levels of L-2HG⁵⁹. Additionally, the enzyme that detoxifies L-2HG (converts L-2HG back into α KG) requires the donation of an electron to the Q pool, a reaction that is diminished upon ETC inhibition⁵⁸. Therefore, upon loss of ETC function, cells accumulate high levels of L-2HG, as it is produced at a higher rate, and its detoxification is diminished. Importantly, L-2HG is also a potent inhibitor of histone demethylases, suggesting that ETC inhibition leads to epigenetic deregulation⁵⁷. In fact, we have recently reported that respiration deficient hematopoietic stem cells (HSC) accumulate large amounts of L-2HG, as well as display widespread histone hypermethylation and massive gene deregulation⁵⁰. This indicates that mitochondria signal by influencing epigenetic regulation. As discussed in chapter 3, respiration deficient endothelial cells do not accumulate L-2HG, nor do they harbor histone deregulation, suggesting that this phenomenon may be cell-type dependent.

Once considered an organelle with ATP generation as its primary function, it is now well appreciated that mitochondria are much more than just the powerhouse of the cell. While they do generate significant amounts of ATP for energy, mitochondria are also now appreciated as key biosynthetic and signaling organelles.

1.2 Endothelial Cells

Endothelial cells (ECs) line the intricate system of vasculature that supplies nearly every tissue and organ in the body with vital oxygen and nutrients. In most healthy adult tissues ECs are quiescent; however, when stimulated can rapidly expand their vast network of vessels. Limited oxygen and nutrient availability are the main drivers of angiogenesis (i.e. the generation of new blood vessels from the existing vasculature). During this intricate process, once quiescent ECs begin to sprout towards areas of low oxygen tension and nutrient availability, forming new blood vessels in their wake. The switch from quiescence to angiogenesis is both a bioenergetically and biosynthetically demanding undertaking; thus, ECs must dramatically alter their metabolism to carry out this task. Angiogenic ECs require additional nutrients to generate the energy needed for migration, as well as to produce the biomass necessary for rapid proliferation. ECs have been categorized as a highly glycolytic cell type that relies little on mitochondrial metabolism, however the study of EC metabolism is an emerging field with much still left to be uncovered.

1.2.1 Angiogenesis

Besides a few exceptions (e.g. the cornea and cartilage are avascular) every tissue in the body relies on blood vessels for the supply of oxygen and nutrients⁶⁰. The vasculature is one of the first organs to develop during embryogenesis, and begins by the differentiation and organization of precursor cells called angioblasts^{60,61}. In a process termed vasculogenesis, angioblasts aggregate and reorganize into a primitive vascular complex known as the vascular plexus^{60,61}. It is from this structure that all other vessels originate, and throughout development expand the vascular plexus via vessel splitting (intussusception) and vessel sprouting (generally referred to as angiogenesis)^{60,61}.

Sprouting angiogenesis:

Sprouting angiogenesis (hereafter referred to as simply, angiogenesis) is the process by which new vessels sprout from the existing vasculature. Angiogenesis is a critical process not only during development, but is also crucial for wound healing and tissue repair, as well as for pathological conditions such as cancer^{62,63}. Tissues in need of oxygen and nutrients produce pro-angiogenic signals (discussed below) that stimulate quiescent ECs to undergo an angiogenic switch. This process begins when the vessel “relaxes” (EC cell-cell contacts loosen, supportive pericyte cells detach, and the basement membrane is broken down) in order to allow the nascent vessel to develop⁶⁰. A single “tip cell” begins to protrude filopodia and invade into the surrounding tissue, migrating toward the pro-angiogenic signal⁶⁴. Behind the tip cell, “stalk cells” proliferate and reorganize to build the growing sprout⁶⁵. Ultimately, the tip cell filopodia from adjacent sprouts connect, and with the help of macrophages, fuse together in a process known as anastomosis⁶⁶. This process generates a new closed circuit with a fully perfused lumen. When the surrounding tissue is fully oxygenated (no longer produce pro-angiogenic signals), ECs resume their quiescence, tightening their cell-cell junctions, establishing basement membrane, and recruiting new pericytes, becoming a fully mature vessel⁶¹. ECs in their quiescent state are referred to as phalanx cells (see Figure 1.2.1.1).

Angiogenic signaling during sprouting:

As mentioned above, tip and stalk cells in the growing sprout exhibit dramatically different cell behaviors. While tip cells extend filopodia and direct the route of the growing vessel (in general they do not proliferate), stalk cells rapidly replicate, follow the leading tip cell, and intricately coordinate their morphology and cell-cell junctions to form a functional vascular lumen (in

general they do not migrate). Accordingly, these two disparate cell types have unique cellular signaling that directs their behavior.

The primary driver that initiates vessel sprouting is vascular endothelial growth factor A (VEGF-A, aka VEGF)⁶². This growth factor, which is released by hypoxic, inflammatory, or tumor tissues, forms a gradient emanating from its source⁶⁷. It is this gradient that guides the tip cell during migration⁶⁷. VEGF binds to VEGF receptor 2 (VEGFR2) expressed on the surface of ECs, and the EC that is exposed to the highest concentration of VEGF becomes the tip cell⁶⁸. There is only one tip cell at the leading edge of a nascent vessel, which must signal to neighboring ECs, suppressing their activation by VEGF to maintain their stalk cell phenotype. VEGF binding to VEGFR2, which is enhanced by co-receptor neuropilin-1 (Nrp1), upregulates expression of the notch ligand delta-like 4 (DLL4) on the surface of tip cells^{68,69}. DLL4 activates notch signaling in adjacent stalk cells, which induces expression of the high-affinity, low-activity decoy VEGF receptor 1 (VEGFR1), while reducing VEGFR2 expression^{68,69}. VEGFR1 acts as a trap to sequester VEGF from binding VEGFR2 receptors left on the surface of stalk cells, thereby reducing VEGF signaling to maintain a stalk cell phenotype^{68,69}. Interestingly, throughout the process of vessel sprouting, ECs continuously compete for the position of the tip cell, dynamically shifting positions, allowing the cell with the highest ratio of VEGFR2/VEGFR1 signaling to lead the vessel⁷⁰. However, the downstream Notch signaling ultimately guides tip and stalk cell behavior. Inhibition of Notch signaling during angiogenesis leads to a hypersprouting phenotype, characterized by increased tip cells, and excessive vessel branching⁷¹⁻⁷⁴. Accordingly, increased Notch signaling decreases tip cell formation and vessel branching^{71,74}. It is through this intricate coordination of VEGF and Notch signaling that tip and

stalk cells communicate to coordinate sprouting angiogenesis (see Figure 1.2.1.1). Besides VEGF, there are several other growth factors that are critical during vessel sprouting, including fibroblast growth factor (FGF), tumor necrosis factor-alpha (TNF- α), transforming growth factor-beta (TGF- β), platelet derived growth factor (PDGF), and angiopoitin (Angpt), which are released both by ECs and by other cells in the microenvironment, and promote the survival, migration, proliferation and maintenance of blood vessels ⁷⁵.

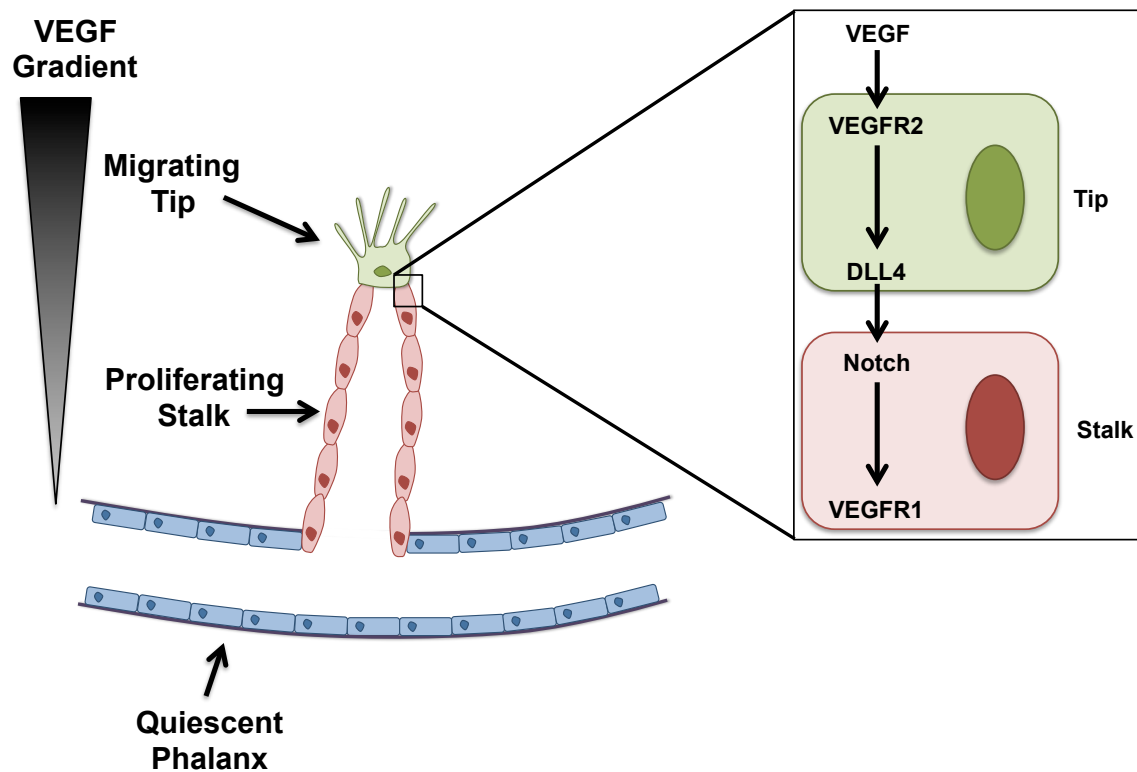


Figure 1.2.1.1 Tip and stalk cell specification during sprouting angiogenesis.

Hypoxic tissues release the pro-angiogenic signal vascular endothelial growth factor (VEGF). The endothelial cell (EC) exposed to the highest concentration of VEGF becomes the tip cell, and migrates toward the pro-angiogenic signal. VEGF receptor 2 (VEGFR2) on the surface of tip cells binds VEGF, leading to increased expression of notch ligand delta-like 4 (DLL4) on the surface of tip cells. DLL4 activates Notch signaling in stalk cells, increasing expression of VEGFR1 on the surface of stalk cells, which decreased VEGFR2 signaling to maintain the stalk cell phenotype.

1.2.2 Endothelial cell metabolism

Unlike quiescent phalanx cells, angiogenic ECs require increased nutrient uptake in order to generate ATP for migration, as well as for the production of cellular biomass (i.e. lipids, amino acids, and nucleotides) for cell growth. In the last several years, the study of EC metabolism has surged, giving insight into the perhaps unique metabolism in this cell type. It is essential to note, however, that the metabolic profiling discussed below is derived from ECs grown in 2-dimensional monolayers with cell culture medium. Such culture conditions can not possibly recapitulate the 3-dimensional complexity and nutrient availability of the *in vivo* microenvironment^{76,77}. It is important to keep this caveat in mind when discussing the catabolism and anabolism of cellular nutrients in any cell type. Despite this limitation, *in vitro* reports of EC metabolism have given insight into their metabolic state, however more studies utilizing *in vivo* metabolic profiling are needed.

Endothelial cells are glycolytic:

Despite having ample access to high concentrations of oxygen in the blood, ECs are highly glycolytic. Although oxidative phosphorylation is an exceedingly more efficient mechanism for ATP production (as discussed in section 1.1.1), ECs prefer to generate nearly 85% of ATP through glycolysis^{74,78,79}. Rat coronary microvascular EC have been shown metabolize the vast majority (up to 98%) of glucose into lactate, only oxidizing about 0.04% into the mitochondrial TCA cycle⁷⁹. In human umbilical vein endothelial cells (HUVECs), flux through glycolysis was calculated to be approximately 200 times higher than either glucose oxidation, fatty acid oxidation, or glutamine oxidation⁷⁴. Notably, the aforementioned studies were conducted under

cultured conditions, and the glucose utilization of ECs their natural *in vivo* environment is currently unknown.

In congruence with evidence that ECs are extremely glycolytic, glycolysis is necessary for their survival, growth and migration. During angiogenesis, VEGF upregulates a number of glycolytic enzymes including glucose transporter 1 (GLUT1), lactate dehydrogenase (LDH), and 6-phosphofructo-2-kinase/fructose-2,6-bisphosphate (PFKFB3), significantly increasing glycolytic flux^{74,80-82}. A hallmark of EC behavior is that they must expand into hypoxic environments, which is one reason it is thought they rely heavily on glycolysis over oxidative metabolism. Accordingly, hypoxia, via hypoxia inducible factor 1 (HIF1), enhances glycolysis in angiogenic ECs⁸³. As ECs rely heavily on glucose for the production of ATP, glycolytic blockade with 2-deoxy-D-glucose (2DG) leads to rapid cell death⁸⁴⁻⁸⁶. Since complete inhibition of glycolysis leads to EC demise, the role of glucose metabolism in ECs has recently been elucidated in the context of partial glycolytic reduction. PFKFB3 indirectly regulates glycolysis, and loss of this enzyme reduces glycolytic flux by approximately 40%⁷⁴. In this model, decreased glycolysis lead to impairment of angiogenesis both *in vitro* and *in vivo*, perturbing both tip cell migration as well as stalk cell proliferation⁷⁴. This critical study also highlighted that while glycolysis is necessary for EC stalk cell proliferation, glycolytic enzymes are primarily localized to tip cell filopodia and lamellipodia (mitochondria were mainly perinuclear), and loss of PFKFB3 reduced the formation of these migratory protrusions⁷⁴. It is postulated that the rapid ATP production generated by glycolysis is necessary for actin cytoskeletal remodeling during migration, and mitochondria are absent from this location by size exclusion. Importantly, EC metabolism was shown to drive tip cell/stalk cell fate, as PFKFB3 loss resulted in a reduced number of tip cells

compared to stalk cells, while PFKFB3 overexpression favored the tip cell phenotype⁷⁴.

Together, these studies highlight not only that glycolysis is required for angiogenesis, but also that metabolism drives endothelial cell fate.

Mitochondrial metabolism in ECs:

ECs rely heavily on glycolysis for ATP production, and produce only small amounts of ATP via oxidative phosphorylation in the mitochondrial ETC. Additionally, ECs are cited to have a relatively low mitochondrial volume and low OCR when compared to other cell types^{74,87}. It is for these reasons that mitochondria metabolism in ECs has been largely overlooked until recently. While some studies indicate that only a minor percentage of glucose derived pyruvate enters the TCA cycle, more recent work estimates that about 20-30% of TCA cycle carbons in cultured HUVECs are derived from glucose^{88,89}. Moreover, ECs have functional mitochondria, indicating that instead of using carbons to fuel ATP production, mitochondria are primarily biosynthetic organelles, utilizing TCA cycle intermediates to generate macromolecules necessary for cellular proliferation.

As discussed in section 1.1.2 above, the TCA cycle intermediate citrate is shuttled out of the mitochondria, where it is converted to acetyl-CoA, which is then used to generate fatty acids by the enzyme fatty acid synthase (FASN). Like other cell types, mitochondria in ECs actively utilize this pathway, as inhibition of FASN diminishes EC proliferation and tumor angiogenesis^{90,91}. In addition to their generation, cells consume fatty acids, which, due to their low aqueous solubility are bound by fatty acid binding proteins (FABPs) during transport within the cell⁹². During angiogenesis, VEGF upregulates FABP4⁹³. Accordingly, loss of FABP4 in ECs results in

diminished proliferation, sprouting, and migration indicating that uptake of fatty acids is necessary for angiogenesis⁹³⁻⁹⁵. Fatty acids are a rich energy source that is broken down in the mitochondria in a process termed fatty acid oxidation (FAO). The rate-limiting enzyme in FAO is carnitine palmitoyltransferase 1 (CPT1), which transfers fatty acids through the outer membrane of the mitochondria. Fatty acids are further transported through the inner membrane and into the mitochondrial matrix by CPT2. In a series of reactions that are coupled to the reduction of 7 molecules of NAD⁺ to NADH, fatty acids are broken down into acetyl-CoA which can enter the TCA cycle²³. In HUVECs, knock-down of CPT1A (the most abundant CPT1 isoform in this cell type) decreased proliferation, albeit quite marginally⁸⁸. *In vivo*, EC-specific CPT1A knock out mice displayed a very slight reduction in post-natal retinal angiogenesis, accompanied by a minor decrease in EC proliferation⁸⁸. The minimal reduction in proliferative capacity in ECs upon loss of FAO is likely due to compensatory mechanisms to upregulate uptake of other anaplerotic carbons. Interestingly, FAO carbons were found to contribute to nucleotide synthesis, which was a unique feature of HUVECs as compared to numerous other cell types⁸⁸. Additionally, loss of CPT1A in HUVECs only slightly decreased oxygen consumption coupled to ATP production, in line with other studies that show the majority of EC ATP is derived from glycolysis⁸⁸. These data support the idea that in ECs mitochondria serve as biosynthetic, rather than bioenergetics organelles.

Glutamine is the most abundant amino acid in human plasma, and after glucose, is the second most consumed nutrient in cultured cancer cells^{96,97}. Likewise, ECs have been shown to readily utilize exogenous glutamine as fuel⁹⁸⁻¹⁰⁰. Glutamine is taken up by cells, where it is then converted to glutamate by glutaminase (GLS)²³. Subsequently, glutamate dehydrogenase

(GLUD) can convert glutamate to α KG to replenish the TCA cycle. In fact, the majority of TCA cycle carbons were found to come from glutamine (as opposed to glucose) in HUVECs grown in culture⁸⁹. In addition to supplying cells with anaplerotic carbons, glutamine is a critical precursor for several transaminase reactions within the mitochondria that generate other non-essential amino acids. Moreover, pyrimidine nucleotide synthesis relies on the conversion of glutamine to glutamate. As carbon and nitrogen from glutamine contribute to numerous biosynthetic pathways, it is no surprise that glutamine deprivation or inhibition of GLS would lead to proliferative defects. Indeed, pharmacological inhibition of GLS in HUVECs causes decreased proliferation and induction of a senescence-like phenotype¹⁰¹. Similarly, HUVECs display impaired proliferative capacity when deprived of glutamine, or after loss of GLS1^{89,102}. Glutamine deprived HUVECs showed decreased nucleotide levels, as well as diminished abundance of several non-essential amino acids (NEAAs)¹⁰². *In vivo*, EC specific loss of GLS1 conferred a modest impairment in retinal angiogenesis, accompanied by decreased EC proliferation^{89,102}. These studies highlight the importance of mitochondrial glutamine metabolism in ECs, and again support the notion that mitochondria in ECs serve a primarily biosynthetic role.

It is unclear why ECs prefer to use aerobic glycolysis as their primary source of cellular energy, however, several theories exist: First, lactate has been shown to be a pro-angiogenic signaling molecule, which is readily generated during glycolysis⁶⁰. Second, the primary purpose of blood vessels is to supply oxygen to tissues, and perhaps consuming less oxygen themselves maximizes oxygen transfer. Third, ECs may rely on glycolysis because they must sprout into hypoxic environments where glucose may not be limited. Regardless, cells cannot rely only on glycolysis

for all of their energetic and biosynthetic demands. As discussed above, loss of fatty acid synthesis, fatty acid oxidation (FAO) or glutamine consumption impairs EC proliferation without appreciable loss of ATP production. While the requirements of individual mitochondrial pathways have been studied in ECs, the role of the mitochondrial electron transport chain (ETC) has never been elucidated. Importantly, loss of ETC function not only abolishes oxygen consumption and ATP production in the mitochondria, but additionally limits other processes such as forward TCA cycle function and FAO due to limited NAD⁺ availability. In chapter 3, I describe in detail the necessity for mitochondrial ETC complex III in endothelial cells during angiogenesis.

2. CHAPTER 2: MATERIALS AND METHODS

2.1 Cell Culture and Drug Treatment

Human umbilical vein endothelial cells (HUVECs) (Lonza) were cultured in Endothelial Basal Medium (MCDB 131) without pyruvate (USBiological) (this media was custom ordered to exclude pyruvate and obtained as a powder), and used at a low passage number (P1-6) for *in vitro* assays. Media was supplemented with EGM-2 SingleQuot growth factors (Lonza) and 1% GlutaMax (Gibco) (supplemented MCDB 131 media). Each vial of P0 cells ordered from Lonza was thawed, and grown for approximately 4 passages in order to expand to about 20 million cells. These cells were then frozen down in 80% EGM2, 10% FBS, and 10% DMSO and kept in liquid nitrogen. Preceding experiments, expanded HUVECs were thawed in EBM2 and kept in culture for at least 24 hours before plating for an experiment. Cells were kept in EBM2 for an additional 24 hours before changing to supplemented MCDB 131 media. Cells were washed 2x with PBS to remove any residual pyruvate. When media was changed and treatment was added was considered time=0. B16-F10 melanoma cells were cultured in RPMI (Corning), with 10% FBS (Corning), 1% sodium pyruvate (Gibco), 1% Non-essential amino acids (Gibco), 1% GlutaMAX (Gibco), 1% antibiotic/antimycotic (Corning), and 0.05mM β -mercaptoethanol (Sigma). Cells were maintained at 37°C with 5% CO₂. HUVECs were treated with: 25nM Antimycin A (Sigma) (dissolved in EtOH), 250nM Piericidin (Sigma) (dissolved in DMSO), 1mM methyl pyruvate (MP) (Sigma) (dissolved in media), and/or indicated doses of L-Aspartic Acid (aspartate) (Sigma) (dissolved in 1M HCl), L-aspartic acid dimethyl ester hydrochloride (methyl aspartate) (Sigma) (dissolved in EtOH), or L-asparagine (asparagine) (Sigma) (dissolved in 1M HCl). Aspartate, methyl aspartate, and asparagine made media quite acidic, so the pH was adjusted using NaOH.

2.2 Oxygen Consumption and Extracellular Acidification Rate

Measurements

Oxygen consumption rate (OCR) and extracellular acidification rate (ECAR) were measured using an XF96 extracellular flux analyzer (Seahorse Bioscience, now Agilent).

2.2.1 In vitro OCR:

30,000 HUVECs per well were plated onto XF96 cell culture plates in supplemented MCDB 131 media and allowed to attach for at least 4 hours, or overnight. Cells were then treated with mitochondrial respiratory chain inhibitor for 2 hours (media was carefully changed by inverting the plate, and washing 2x with PBS to remove any residual pyruvate). Basal respiration was measured by subtracting the OCR values after treatment with 2 μ M antimycin A (Sigma) and 2 μ M rotenone (Sigma). Coupled respiration was determined by treatment with 2.5 μ M oligomycin A (Sigma), and subtracting oligomycin A values from basal respiration. To measure ECAR, cells were treated in supplemented MCDB 131 media without sodium bicarbonate. Basal ECAR was measured by subtracting the ECAR rate after treatment with 20mM 2-deoxyglucose (2-DG) (Sigma). Maximum ECAR rate was measured by subtracting the rate after after 2-DG treatment from the rate after treatment with 2.5uM Oligomycin A.

2.2.2 In vivo OCR:

100,000 lung ECs were plated onto XF96 cell culture plates in supplemented MCDB 131 media and attached using Cell-Tak following the manufacturer's protocol (Corning). Briefly, Cell-Tak was dissolved in a sodium bicarbonate buffer at 22.4ug/mL. 25uL of this solution was added to

each seahorse well and incubated for 20min at room temperature. Wells were washed 2x with water and cells are added in 50uL and spun at 200xg for 1 minute with no brake. Basal respiration was measured by subtracting the OCR values after treatment with 2 μ M antimycin A (Sigma) and 2 μ M rotenone (Sigma). Coupled respiration was determined by treatment with 2.5 μ M oligomycin A (Sigma), and subtracting oligomycin A values from basal respiration.

2.3 HUVEC Proliferation And Viability Assays

2.3.1 Proliferation:

For proliferation curves, HUVECs were thawed in EBM2 and allowed to recover for 24 hours. HUVECs were then plated onto 6 well plates in EBM2 media and again allowed to attach/recover for 24 hours. Media was then removed and cells were washed 2x with PBS to remove any residual pyruvate and replaced with supplemented MCDB 131 media with or without drug treatments (this was time=0). Cells were then counted at each timepoint (24, 48, 72, or 96 hours) via flow cytometry using AccuCount Fluorescent Particles (Spherotech). Briefly, all of the cells from each 6-well well were collected in a flow tube, spun down at 300xg, and resuspended in 190uL PBS and 10uL sperotech beads (200uL total). The flow machine then counted 10,000 beads (1/10 of the sample). The number of cells counted on the flow cytometer was then multiplied by 10 to achieve the total number of cells per well.

2.3.2 Viability:

For viability, HUVECs were plated and treated as described above. Viability was assessed at 96 hours post-treatment via flow cytometry by adding 100ng/mL of 4',6-Diamidino-2-phenylindole dihydrochloride (DAPI) and assessing the percentage of DAPI negative cells by flow cytometry.

To measure apoptosis and viability, HUVECs were plated and treated as described above.

After 48 or 96 hours, cells were collected and stained with AnnexinV and Propidium Iodide (PI) according to the manufacturers protocol (eBioscience AnnexinV apoptosis detection kit). For AnnexinV/PI staining, cells were collected and washed once in PBS and once in 1x binding buffer. Cells were spun down and resuspended in 100uL 1x binding buffer, 5uL of AnnexinV antibody was added and incubated 15 minutes at room temperature. Cells were spun down and resuspended in 200uL 1x binding buffer to which 5uL of PI was added, and analyzed by flow cytometry.

2.4 Measurement of HUVEC mitochondrial membrane potential and content

HUVECs were plated and treated as described above and collected after 48 or 96 hours. To measure membrane potential, cells were stained with 50nM TMRE (Tetramethylrhodamine ethyl ester perchlorate, Molecular Probes) for 20 minutes at 37°C. Median fluorescence intensity (MFI) (PE) was measured by flow cytometry and corrected by subtracting the MFI of each sample after addition of 25uM CCCP (carbonyl cyanide m-chlorophenyl hydrazine). To measure mitochondrial content, cells were stained with 25nM MitoTracker Green (Molecular Probes) for 20 minutes at 37°C. MFI (FITC) was measured by flow cytometry.

2.5 Quantitative RT-PCR and western blot analysis

2.5.1 qRT-PCR:

To measure QPC expression, RNA was isolated using the E.Z.N.A Total RNA Kit I by following the manufacturer's protocol (Omega). CYBRFast 1-Step RT-qPCR Lo-ROX Kit (Tonbo) was used to measure QPC expression with the following primers: QPC-F: 5'-GAGACTGAGGATATCGATTG-3', and QPC-R: 5'-GGATGCGCTCGCGAGTGCGG-3'. To measure mitochondrial DNA content, genomic DNA was purified using the QIAamp DNA Mini Kit (Qiagen), and qRT-PCR was performed using iQ SYBR Green Supermix (Bio-Rad) using the following primers: ND2-F: 5'-GCCCTAGAAATAAACATGCTA-3'; ND2-R: 5'-GGGCTATTCCTAGTTTTATT-3'; COX2-F: 5'-CTGAACCTACGAGTACACCG-3'; COX2-R: 5'-TTAATTCTAGGACGATGGGC-3'; CYTB-F: 5'-CATTTATTATCGCGGCCCTA-3'; CYTB-R: 5'-TGGGTTGTTTGATCCTGTTTC-3'; SDHA-F: 5'-TCCACTACATGACGGAGCAG-3'; SDHA-R: 5'-CCATCTTCAGTTCTGCTAAACG-3'; b-actin-F: 5'-TCCACCTTCCAGCAGATGTG-3'; b-Actin-R: 5'-GCATTTGCGGTGGACGAT-3'. Each sample was run in triplicate, and 3 Cq values for each sample were averaged. The normalized expression (delta Cq) for each sample was determined by subtracting the actin Cq value from the sample Cq value. The delta Cq expression value for each sample was determined using the following formula ($2^{(-\text{deltaCq})}$). This value for each mitochondrial gene was divided by the value for Sdha (nuclear) to determine the ratio of mitochondrial to nuclear DNA.

2.5.2 Western blot:

For western blot analysis, cells were lysed in 1x Cell Lysis Buffer (Cell Signaling) containing PMSF (phenylmethane sulfonyl fluoride). Protein was quantified using Pierce BCA protein assay

reagents (Thermo scientific). Relative protein abundance was measured using the Wes system (ProteinSimple) using the manufacturer's protocol and the following antibodies: SHMT2 (Cell Signaling, 12762), PHGDH (Abcam, Ab211365), GAPDH (Sigma, G9545), Tie2/TEK (Millipore, 05-584), and Angpt2 (Invitrogen, PA5-23612).

2.6 HUVEC Sprouting Assay

2.6.1 Methylcellulose stock:

1.2g of methylcellulose (MC) (Sigma, M0512, 4000cP viscosity) was weighed into a flask with a stirbar, and autoclaved to sterilize. 50mL EBM2 media that was preheated to 55°C was added to MC and mixture was incubated at 55°C for 20 minutes, swirling every few minutes. Remaining 50mL EBM2 was added and the flask was placed on a stirplate in the cold room for 2 hours (or until the MC was completely dissolved and had an even consistency). This solution was then transferred to two 50mL conical tubes, which were centrifuged for 2 hours at 4000xg at room temperature. The last ~5mL at the bottom was not used, as this contains insoluble fibers that can cause issues). Solution was stored at 4°C.

2.6.2 Sprouting Assay:

HUVECs were first resuspended in 20% methylcellulose (Sigma, 4000cP viscosity) (80% EGM2) at a concentration of 1000 cells per 25uL. This suspension was then dropped onto non-adherent plates (25uL drops), flipped upside-down, and HUVECs were allowed to form spheroids overnight in hanging drops. Spheroids were collected in PBS + 10% FBS and spun down at 300xg for 5 minutes and then 500xg for 3 minutes at room temperature with no brake. Spheroids were then resuspended in 40% FBS in methylcellulose, combined with collagen type I

(EMD Millipore) (187.5uL per well), NaHCO₃ (15.5mg/mL) (75uL per well), and NaOH (1M) (5uL per well), plated in 24-well plates, and allowed to polymerize at 37°C. Wells were then topped with an equal volume of supplemented MCDB 131 media with or without drug treatments. Media contained 2ug/mL mitomycin C (Sigma) to inhibit proliferation. Spheroids were allowed to sprout for 24 hours before fixation with 4% paraformaldehyde.

2.7 HUVEC Scratch-Wound Cell Migration Assay

Scratch-wound cell migration assays were performed using the IncuCyte ZOOM 96-well scratch wounds cell migration system (Essen BioScience). HUVECs were plated onto 96-well Image Lock tissue culture plates (Essen BioScience, 4379) at a density of 30,000 cells per well in supplemented MCDB 131 media and allowed to attach overnight. Cells were then treated with 5ug/mL mitomycin C for 2 hours to inhibit proliferation. Monolayers were then wounded using the 96-well WoundMaker (Essen BioScience) following the manufacturer's protocol. Media was then replaced with supplemented MCDB 131 with or without drug treatments and images of wounds were taken every 4 hours until closure.

2.8 Lentiviral constructs

2.8.1 Virus Production:

Empty vector (EV) and AOX pWPI GFP¹⁰³, or EV and LbNOX pLV-EF1 RFP¹⁰⁴ (VectorBuilder, VB160708-1059xrd) lentiviral constructs were transfected into COS1 cells using jetPRIME transfection reagent (Polyplus), along with pMD2.G and psPAX2 packaging vectors to produce EV-GFP, AOX-GFP, EV-RFP, and LbNOX-RFP lentiviruses. Briefly, COS1 cells were plated onto 10cm dishes so that they were about 50-60% confluent. 10ug of total DNA

was diluted in JetPrime buffer (500uL per reaction). 5ug of each lentiviral vector were used, along with 3.75ug of psPAX2 and 1.25ug of pMD2G packaging vectors. 20uL of JetPrime was added to each reaction and incubated for 10 minutes at room temperature. Fresh media was added to each 10cm dish of COS1 cells and 500uL of the JetPrime/DNA mixture was added dropwise to each plate while swirling. These plates were left untouched for 48hours and then viral supernatant was collected, filtered through a 0.22um filter, and stored at -80°C until use.

2.8.2 HUVEC viral transduction:

HUVECs were plated at 500,000 cells per 10cm dish and allowed to recover overnight. In the morning, media was removed and 2mL of fresh EBM2 was added to each dish. 1.5mL of viral supernatant was then added to each plate dropwise while swirling. In the evening, 3mL of fresh EBM2 media was added and the plate was incubated overnight. The media was changed the following morning. After 48 hours, HUVECs were collected and either GFP+ or RFP+ cells were sorted using fluorescence-activated cell sorting (FACS). Cells were allowed to recover overnight and then plated for each assay.

2.9 Mice and Tamoxifen Administration

2.9.1 Mice:

C57BL/6 mice harboring a loxp flanked exon 1 of the *Uqcrq* gene (encodes QPC) were generated by Ozgene (Figure 3.2.4.1). Mice were genotyped using the following primers: 1. 5'-CTTCCGCTCCTCCCGGAAGT-3', 2. 5'-TTCCCAAACCTCGCGGCCCATG-3' and 3. 5'-CAATTCCAGCCAACAGTCCC-3' which allow identification of the QPC wild-type, loxp-flanked, and excised alleles. QPC-floxed mice were crossed with *Cdh5Cre^{ERT2}* mice, which have

a tamoxifen-inducible Cre allele under the endothelial-specific Cadherin 5 (Cdh5, aka VE-cadherin) promoter¹⁰⁵. The Cre allele was detected by using the following primers: 1. 5'-AATCTCCCACCGTCAGTACG-3', and 2. 5'-CGTTTTCTGAGCATACTGGGA-3'. Lox-stop-lox TdTomato mice were purchased from Jackson (stock no. 007914).

2.9.2 Tamoxifen Administration:

Tamoxifen stock was prepared by dissolving tamoxifen (Sigma) in corn oil by shaking at 37°C for 2 hours. Tamoxifen was administered to mouse pups orally by dropping 2.5µL of 40mg/mL tamoxifen stock into the mouth using a p10 pipet. Pups were given 5 doses of tamoxifen from P0-P4 at a dose of 100µg/pup/day. For tumor angiogenesis assays, adult mice were fed tamoxifen chow (Envigo) for 2 weeks prior to tumor injection and remained fed with tamoxifen chow for the entirety of the experiment. All animal procedures were approved by the Institutional Animal Care and Use Committee (IACUC) at Northwestern University.

2.10 Postnatal retinal angiogenesis assay

Mouse pups were dosed with tamoxifen as described above. Eyeballs were harvested on P7 as previously described¹⁰⁶. Eyeballs were immediately placed in ice cold PBS, and then fixed in 4% paraformaldehyde at room temperature for 2 hours while on a rocker, rinsed with PBS and stored at 4°C in PBS until dissection. To dissect retinas, an incision was made over the cornea, and the cornea was removed. Outer layers of the eye were then removed, including the sclera, choroid, cornea layers and pigmented layers. The lens was removed from the retina, and the hyaloid vessels were removed. Retinas were blocked/permeabilized in PBS + 5% bovine serum albumin (BSA) (OmniPur) + 0.5% TritonX-100 (Sigma) for 4 hours at room temperature (RT)

while rocking. Retinas were then stained with primary antibodies overnight at 4°C and washed the next day in 5% BSA + 0.3% TritonX-100 (wash buffer). Retinas were then incubated with fluorescently labeled secondary antibodies and IB4 overnight at 4°C and washed for 4 hours with wash buffer, and then in PBS. Retinas were then cut into cloverleaves, and whole-mounted onto slides using Prolong Diamond Antifade Mounting Media (Molecular Probes).

2.11 Isolation of endothelial cells from mouse lungs

2.11.1 Preparation of single cells lung homogenates:

Whole lungs were harvested from QPC-WT and -KO mice dosed with tamoxifen. P15 pups were euthanized in a humane manner, and lungs were resected. Lungs were then perfused with phosphate buffered saline (PBS) and then with dispase (corning). Lungs were then cut into small pieces using scissors and digested while shaking at 37°C in 5 mg/mL Collagenase type I (Gibco) and 1 mg/mL DNase I (Roche). Lung tissue was homogenized by passing it through a 28G needle several times, and filtering through a 70um filter. Red cell lysis was performed by resuspending homogenized lung pellets in 1mL of RBC lysis (ACK) buffer for 2 minutes, adding PBS to dilute RBC buffer, and then cells were pelleted and resuspended in PBS + 0.5% BSA and kept on ice.

2.11.2 Isolation of lung ECs for RNAseq:

For RNAseq, homogenized lungs were stained with biotinylated CD45 and depleted of CD45+ cells using EasySep Mouse Streptavidin RapidSpheres Isolation Kit (Stemcell) by using the manufacturer's protocol. CD31+ cells were then sorted by FACS and RNA was isolated to be used for RNAseq.

2.11.3 Isolation of lung ECs for metabolomics:

For Metabolomics, Homogenized lungs were stained with both biotinylated CD45 and biotinylated CD326/EpCAM and depleted of CD45+ and EpCAM+ cells using EasySep Mouse Streptavidin RapidSpheres Isolation Kit (Stemcell) by using the manufacturer's protocol. Cells were then stained with CD31-FITC, and CD31+ cells were enriched using the Mouse FITC Selection Kit (Stemcell). Cell pellets were frozen at -80°C until metabolites could be extracted.

2.12 Histological analysis

2.12.1 Tumor Histology:

Tumors were fixed in 4% paraformaldehyde for 24 hours, and submitted for histological analysis at Northwestern histology core. The following was performed by the histology core: Briefly, organs were paraffin embedded and sectioned onto slides. Following standard deparaffinization, antigen retrieval was performed using pH6 sodium Citrate buffer at 110 degrees C for 20 minutes in a biocare decloaking chamber. Slides were blocked and incubated with primary antibodies overnight at 4°C. Blocking and secondary antibody steps were performed using an automated Intellipath staining system made by BioCare.

2.12.2 Lung histology:

Lungs were dissected and perfused through the trachea with a 1:1 solution of optimal cutting temperature (OCT) medium (Fisher), embedded in OCT, and frozen in 2-methylbutane on dry ice. Sections were stored at -80°C until sectioning. Frozen tissue was cryo-sectioned (7µm) and placed on slides, and fixed with acetone (submerged in cold acetone at -20°C for 10 minutes and then dried on the bench overnight). The next day, a pap pen was used to draw a hydrophobic

barrier around the tissue. Sections were rehydrated in PBS for 10 minutes at room temperature, and then blocked/permeabilized in PBS + 5% BSA + 0.3% tritonX for 1 hour at room temperature. Antibodies were diluted in blocking solution and incubated for 1 hour at room temperature in the dark. Slides were then washed 3x 5 minutes with PBS. Sections were then coverslipped with prolong diamond mounting media.

2.13 Antibodies, flow cytometry and cell sorting

2.13.1 Antibodies:

Lung homogenates were stained with the following antibodies: anti-mouse CD45 biotin (ebioscience, 13-0451-82, clone 30-F11), anti-mouse CD326/EpCAM biotin (ebioscienceInvitrogen, 2020-10-01, clone G8.8), anti-mouse CD31-FITC (BioLegend, 102406, clone 390). For flow cytometry, live cells were gated by staining with GhostDye viability stain (Tonbo Biosciences). Retinas were stained with the following antibodies/stains: GS Isolectin-B4 (IB4) (Invitrogen, I21411, Alexa-Fluor 488) and), anti-phospho-histone 3 (Ser10) (Alexa Fluor 647, EMD Millipore, 06-570, polyclonal).), Collagen IV (Goat, EMD Millipore, AB769, polyclonal), Cleaved Caspase-3 (Rabbit, Cell Signaling, 9661, polyclonal), Alexa Fluor 647 AffiniPure Bovine Anti-Goat (Jackson Immuno., 805-605-180) and DyLight 405 AffiniPure Donkey Anti-Rabbit (Jackson Immuno., 711-475-152). Tumors sections were stained with the following antibodies: anti-CD31 (Goat, Santa Cruz, sc-1506, M-20), anti-phospho-histone 3 (Ser10) (Rabbit, abcam, ab5176, polyclonal), anti-Goat Cy3 (Jackson Immuno), and anti-Rabbit Alexa-Fluor 488 (Jackson Immuno). Lungs sections were stained with the following antibodies: anti-CD31 (PE-CF594, BD Horizon, 563616, MEC 13.3), and anti-phospho-histone 3 (Ser10)

(Alexa Fluor 647, EMD Millipore, 06-570, polyclonal). Tumors and lung section nuclei were stained with 100ng/mL of 4',6-Diamidino-2-phenylindole dihydrochloride (DAPI).

2.13.2 Flow cytometry and cell sorting:

Flow cytometry, samples were run on LSR Fortessa flow cytometers (BD) and data was analyzed using FlowJo software. Cell sorting was performed using the FACS Aria II (BD).

2.14 Microscopy and image analysis

Images of HUVEC spheroids were taken using a Nikon AZ100 Multi-purpose Zoom Microscope and Nikon imaging software. Images were analyzed using ImageJ software. Images of scratch-wound assays were taken every 4 hours using the automated IncuCyte live-cell analysis system (Essen BioScience). Percent wound closure was analyzed and calculated using IncuCyte scratch wound software (Essen BioScience). Retinal, lung, and tumor images were taken using the Nikon A1 Confocal Laser Microscope System and analyzed using ImageJ software. Branchpoint analysis was performed using AngioTool software.

2.15 Metabolite analysis

2.15.1 In vitro cell collection for metabolomics:

HUVECs were plated in supplemented MCDB 131 media and allowed to attach overnight. Media was then replaced with supplemented MCDB 131 media with or without the various drugs/supplements and treated for 24 hours. Cells were washed 2x with PBS and trypsinized and collected in media. Cells were spun and washed 2x with PBS to remove all media. HUVECs

were then resuspended in 1mL of PBS and counted using the Countess cell counter. Cells were then pelleted and flash frozen in liquid nitrogen in cryovials.

2.15.2 In vivo cell collection for metabolomics:

Endothelial cells were isolated from P15 mouse lungs as described above (see section 2.11.1 and 2.11.3 above) and pellets were flash frozen in liquid nitrogen. Frozen pellets were stored at -80°C until extraction.

2.15.3 Metabolite sample preparation and analysis

Samples were thawed and resuspended in 500uL of ice cold 80% methanol (HPLC grade) and subjected to 3 freeze-thaw cycles alternating between liquid nitrogen and a 37°C water bath. Samples were vortexed for 15 seconds and then were centrifuged at 18,000xg for 10 minutes at 4°C to pellet cell debris. The resulting supernatants (containing metabolites) were transferred to fresh tubes and delivered to Peng Gao in the Northwestern metabolomics core. Peng then dried samples and resuspended them a predetermined volume. Samples were analyzed by High-Performance Liquid Chromatography and High-Resolution Mass Spectrometry and Tandem Mass Spectrometry (HPLC-MS/MS). Specifically, the system consisted of a Thermo Q-Exactive in line with an electrospray source and an Ultimate3000 (Thermo) series HPLC consisting of a binary pump, degasser, and auto-sampler outfitted with an Xbridge Amide column (Waters; dimensions of 4.6 mm × 100 mm and a 3.5 µm particle size). The mobile phase A contained 95% (vol/vol) water, 5% (vol/vol) acetonitrile, 20 mM ammonium hydroxide, 20 mM ammonium acetate, pH = 9.0; B was 100% Acetonitrile. The gradient was as following: 0-1 min, 15% A; 18.5 min, 76% A; 18.5-20.4 min, 24% A; 20.4-20.5 min, 15% A; 20.5-28 min, 15% A with a

flow rate of 400 $\mu\text{L}/\text{min}$. The capillary of the ESI source was set to 275 $^{\circ}\text{C}$, with sheath gas at 45 arbitrary units, auxiliary gas at 5 arbitrary units and the spray voltage at 4.0 kV. In positive/negative polarity switching mode, an m/z scan range from 70 to 850 was chosen and MS1 data was collected at a resolution of 70,000. The automatic gain control (AGC) target was set at 1×10^6 and the maximum injection time was 200 ms. The top 5 precursor ions were subsequently fragmented, in a data-dependent manner, using the higher energy collisional dissociation (HCD) cell set to 30% normalized collision energy in MS2 at a resolution power of 17,500. The sample volumes of 10 μl were injected which contained 200,000 cells. Data acquisition and analysis were carried out by Xcalibur 4.0 software and Tracefinder 2.1 software, respectively (both from Thermo Fisher Scientific).

2.15.4 Measurement of NAD⁺ and NADH metabolites:

NAD⁺/NADH ratio was measured using the NAD/NADH-glo Assay (Promega) by following the manufacturer's protocol. Briefly, 25,000 HUVECs were plated in a 24-well plate and allowed to attach/recover overnight. The next morning, cells were washed 2x with PBS and media containing drugs/supplements was added to each well and treated for the indicated time (4 or 16 hours). Cells were then collected by trypsinization, resuspended in 50 μL of PBS and added to a 96 well, opaque white plate. 50 μL of base solution (0.2N NaOH) + 1% DTAB was added to each well and pipetted up and down to mix. 50 μL of each well was then transferred to a new well. To these wells, 25 μL of 0.4N HCl was added, a plate seal was added, and the whole plate was incubated at 60 $^{\circ}\text{C}$ for 15 minutes and then allowed to cool at room temperature for 10 minutes. To the acid treated wells, 25 μL of 0.5M tris base was added, and to the remaining wells, 50 μL of a 1:1 solution of 0.5M tris base and 0.4N HCl was added. The detection reagent was prepared as

follows: 1mL luciferin detection reagent, 5uL reductatse, 5uL reductase substrate, 5uL NAD cycling enzyme, and 25uL of NAD cycling substrate. Enough of this was made to add 100uL to each well. 100uL of this detection reagent was added to each well and gently tapped to mix. The plate was incubated at room temperature for 1hour and then the luminescence was read on a plate reader. The luminescence of the acid-treated wells (NAD⁺) was divided by the luminescence of the base-treated wells (NADH) to obtain the ratio of NAD⁺/NADH.

2.16 RNA sequencing analysis

Mouse pups were dosed with tamoxifen and endothelial cells were isolated from P15 mouse lungs as described above (see sections 2.9.2, 2.11.1, and 2.11.2 above). Cells were lysed with RLT buffer + 0.1% β -mercaptoethanol from the RNeasy Plus Micro Kit (Qiagen) and stored at -80°C until RNA was extracted. RNA isolation were performed using the RNAeasy Plus Micro Kit (Qiagen) following the manufacturer's instructions with an additional on-column DNase treatment using RNase-free DNase Set (Qiagen). RNA quality and quantity were measured using Agilent 4200 Tapestation using high Sensitivity RNA ScreenTape System (Agilent Technologies). NEBNext Ultra™ RNA (New England Biolabs, Inc) was used for full-length cDNA synthesis and library preparation. Libraries were pooled, denatured and diluted, resulting in a 2.0 pM DNA solution. PhiX control was spiked at 1%. Libraries were sequenced on an Illumina NextSeq 500 instrument (Illumina Inc) using NextSeq 500 High Output reagent kit (Illumina Inc) (1x75 cycles) with a target read depth of approximate (8-16) million aligned reads per sample. FASTQ reads were trimmed using Trimmomatic to remove end nucleotides with a PHRED score less than 30 and requiring a minimum length of 20 bp. Reads were then aligned to the mm10 genome using tophat version 2.1.04 using the following options --no-novel-juncs --

read-mismatches 2 --read-edit-dist 2 --max-multihits 20 --library-type fr- unstranded. The generated bam files were then used to count the reads only at the exons of genes using htseq-count5 with the following parameters -q -m intersection-nonempty -s no -t exon. Differential expression analysis was done using the R package edgeR6. Bigwig tracks of RNA-Seq expression were generated by using the GenomicAlignments package in R in order to calculate the coverage of reads in counts per million (CPM) normalized to the total number of uniquely mapped reads for each sample in the library. GSEA analysis was done using the Broad Institute GSEA software7. In brief, the gene list output from edgeR was ranked by calculating a rank score of each gene as $-\log_{10}(\text{PValue}) \cdot \text{sign}(\log\text{FC})$. A pre-ranked GSEA analysis was done using 3000 permutations and the Hallmark pathway database.

2.17 Tumor angiogenesis assay

8 week old mice were dosed with tamoxifen as described above (see section 2.9.2 above). The right flank was shaved and 100,000 B16-F10 melanoma cells (ATCC) were injected subcutaneously. Tumor size was measured using calipers every 2-3 days for 21 days. Tumor volume was calculated by first determining the geometric mean between the length and width, then using the equation: $(4/3) \cdot (\pi) \cdot (\text{geometric mean}/2)^3$. On day 21, tumors were harvested, weighed, tumor size was measured, and volume was calculated using the equation: $(4/3) \cdot (\pi) \cdot (\text{length}/2) \cdot (\text{width}/2) \cdot (\text{depth}/2)$.

2.18 Mass spectrometry to identify histone modifications

Nuclei were isolated using gentle detergent treatment (0.3% NP-40 in NIB-250 buffer) of cells and centrifugation at 0.6g. Detergent was removed by 2x washing of obtained pellets with NIB-

250, no NP-40 buffer. Histones from isolated nuclei were acid-extracted and derivatized with propionic anhydride both prior to and following trypsin digestion as previously described¹⁰⁷. Propionylated histone peptides were resuspended in 50 μ l water with 0.1% TFA and 3 μ l was injected in 3 technical replicates on a nanoLC/triple quadrupole MS that consisted of a Dionex UltiMate 3000 coupled to a Thermo Fisher Scientific TSQ Quantiva triple quadrupole mass spectrometer. Buffer A was 100% LC-MS-grade water with 0.1% formic acid and buffer B was 100% ACN. The propionylated peptides were loaded onto an in-house packed C18 trapping column (4 cm \times 150 μ m; Magic AQ C18, 3 μ m, 200 Å-Michrom) for 10 min at a flow rate of 2.5 μ l min⁻¹ in 0.1% TFA loading buffer. The peptides were separated by a gradient from 1 to 35% buffer B from 5 to 45 min. The analytical column was 10 cm \times 75 μ m PicoChip (1PCH7515-105H253-NV New Objective) and consisted of the same C18 material as the trapping column. The triple quadrupole settings were as follows: collision gas pressure of 1.5 mtorr; Q1 peak width of 0.7 (full-width at half-maximum); cycle time of 3 s; skimmer offset of 10 V; electrospray voltage of 2.5 kV. SRM mass spectrometer transitions were developed as described previously^{108,109}. Data were analysed using Skyline software (v3.5; MacCoss Lab, University of Washington) with Savitzky-Golay smoothing of peaks¹¹⁰. Automatic peak assignment and retention times were checked manually.

3. CHAPTER 3: MITOCHONDRIAL COMPLEX III IS NECESSARY FOR ENDOTHELIAL CELL PROLIFERATION DURING ANGIOGENESIS

3.1 Significance

While largely quiescent in healthy adult tissues, endothelial cells (ECs) are dynamic, undergoing rapid migration and proliferation during angiogenesis; thus, increasing their biosynthetic and bioenergetic demand. Recent findings indicate that metabolism is a critical regulator of EC function during angiogenesis. ECs are classically described as being highly glycolytic, and numerous studies have described the necessity of glycolysis in ECs during vessel sprouting¹¹¹. Despite having abundant access to oxygen in the bloodstream, ECs generate up to 85% of their ATP from glycolysis⁷⁴. When vessel sprouting is stimulated by pro-angiogenic signals such as vascular endothelial growth factor A (VEGFA), glycolysis is enhanced due to upregulation of glycolytic enzymes, nearly doubling flux through glycolysis^{74,81,82}. This increased glycolytic flux is critical, as decreased expression of the glycolytic activator phosphofructokinase-2/fructose-2,6-bisphosphatase (PFKFB3), severely impairs both migration and proliferation of ECs *in vitro* and *in vivo*⁷⁴. Furthermore, inhibition of PFKFB3 in ECs decreased pathological neovascularization in ocular and inflammatory models, as well as cancer cell metastasis^{112,113}. Moreover, decreased levels of other glycolytic enzymes including hexokinase 2 (HK2), pyruvate kinase M2 (PKM2), and glucose transporter 1 (GLUT1) cause impaired angiogenesis^{114–116}. Collectively these data indicate that glycolytic flux in ECs is necessary for angiogenesis.

Since ECs undergo high levels of aerobic glycolysis, and thus oxidize only small amounts of glycolysis-derived pyruvate within the mitochondria, mitochondrial function was previously surmised to play a marginal role in EC metabolism⁷⁴. In addition to importing glucose, ECs take up fatty acids from their environment and break them down into acetyl-CoA in the mitochondria in a process known as fatty acid oxidation (FAO). Fatty acid-derived acetyl-CoA is then utilized to fuel the tricarboxylic acid (TCA) cycle¹¹⁷. FAO has been shown to be critical in ECs, as knock down of fatty acid binding protein 4 (FABP4) or carnitine palmitoyltransferase 1A (CPT1A) leads to diminished angiogenesis^{88,94,95}. Glutamine is also readily imported into ECs where it is metabolized into alpha-ketoglutarate (α KG), which is used to replenish the mitochondrial TCA cycle (i.e. anaplerosis). Limiting EC glutamine utilization results in diminished angiogenesis both *in vitro* and *in vivo*^{89,102}. While FAO and glutamine utilization fuel metabolism during vessel sprouting, loss of either of these two pathways result in a relatively modest decrease in angiogenesis compared to inhibition of PFKFB3. It is likely that restricting one particular carbon source to fuel the TCA cycle will not markedly impair mitochondrial metabolism.

In the present study, we directly tested the necessity for mitochondrial metabolism during angiogenesis by inhibiting the mitochondrial respiratory chain complex III. Respiration is initiated by the donation of electrons to complexes I and II by the TCA cycle-generated reducing equivalents NADH and FADH₂, respectively. Mitochondrial complexes I and II pass electrons to complex III, and finally to oxygen via complex IV. This electron flow drives the pumping of hydrogen ions into the intermembrane space to generate membrane potential required for ATP production by ATP synthase (complex V). Respiration is linked to three distinct mitochondrial

functions: (1) oxidative phosphorylation for ATP generation; (2) oxidative TCA cycle flux to produce metabolites for macromolecule biosynthesis; and (3) release of reactive oxygen species (ROS) and metabolites to determine cell fate and/or function. Thus, loss of mitochondrial complex III could have multiple effects on cells, including death due to a bioenergetic collapse, decreased proliferation due to diminished oxidative TCA cycle function for macromolecule synthesis, and loss of cell fate and/or function due to changes in angiogenic gene expression. Thus, we utilized mitochondrial complex III inhibitors *in vitro*, and an EC-specific mitochondrial complex III-deficient mouse model to test which mechanisms linked to mitochondrial respiration in ECs are required for angiogenesis.

3.2 Results

3.2.1 Mitochondrial complex III is required for endothelial cell proliferation *in vitro*

To study the effects of mitochondrial respiratory chain inhibition on EC behavior, we cultured human umbilical vein endothelial cells (HUVECs) with the mitochondrial complex III inhibitor antimycin A to induce loss of mitochondrial respiration (Figure 3.2.1.1a). At low nanomolar concentrations (25nM) antimycin A irreversibly inhibits mitochondrial respiratory complex III¹¹⁸. When electron transport is inhibited, cells can no longer generate ATP via oxidative phosphorylation, and therefore must increase glycolytic flux in order to generate the necessary ATP. Since respiratory capacity was abolished, we confirmed that HUVECs were performing maximal glycolysis basally (Figure 3.2.1.1 b). Importantly, even after 96 hours of treatment with antimycin A in culture, no significant decrease in cell viability was observed, indicating that respiratory chain inhibition does not cause HUVEC death or apoptosis (Figure 3.2.1.2). This suggests that HUVEC are able to generate sufficient levels of ATP for cell survival by glycolysis

alone. Furthermore, antimycin A treatment does not lead to mitochondrial demise *in vitro*, as we observed no loss of mitochondrial membrane potential, mitochondrial content, or mitochondrial DNA (Figure 3.2.1.3). Two important processes activated in ECs in response to angiogenic signaling are sprouting (i.e. invasion and migration) and proliferation¹¹⁹. We therefore utilized HUVECs in culture to explore how mitochondrial inhibition affects these key angiogenic functions. First, we used an *in vitro* sprouting assay where HUVEC spheroids sprout and migrate through a 3D collagen matrix. After 24 hours, spheroids treated with antimycin A showed no changes in sprout length or number (Figure 3.2.1.4 a-c). Additionally, respiration-deficient HUVECs migrated similar to controls in a 2D scratch wound migration assay (Figure 3.2.1.4 d). Interestingly, HUVECs treated with antimycin A displayed a striking defect in proliferation, as they completely failed to grow over a period of 96 hours (Figure 3.2.1.5). Similar results were obtained when HUVECs were treated with the mitochondrial complex I inhibitor, piericidin (Figure 3.2.1.6). Together, these data clearly show that the mitochondrial respiratory chain is necessary for HUVEC proliferation *in vitro*, while it is dispensable for migration and sprouting.

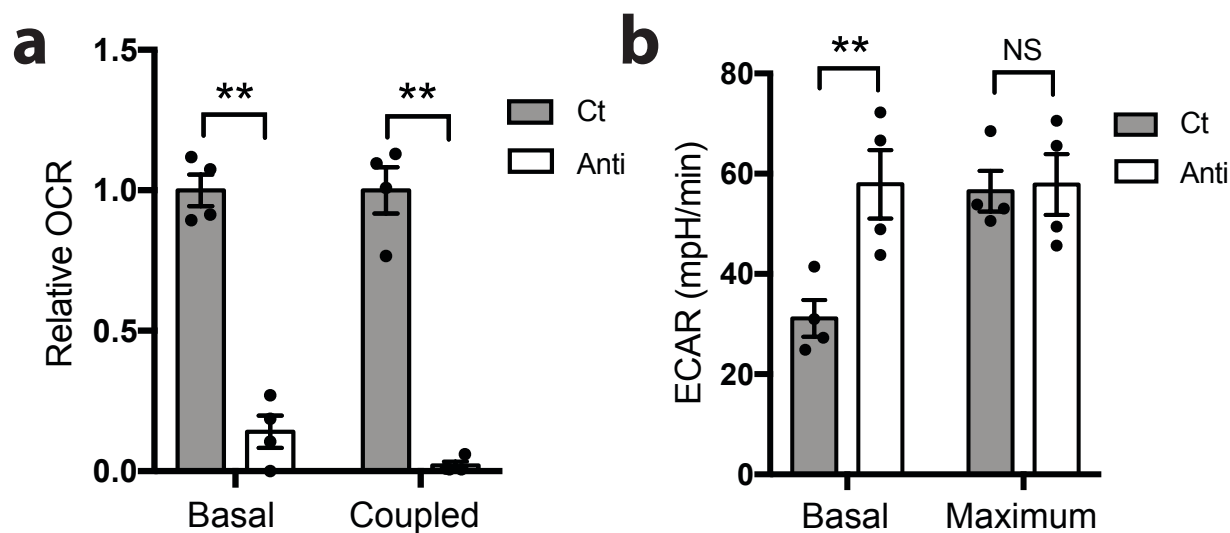


Figure 3.2.1.1 Antimycin treated HUVECs lose oxygen consumption and perform maximum glycolysis
a. Relative basal and coupled oxygen consumption rate (OCR) of control (Ct) or antimycin A (Anti) treated HUVECs, measured after 2 hours treatment. Values are normalized to control mean (n=4). **b.** Basal and maximum extracellular acidification rate (ECAR) of Ct or Anti treated HUVECs, measured after 2 hours treatment (n=4). HUVECs were treated with 25nM antimycin A. Data represents mean +/- SEM and were analyzed with a two-tailed t-test (*p<0.05, **p<0.01, NS=not significant).

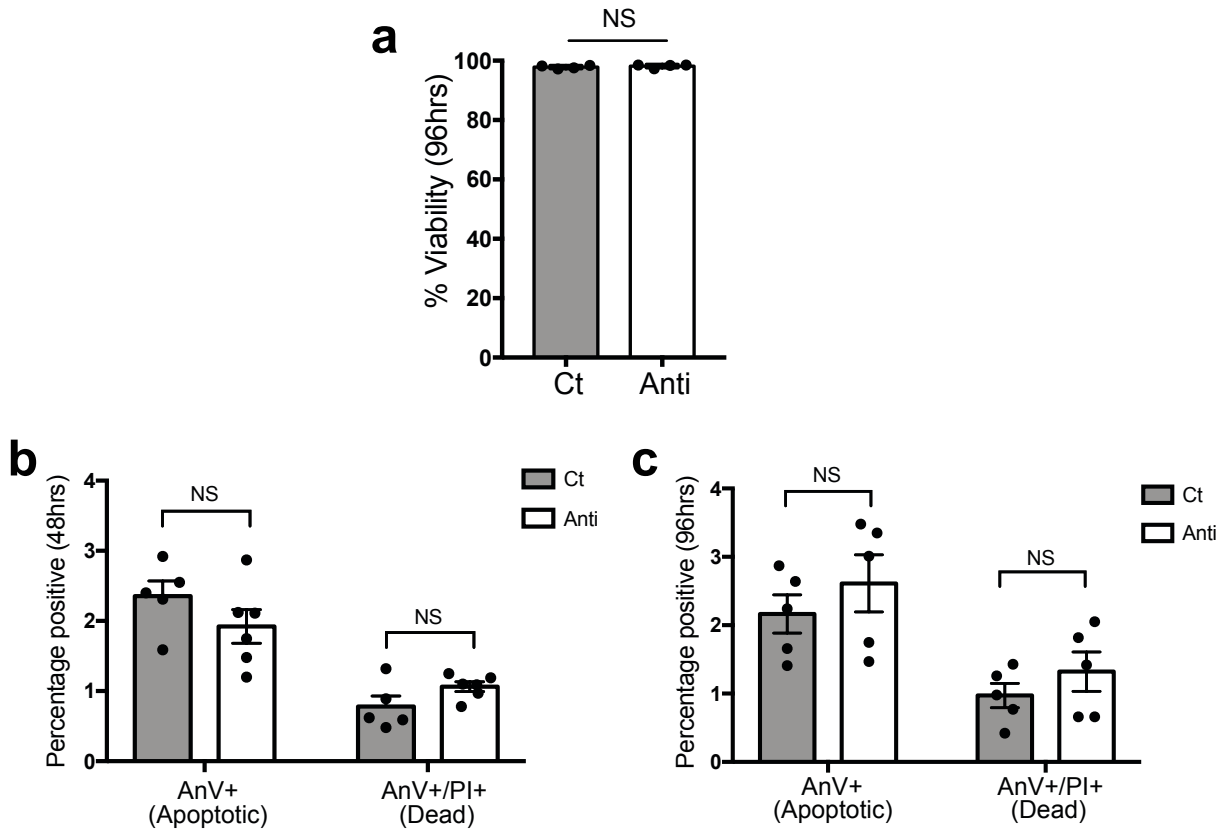


Figure 3.2.1.2 Antimycin A treated HUVECs do not increase cell death or apoptosis

a. Cell viability (% Dapi negative cells) of Ct or Anti treated HUVECs, measured after 96 hours treatment (n=4).
b-c. Percentage of AnnexinV (AnV) positive (apoptotic) or AnV/propidium iodide (PI) double positive (dead) HUVECs, control (Ct) or antimycin A (Anti) treated for 48 (b) or 96 (c) hours (n=5). HUVECs were treated with 25nM antimycin A. Data represents mean +/- SEM and were analyzed with a two-tailed t-test (*p<0.05, **p<0.01, NS=not significant).

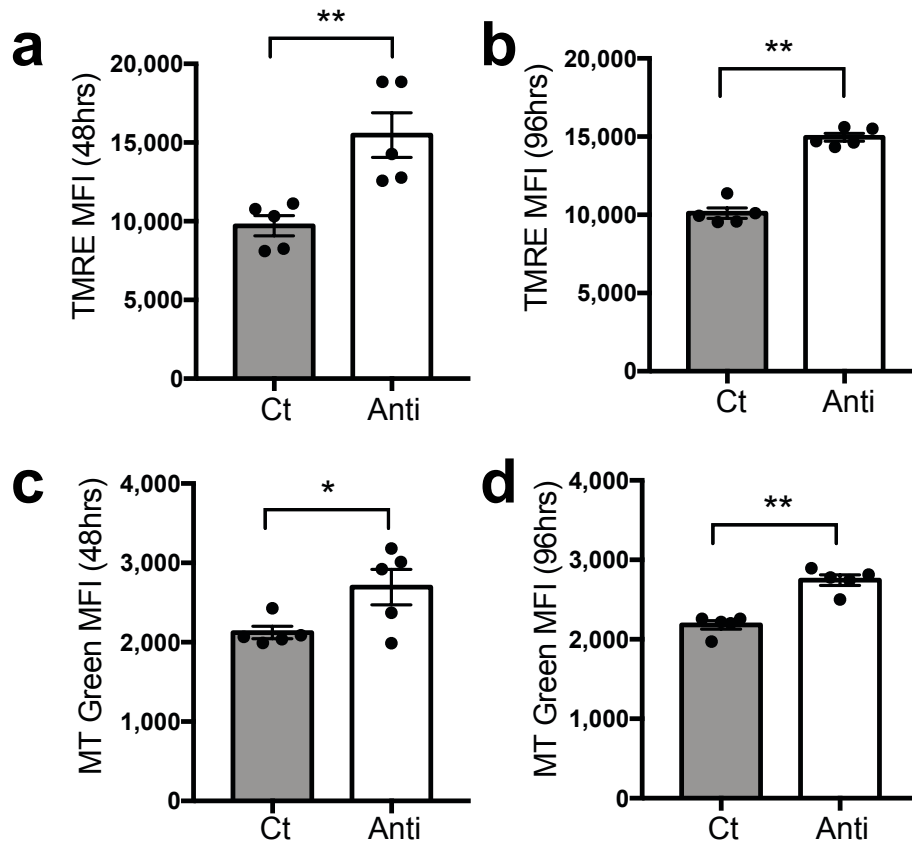


Figure 3.2.1.3 Antimycin A treated HUVECs have increased mitochondrial membrane potential and content

a-b. TMRE median fluorescence intensity (MFI) in HUVECs, Ct or Anti treated for 48 (a) or 96 (b) hours (n=5). **c-d.** MitoTracker Green MFI in HUVECs, Ct or Anti treated for 48 (c) or 96 (d) hours (n=5). HUVECs were treated with 25nM antimycin A. Data represents mean \pm SEM and were analyzed with a two-tailed t-test (*p<0.05, **p<0.01, NS=not significant).

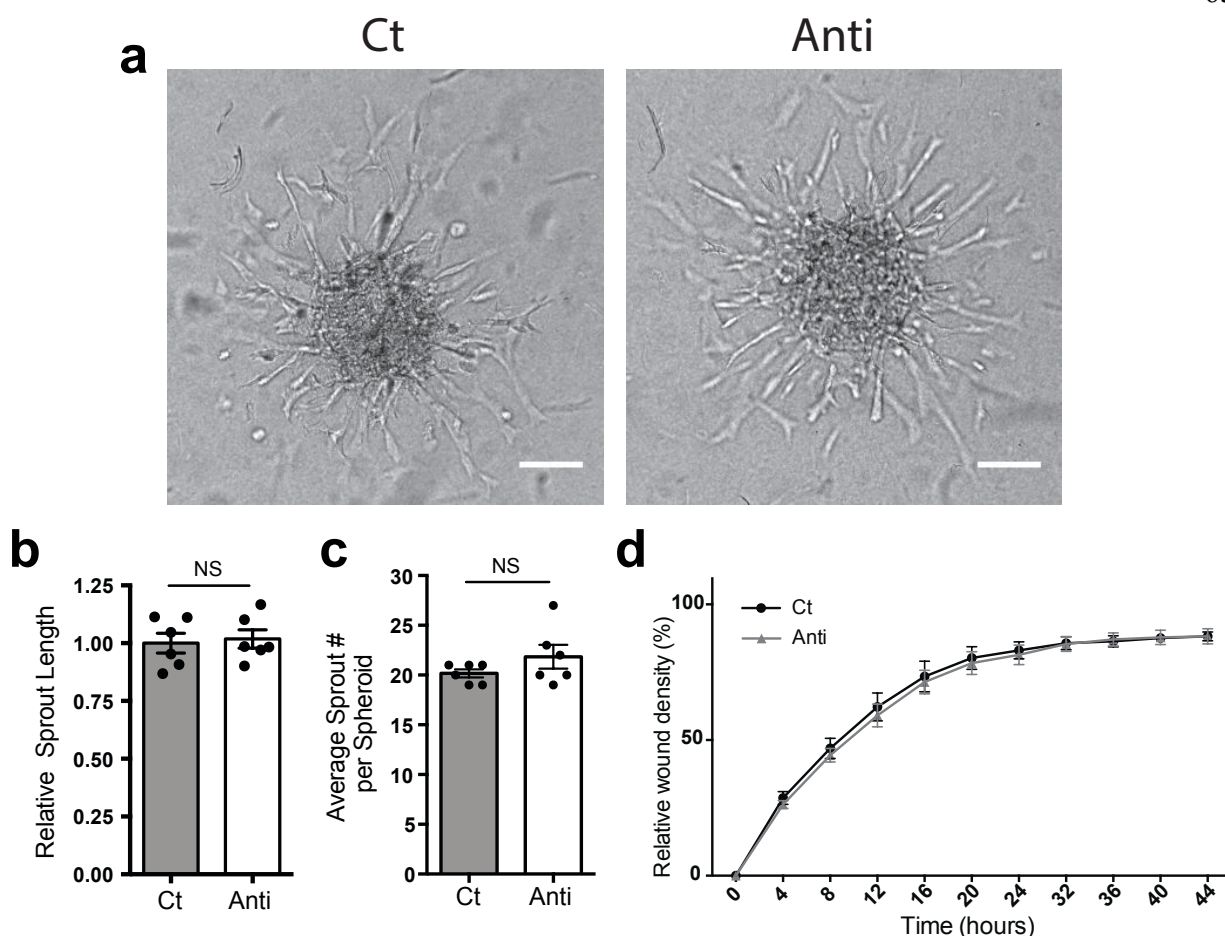


Figure 3.2.1.4 Complex III function in HUVECs is not required for sprouting or migration

a. Representative images of Ct or Anti treated HUVECs in a sprouting assay after 24 hours. Scale bar represents 50 μ m. **b.** Quantification of relative sprout length of Ct or Anti treated HUVECs after 24 hours. Values are normalized to control mean (n=6). **c.** Quantification of the average number of sprouts per spheroid of Ct or Anti treated HUVECs after 24 hours. (n=6). **d.** Relative wound density % over time in a scratch wound migration assay in Ct or Anti treated HUVECs (Ct: n=15; Anti: n=7). HUVECs were treated with 25nM antimycin A. In sprouting and migration assays, media contained 2 μ g/mL mitomycin C to inhibit proliferation. Data represents mean \pm SEM and were analyzed with a two-tailed t-test (*p<0.05, **p<0.01, NS=not significant).

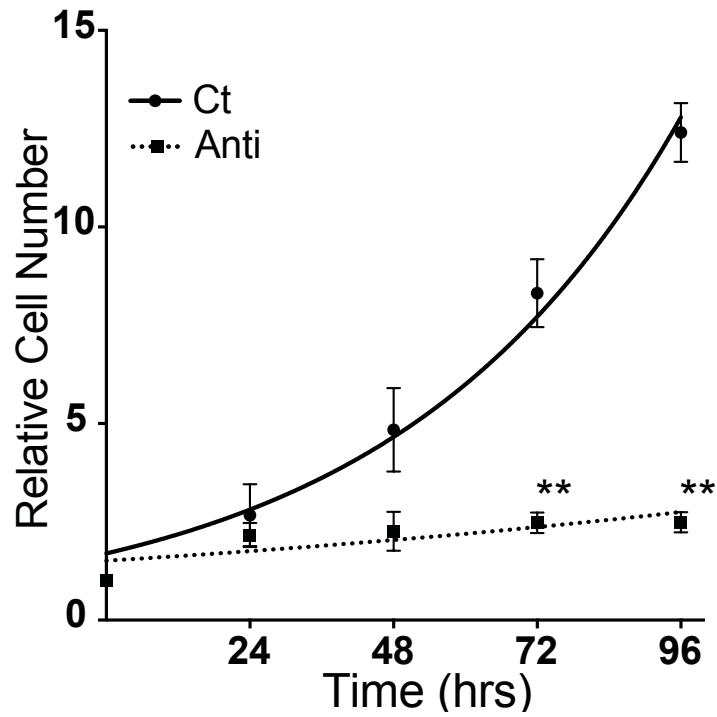


Figure 3.2.1.5 Complex III deficient HUVECs fail to proliferate

Relative cell number in Ct or Anti treated HUVECs at 0, 24, 48, 72, and 96 hours. Cell number relative to number of cells plated on day 0 (n=5). HUVECs were treated with 25nM antimycin A. Data represents mean +/- SEM and were analyzed with a two-tailed t-test (*p<0.05, **p<0.01, NS=not significant).

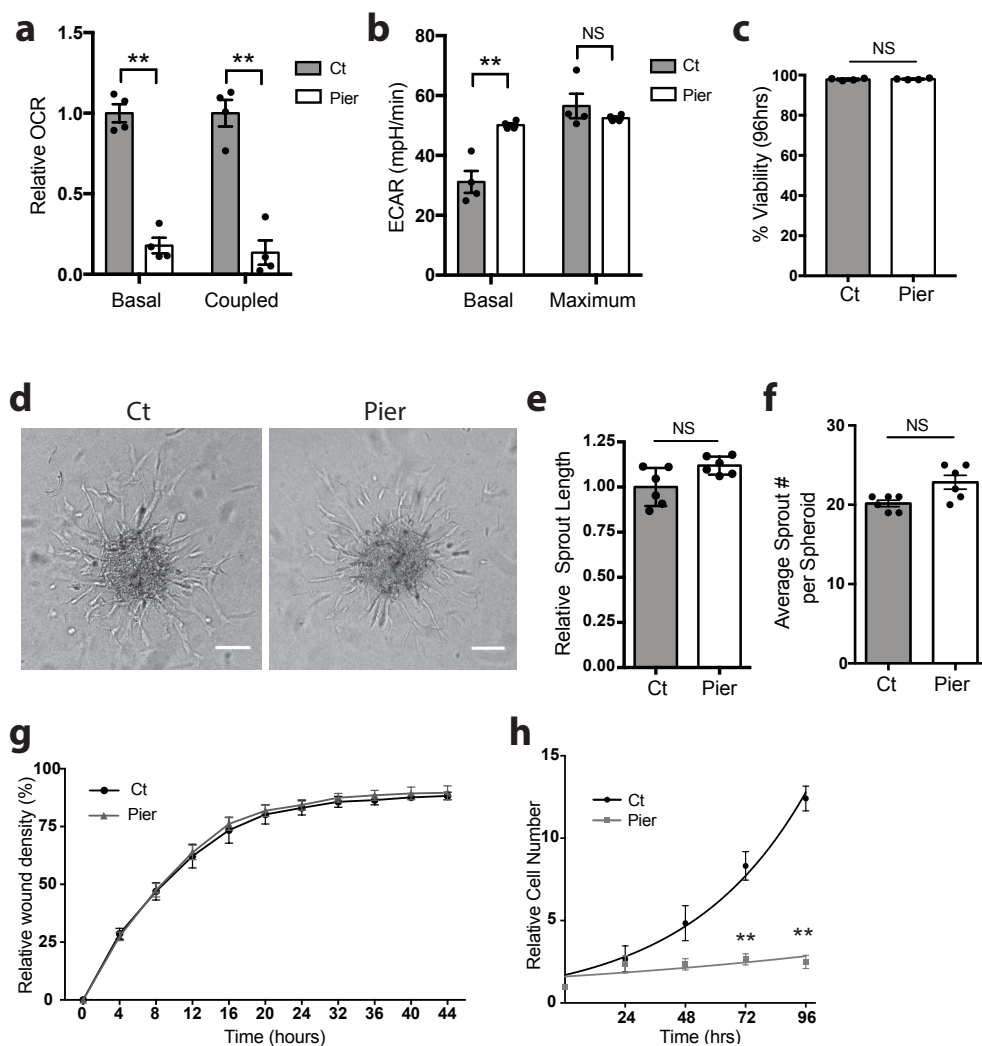


Figure 3.2.1.6 Mitochondrial complex I is required for endothelial cell proliferation *in vitro*

a. Basal and coupled oxygen consumption rate (OCR) of control (Ct) or piericidin (Pier) treated HUVECs, measured after 2 hours treatment. Values are normalized to Ct mean (n=3). **b.** Basal and maximum extracellular acidification rate (ECAR) of Ct or Pier treated HUVECs, measured after 2 hours treatment (n=3). **c.** Cell viability (% Dapi negative cells) of Ct or Pier treated HUVECs, measured after 96 hours treatment (n=4). **d.** Representative images of Ct or Pier treated HUVECs in a sprouting assay after 24 hours. Scale bar represents 50 μ m. **e.** Quantification of relative sprout length of Ct or Pier treated HUVECs allowed to sprout for 24 hours. Values normalized to control mean (n=6). **f.** Quantification of the average number of sprouts per spheroid in Ct or Pier treated HUVECs allowed to sprout for 24 hours. (n=6). **g.** Relative wound density over time in a scratch wound migration assay in Ct or Pier treated HUVECs (Ct: n=15; Anti: n=7). **h.** Proliferation assay showing relative cell number in Ct or Pier treated HUVECs at 0, 24, 48, 72, and 96 hours. Cell number relative to number of cells plated on day 0 (n=5). HUVECs were treated with 250nM piericidin. In sprouting and migration assays, media contained 2 μ g/mL mitomycin C to inhibit proliferation. Data represents mean \pm SEM and were analyzed with a two-tailed t-test (*p<0.05, **p<0.01, NS=not significant).

3.2.2 Mitochondrial complex III in HUVECs maintains NAD⁺/NADH ratio, necessary for endothelial cell proliferation

The mitochondrial TCA cycle is critical for cellular proliferation, as it produces metabolic intermediates that are used as building blocks for biosynthetic macromolecules¹¹. Metabolic profiling revealed that respiration-deficient HUVECs displayed decreased levels of TCA cycle intermediates (Figure 3.2.2.1 a). Broadly, amino acid levels in HUVECs treated with antimycin A were not impaired, with the exception of aspartate, which was significantly decreased (Figure 3.2.2.1 b). Nucleotide metabolite abundance remained relatively unchanged in respiration-deficient HUVECs (Figure 3.2.2.1 c-d).

To test specificity of antimycin A, we expressed the *Ciona intestinalis* alternative oxidase (AOX) in HUVECs, which is refractory to antimycin treatment^{120,121}. AOX has the capability to accept electrons from ubiquinol and transfer them to oxygen, bypassing complex III and IV functions, and restoring electron transport chain activity in the presence of complex III inhibition^{120,121}. We found that HUVECs expressing AOX maintain oxygen consumption and NAD⁺/NADH in the presence of antimycin A, indicating that AOX is functioning properly (Figure 3.2.2.2 a-b). Importantly, AOX was able to rescue proliferative capacity after antimycin A treatment, as it restores both TCA cycle metabolites and aspartate levels (Figure 3.2.2.2 c and Figure 3.2.2.3). Together, these data highlight the specificity of antimycin A, and demonstrate that its effects on HUVECs are due to its inhibition of complex III.

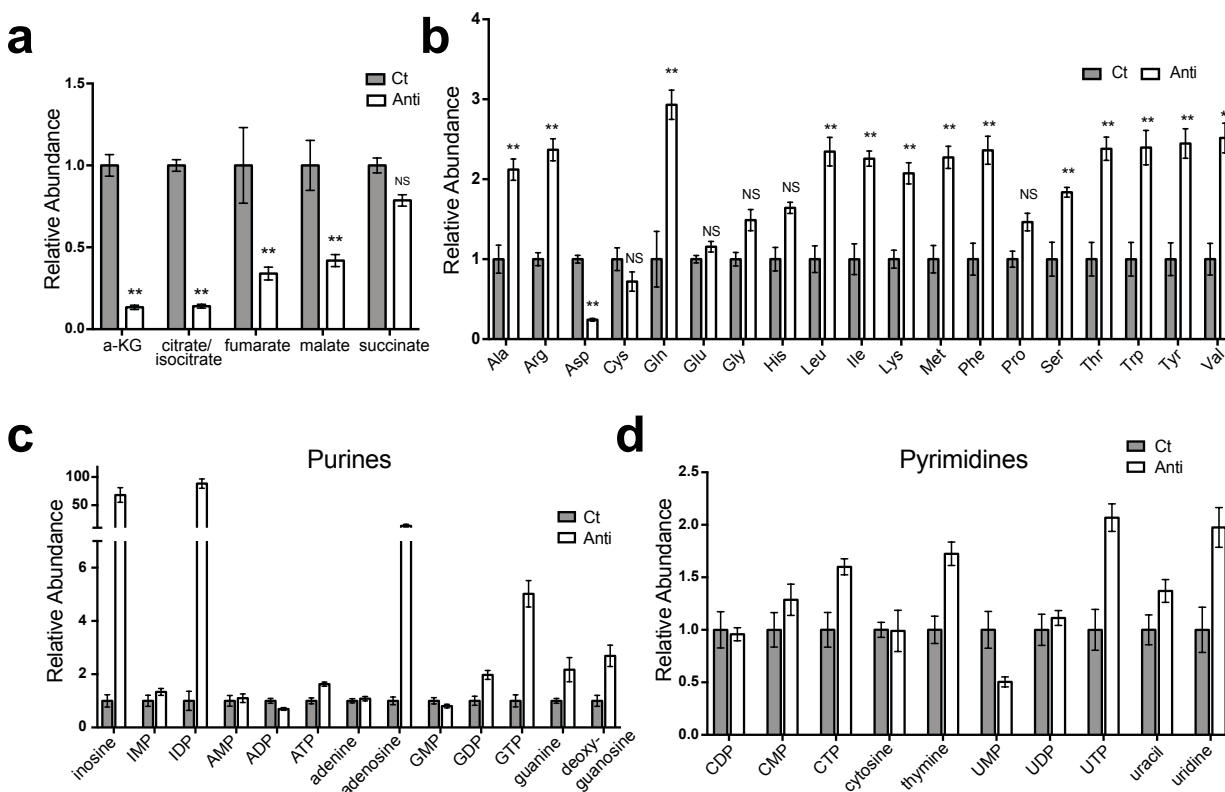


Figure 3.2.2.1 Mitochondrial complex III is required to maintain aspartate levels

a-b. Relative abundance of TCA cycle (a), and amino acid (b) metabolites from control (Ct) or antimycin A (Anti) treated HUVECs, after 24 hours treatment. Values are normalized to control mean (n=6). **c-d.** Relative abundance of purine (c) and pyrimidine (d) nucleotides from control (Ct) or antimycin A (Anti) treated HUVECs, after 24 hours treatment. (n=6). All values are relative to Ct mean. Data represents mean \pm SEM and were analyzed using 2-way ANOVA and Tukey's multiple comparisons test (* $p < 0.05$, ** $p < 0.01$, NS=not significant).

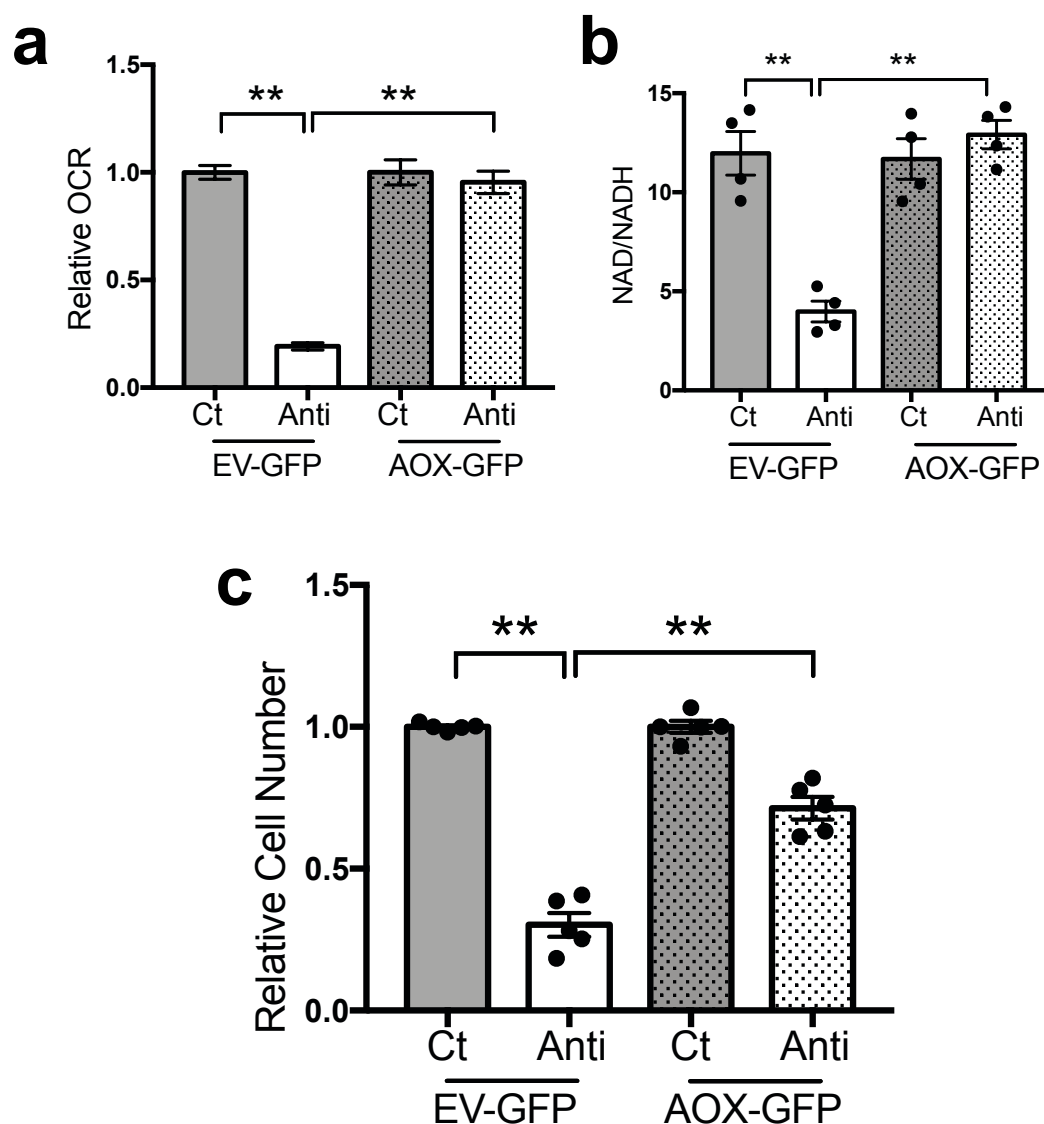


Figure 3.2.2.2 AOX rescues OCR, NAD⁺/NADH, and proliferation in antimycin A treated HUVECs

a. Relative oxygen consumption (OCR) in empty vector (EV)-GFP or AOX-GFP expressing HUVECs, Ct or Anti treated for 2 hours (representative of n=3 independent experiments). **b.** Ratio of NAD⁺/NADH in EV-GFP or AOX-GFP expressing HUVECs, Ct or Anti treated for 4 hours (n=4). **c.** Relative cell number after 72 hours proliferation in EV-GFP or AOX-GFP expressing HUVECs, Ct or Anti treated (n=5). Values are normalized to control mean (n=6). Data represents mean \pm SEM and were analyzed using one or two-way ANOVA and Tukey's multiple comparisons test (*p<0.05, **p<0.01, NS=not significant).

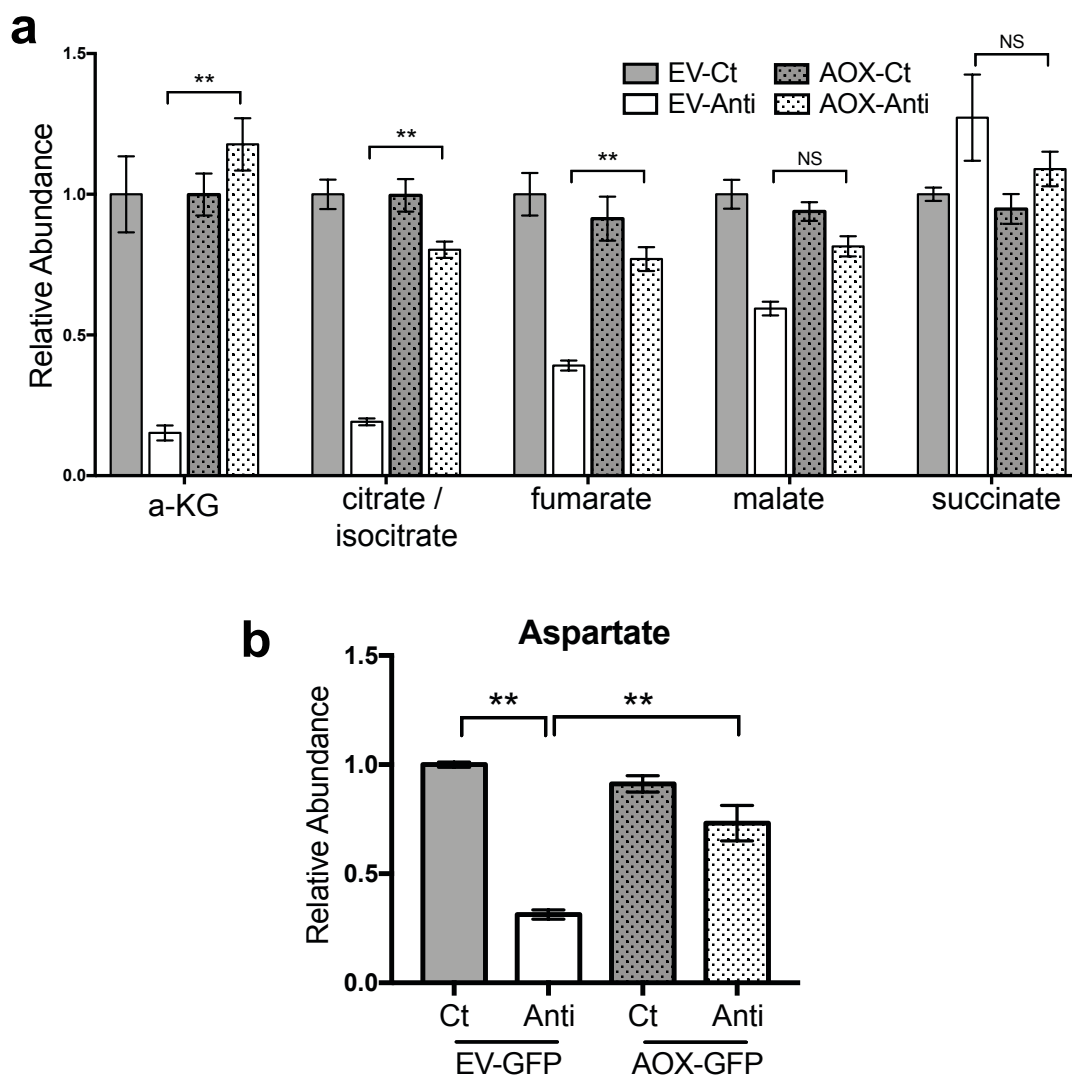


Figure 3.2.2.3 AOX rescues TCA cycle metabolites and aspartate levels in antimycin A treated HUVECs
a-b. Relative abundance of TCA cycle metabolites (a), and aspartate (b) in EV-GFP or AOX-GFP expressing HUVECs, Ct or Anti treated for 24 hours. Values are normalized to control mean (n=6). Data represents mean +/- SEM and were analyzed using one or two-way ANOVA and Tukey's multiple comparisons test (* $p < 0.05$, ** $p < 0.01$, NS=not significant).

Cells use complex I of the ETC to oxidize NADH to NAD⁺; thus, after complex III inhibition, there is a decreased capacity to regenerate NAD⁺, causing decreased TCA cycle flux. Previously it has been demonstrated that restoration of NAD⁺/NADH is sufficient to rescue proliferation in respiration-deficient cancer cells^{25,104}. To test this hypothesis in HUVECs, we expressed an NADH oxidase from *Lactobacillus brevis* (LbNOX) which generates NAD⁺ from NADH independent of ETC function¹⁰⁴. We found that expressing LbNOX in the cytosol did not restore OCR, but was able to rescue NAD⁺/NADH, and proliferation in antimycin A treated HUVECs (Figure 3.2.2.4). Additionally, respiration-deficient HUVECs expressing LbNOX accumulate large amounts of succinate, due to complex III inhibition (Figure 3.2.2.5 a). Finally, expressing LbNOX in antimycin A treated HUVECs was able to increase aspartate levels relative to EV (Figure 3.2.2.5 b). These data indicates that an essential function of the ETC in HUVECs is to maintain NAD⁺/NADH to support cellular proliferation.

Numerous studies have reported that cells lacking a functional respiratory chain are able to proliferate *in vitro* upon supplementation with supra-physiological levels of pyruvate in the culture media^{24,25,122}. Similarly, we observed that addition of methyl pyruvate (MP), while not rescuing OCR, was able to restore proliferative capacity in antimycin A treated HUVECs (Figure 3.2.2.6 a-b). Additionally, antimycin A treated HUVECs with MP accumulated succinate due to complex III inhibition and displayed restored aspartate levels (Figure 3.2.2.6 c-d).

The mechanism by which pyruvate is able to restore proliferation in respiration deficient cells is currently not well understood. It has been hypothesized that in respiration-deficient cancer cells, pyruvate is sufficient to restore NAD⁺/NADH²⁵. The enzyme, lactate dehydrogenase (LDH)

converts pyruvate to lactate, and is coupled to the oxidation of NADH to NAD⁺. One theory is that cells lacking a functional respiratory chain require supra-physiological levels of pyruvate to generate NAD⁺ from NADH via this LDH reaction²⁵. In fact, it has been shown that in respiration deficient cancer cells, pyruvate is able to restore both NAD⁺/NADH and proliferation²⁵. Interestingly, in HUVECs, methyl pyruvate was not able to rescue NAD⁺/NADH after neither 4 nor 16 hours of treatment (Figure 3.2.2.7). This indicates that pyruvate restores proliferation in antimycin A treated HUVECs by an alternative mechanism that is independent of NAD⁺/NADH. Others have shown that pyruvate can directly be converted to oxaloacetate via the enzyme pyruvate carboxylase (PC) in order to replenish aspartate levels required for proliferation¹²³. It is therefore possible that in antimycin A treated HUVECs, pyruvate is converted to oxaloacetate by PC to generate aspartate for proliferation, however this hypothesis remains untested.

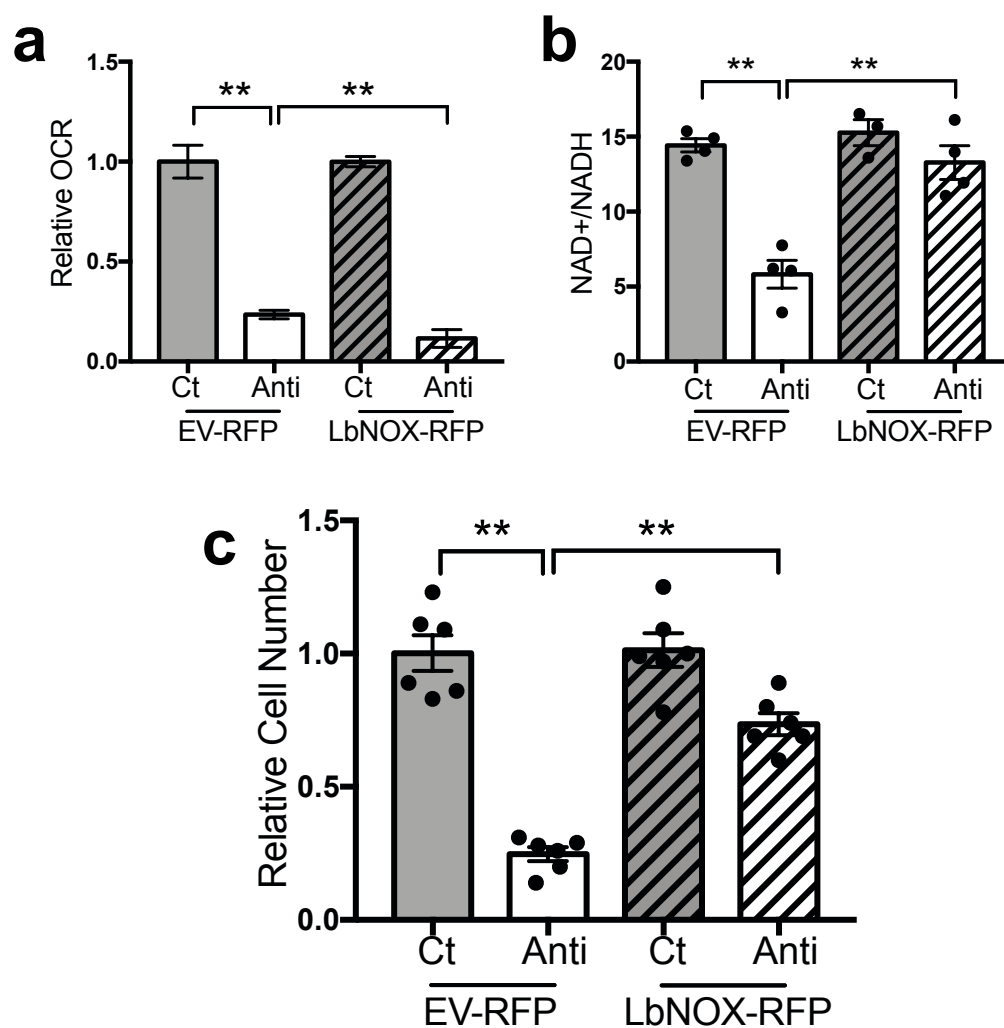


Figure 3.2.2.4 LbNOX rescues OCR, NAD⁺/NADH, and proliferation in antimycin A treated HUVECs
a. Relative OCR in EV-RFP or LbNOX-RFP expressing HUVECs, Ct or Anti treated for 2 hours (representative of n=3 independent experiments). **b.** Ratio of NAD⁺/NADH in EV-RFP or LbNOX-RFP expressing HUVECs, Ct or Anti treated for 4 hours (n=4). **c.** Relative cell number after 72 hours proliferation in EV-RFP or LbNOX-RFP expressing HUVECs, Ct or Anti treated (n=6). Values are normalized to control mean. (n=6). HUVECs were treated with 25nM antimycin A. Data represents mean +/- SEM and were analyzed using one or two-way ANOVA and Tukey's multiple comparisons test (*p<0.05, **p<0.01, NS=not significant).

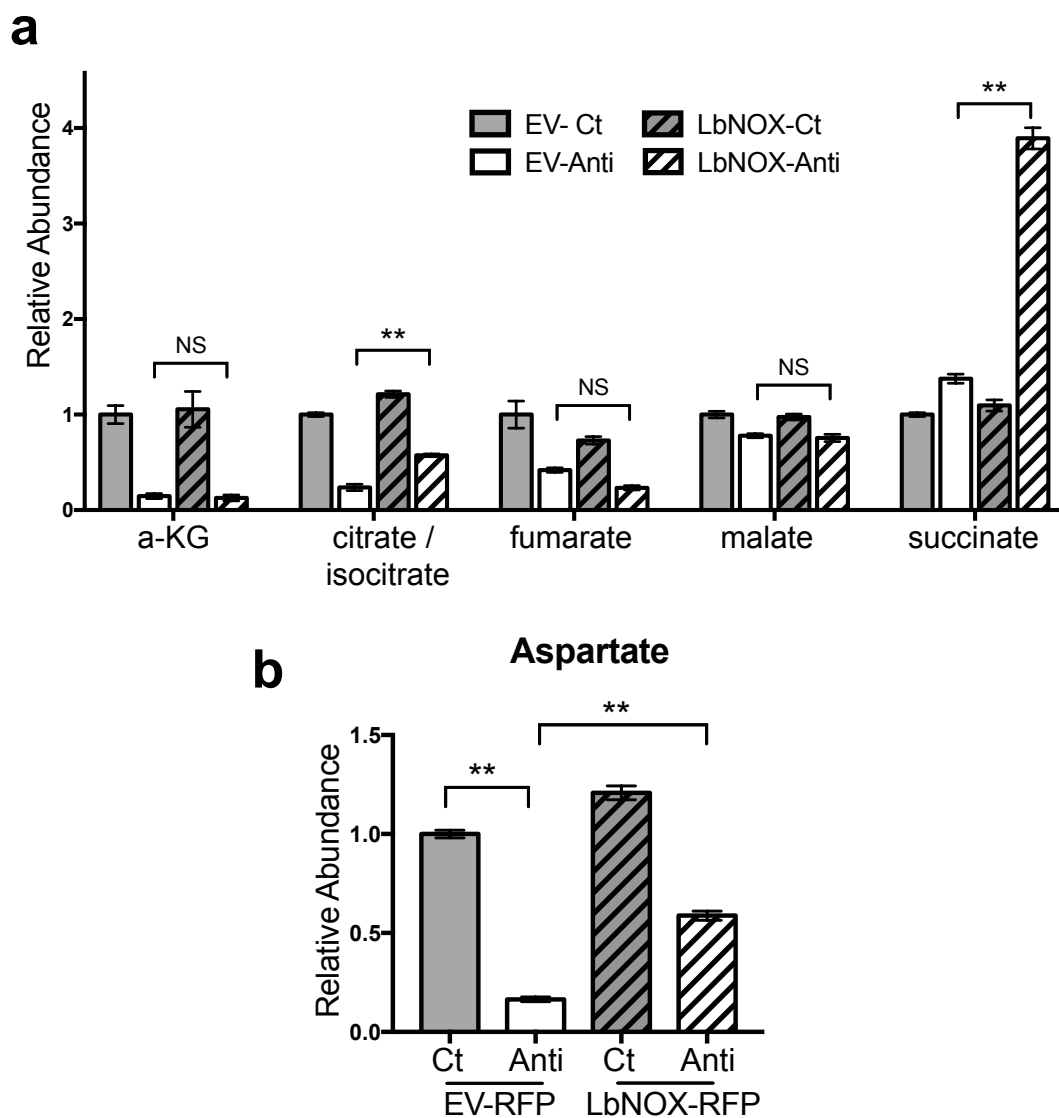


Figure 3.2.2.5 Antimycin A treated HUVECs accumulate succinate and partially maintain aspartate levels

a-b. Relative abundance of TCA cycle metabolites (a), and aspartate (b) in EV-RFP or LbNOX-RFP expressing HUVECs, Ct or Anti treated for 24 hours. Values are normalized to control mean. (n=6). HUVECs were treated with 25nM antimycin A. Data represents mean \pm SEM and were analyzed using one or two-way ANOVA and Tukey's multiple comparisons test (* $p < 0.05$, ** $p < 0.01$, NS=not significant).

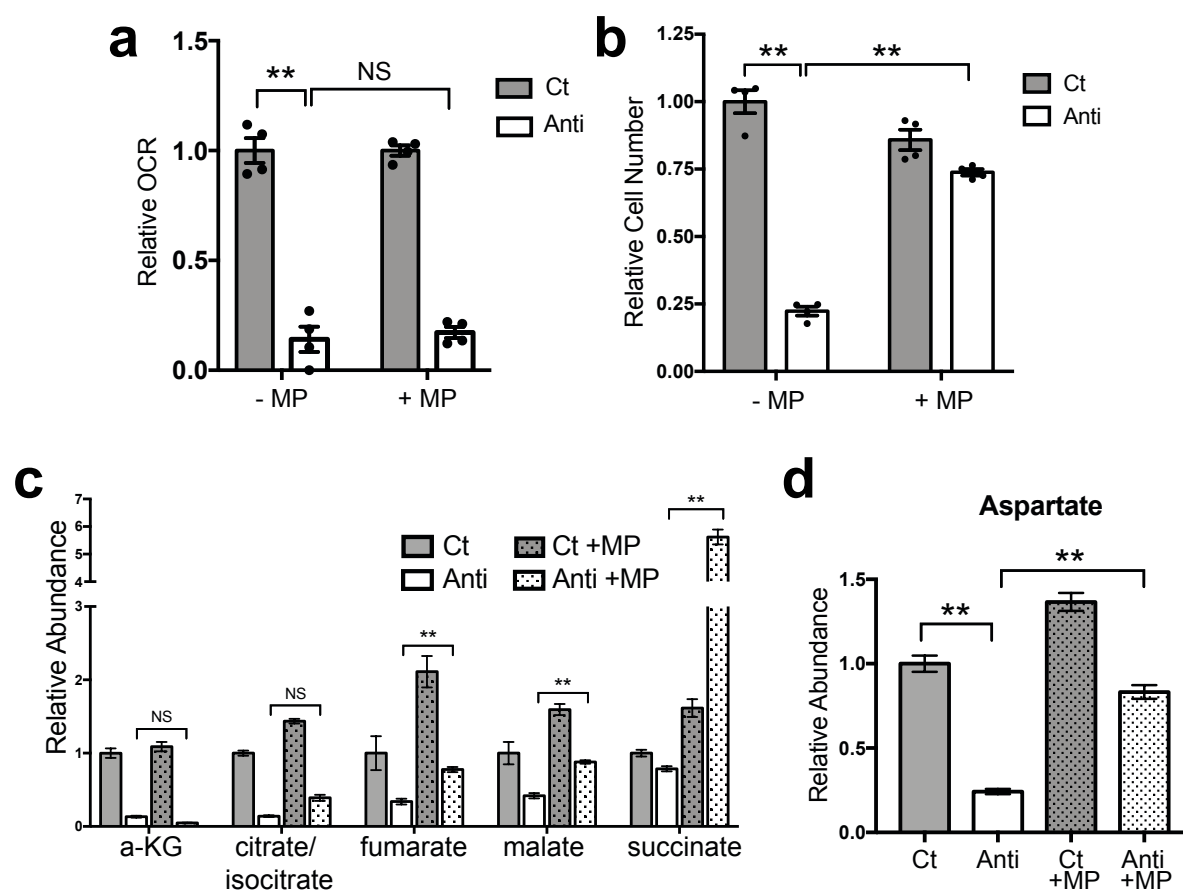


Figure 3.2.2.6 Methyl Pyruvate maintains proliferation and aspartate levels in antimycin A treated HUVECs

a. Relative oxygen consumption (OCR) in Ct or Anti treated HUVECs with or without 1mM methyl pyruvate (MP), after 2 hours treatment (n=4). **b.** Relative cell number after 72 hours proliferation in Ct or Anti treated HUVEC with or without 1mM MP (n=4). **c-d.** Relative abundance of TCA cycle intermediates (e) and aspartate (f) in Ct or Anti treated HUVECs with or without 1mM MP, after 24 hours treatment. All values are relative to Ct mean. Data represents mean +/- SEM and were analyzed using either two-tailed t-test, or 2-way ANOVA and Tukey's multiple comparisons test (*p<0.05, **p<0.01, NS=not significant).

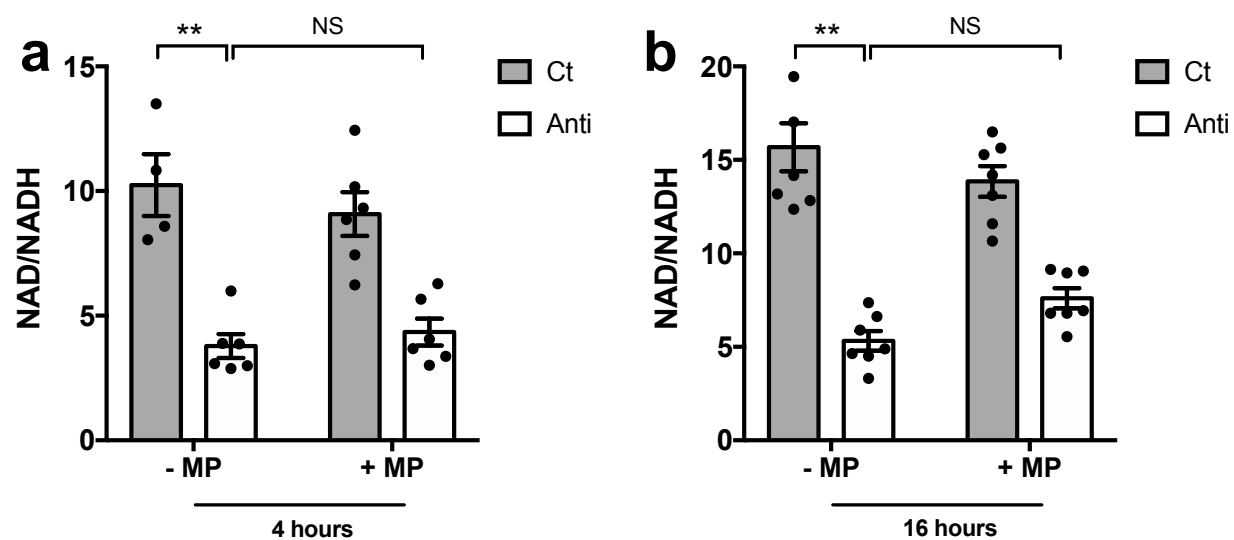


Figure 3.2.2.7 Methyl pyruvate does not restore NAD⁺/NADH in antimycin A treated HUVECs
a-b. Ratio of NAD⁺/NADH in antimycin A treated HUVECs, with or without 1mM methyl pyruvate after 4 hours (a) or 16 hours (b). Data represents mean ± SEM and were analyzed using one or two-way ANOVA and Tukey's multiple comparisons test (*p<0.05, **p<0.01, NS=not significant).

As aspartate levels are decreased in antimycin A treated HUVECs and are rescued upon expression of AOX, LbNOX or addition of MP, we hypothesized that supplementation with aspartate would allow proliferation after ETC inhibition. Previous studies have reported that in respiration deficient cancer cells, aspartate is sufficient to support proliferation in the absence of pyruvate^{24,25}. Surprisingly, aspartate was not able to rescue proliferation in antimycin A treated HUVECs (Figure 3.2.2.8 a). Additionally, neither cell permeable methyl aspartate nor asparagine (which is converted to aspartate by the enzyme asparaginase) were able to restore proliferation (Figure 3.2.2.8 b-c). Together, these data reveal that in HUVECs, mitochondrial complex III fulfills biosynthetic requirements by supporting NAD⁺ regeneration. It is likely that NAD⁺ dependent aspartate synthesis is necessary but not sufficient for cell proliferation.

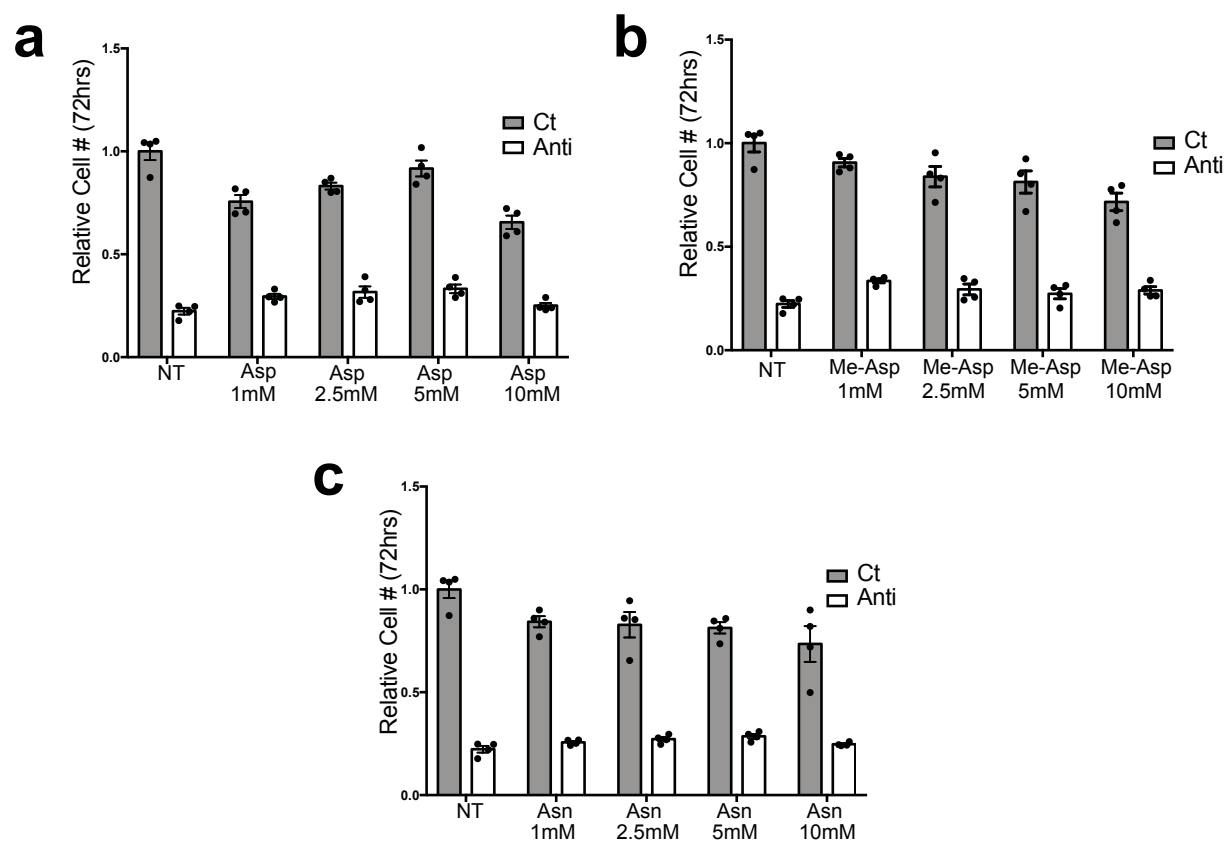


Figure 3.2.2.8 Aspartate, methyl aspartate, or asparagine are not sufficient to support proliferation in antimycin treated HUVECs

a-c. Relative cell number after 72 hours proliferation in Ct or Anti treated HUVECs with or without the indicated dose of aspartate (Asp) (a), methyl aspartate (Me-Asp) (b) or asparagine (Asn) (c) (n=4). All values are relative to Ct mean. Data represents mean \pm SEM.

3.2.3 Inhibiting mitochondrial complex III respiration in HUVECs does not broadly disrupt histone modifications

In addition to fulfilling a biosynthetic demand, mitochondrial metabolites have recently been shown to be necessary to maintain histone acetylation^{14,50}. Accumulation of the TCA cycle intermediates succinate and fumarate, as well as the metabolite L-2-hydroxyglutarate (2HG), leads to competitive inhibition of alpha-ketoglutarate (α KG)-dependent dioxygenases, including JmJC domain-containing histone lysine demethylases (KDMs) and the ten-eleven translocation (TET) family of 5-methylcytosine (5mC) hydroxylases^{52,53}. Recently, we reported that build-up of these three metabolites in mitochondrial complex III KO hematopoietic stem cells, resulted in hyper-methylation of DNA and histones⁵⁰. In the present study, we unexpectedly observed a decrease in 2HG, as well as the expected increase in 2HG: α KG, Succinate: α KG, and Fumarate: α KG (Figure 3.2.3.1). Others have reported that fatty acid oxidation is necessary to maintain H3K9 acetylation in lymphatic endothelial cells¹²⁴. However, we found that histone modifications in HUVECs treated with antimycin A were largely unchanged (Figure 3.2.3.2 a). Specifically, we did not observe changes in H3K9 acetylation or methylation, and saw minimal alterations in other major histone marks linked to gene expression (Figure 3.2.3.2 b-f). Together, these data indicate that mitochondrial complex III in HUVECs *in vitro* is not required for maintenance of chromatin modifications.

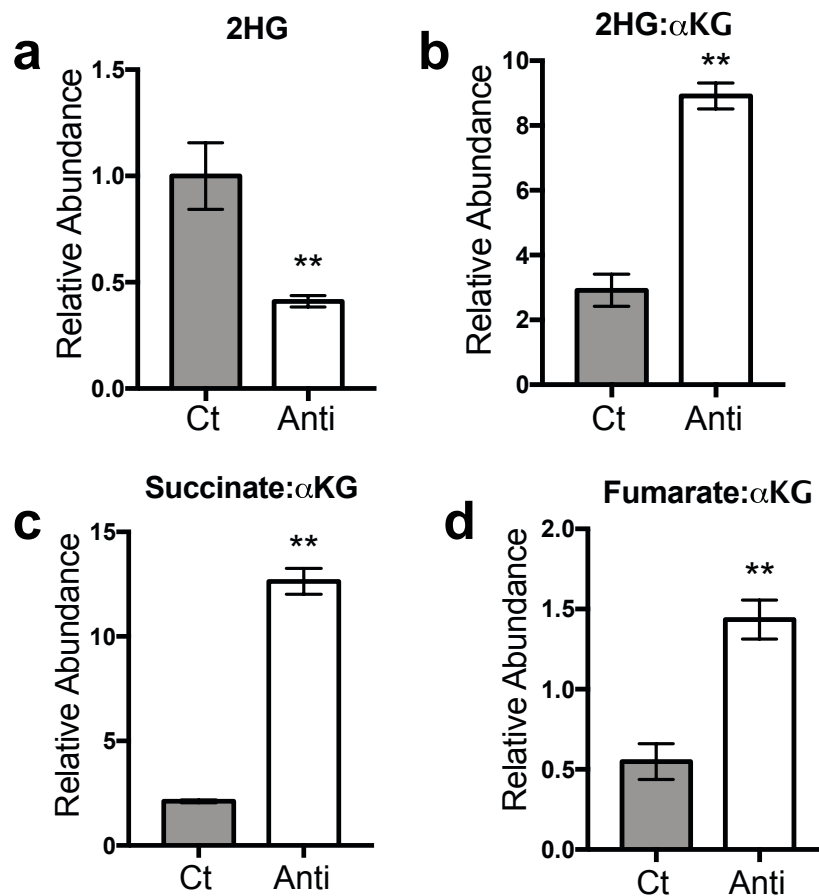


Figure 3.2.3.1 Respiratory deficient HUVECs have decreased 2HG, and increased 2HG:αKG, Succinate:αKG, and Fumarate:αKG

a-d. Relative abundance of L-2-hydroxyglutarate (2HG) (a), 2HG:αKetoglutarate (αKG) (b), Succinate:αKG (c), and Fumarate:αKG (d) from Ct or Anti treated HUVECs, after 24 hours treatment. (n=6). All values are relative to Ct mean. Data represents mean +/- SEM and were analyzed using either two-tailed t-test (*p<0.05, **p<0.01, NS=not significant).

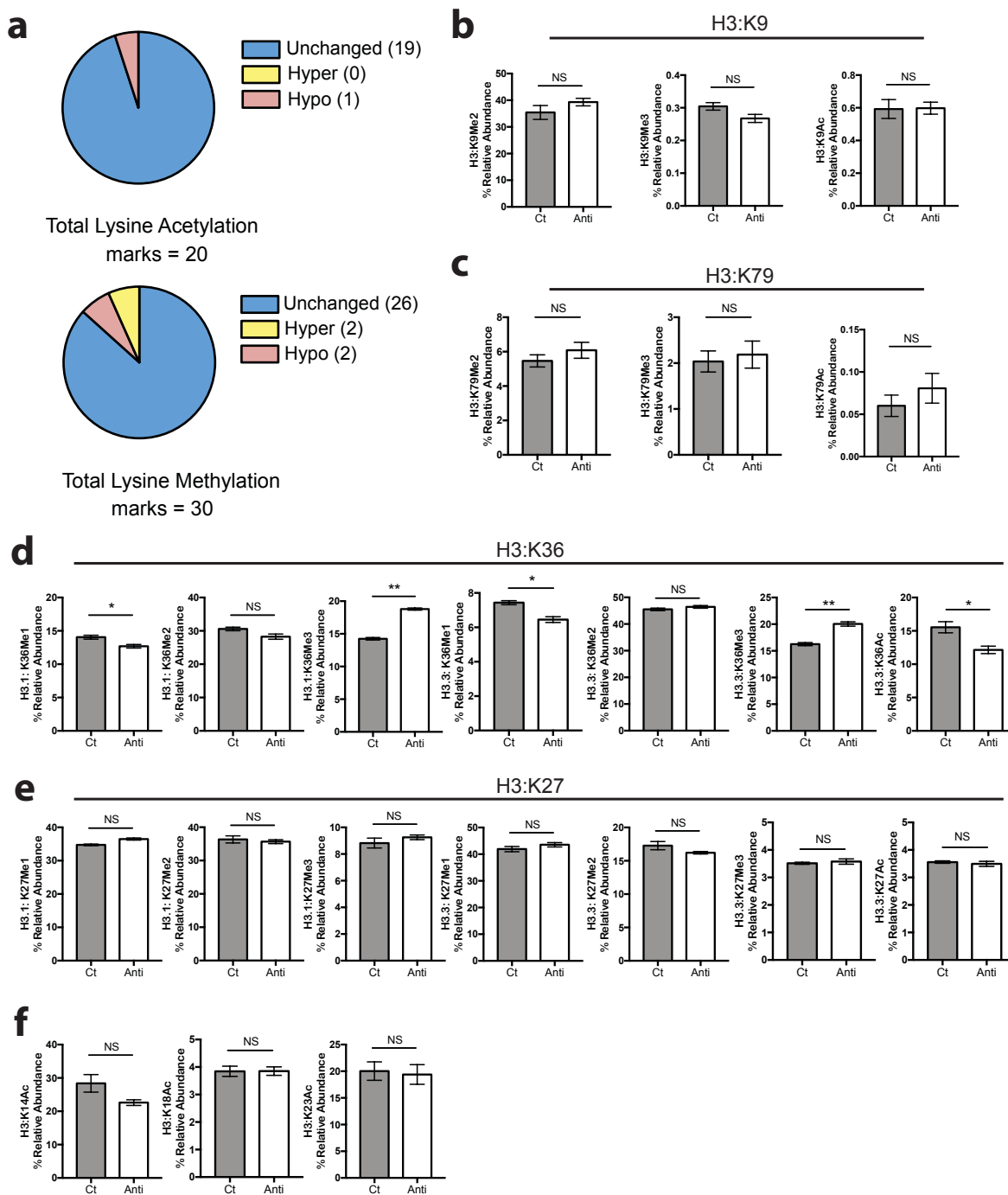


Figure 3.2.3.2 Inhibiting mitochondrial complex III respiration in HUVECs does not broadly disrupt histone modifications

a. Proportion of total lysine acetylation or methylation marks that were unchanged, hyper- or hypo-acetylated and methylated in control (Ct) or antimycin A (Anti) treated HUVECs after 24 hours treatment (n=4). **b-f.** Percent relative abundance of H3:K9 (b), H3:K79 (c), H3:K36 (d), H3:K27 (e), and H3:K14/18/23 (f) methylation and/or acetylation marks in Ct or Anti treated HUVECs after 24 hours treatment (n=4). Data represents mean \pm SEM and were analyzed with a two-tailed t-test (* $p < 0.05$, ** $p < 0.01$, NS=not significant).

3.2.4 Mitochondrial complex III respiration in ECs is required for post-natal retinal angiogenesis

The microenvironment and nutrient availability of ECs differs greatly between cell culture and a living organism, prompting us to ask what the requirements are for EC mitochondrial complex III function *in vivo*. To explore the effect of mitochondrial respiratory chain inhibition *in vivo*, we crossed mice with a floxed *Uqcrcq* gene, which encodes for ubiquinol binding protein, (a critical subunit of the mitochondrial respiratory chain complex III) (QPC^{fl/fl}), with Cdh5Cre^{ERT2} mice, to allow for tamoxifen-inducible, endothelial-specific loss of mitochondrial respiration (QPC-KO) (Figure 3.2.4.1) ¹⁰⁵.

To understand the role of EC mitochondrial complex III respiration in vessel sprouting *in vivo*, we studied angiogenesis in the post-natal mouse retina. Mouse pups were administered 5 doses of tamoxifen on post-natal days 0-4 (P0-P4) to induce Cre recombination and loss of respiration in ECs. To ensure recombination, QPC-WT and -KO mice were crossed to mice harboring a lox-stop-lox TdTomato allele (Figure 3.2.4.2). Retinal whole mounts from P7 pups stained with isolectin-B4 (IB4) revealed a dramatic impairment in retinal angiogenesis in QPC-KO mice (Figure 3.2.4.3 a). By P7, vessels should nearly reach the outer edge of the retina, however radial expansion was massively impaired in QPC-KO mice, as vessels only reached about half the distance to the outer retinal edge (Figure 3.2.4.3 a-b). Additionally, a striking decrease in vascular density can be observed in QPC-KO retinas, which show substantially fewer branchpoints/mm² (Figure 3.2.4.3 a,c). Further staining revealed that QPC-KO retinas had significantly fewer phospho-histone 3 (pH3) positive ECs, indicating a proliferative impairment congruent with what was observed *in vitro* (Figure 3.2.1.5, and Figure 3.2.4.4 a-b). Moreover,

filopodia of QPC-KO ECs on the outer retinal edge were unremarkable in both appearance and number as compared to QPC-WT, suggesting no defect in migration, again consistent with our *in vitro* data (Figure 3.2.1.4, and Figure 3.2.4.4 c-d). Although decreased EC proliferation was observed in QPC-KO retinas, it is possible that EC death was also contributing to the decreased vascularity. For this reason, we stained retinas with cleaved caspase 3 (Casp3) to quantify apoptotic ECs, however cell death was not increased in QPC-KO ECs (Figure 3.2.4.5). Additionally, during sprouting angiogenesis, vessels are continuously being remodeled and undergoing vessel pruning (i.e. vessel regression), which leaves behind empty collagen IV sleeves¹²⁵. An accelerated rate of vessel regression could contribute to decreased vascularity in QPC-KO retinas, however no increase in empty collagen sleeves was observed in QPC-KO mice compared to WT (Figure 3.2.4.5). This indicates that decreased retinal vascularity was not due to EC death or regression. In fact, cell death and vessel pruning were decreased by approximately one half in QPC-KO retinas, which contained about half the number of vessels, suggesting likely no appreciable change in cell death or vessel pruning. We conclude that complex III inhibition *in vivo*, decreases EC proliferation, but does not alter migration, apoptosis, or regression of vessels during post-natal retinal angiogenesis.

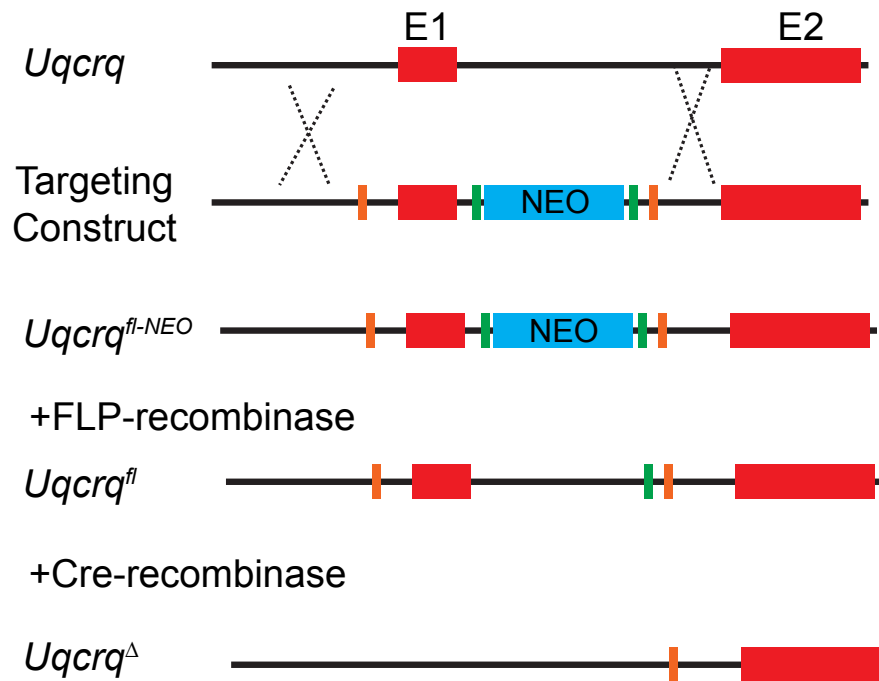


Figure 3.2.4.1 Illustration of the strategy utilized to generate *Uqcrq* floxed and excised alleles. (Figure created by Samuel E. Weinberg, and used with his permission)

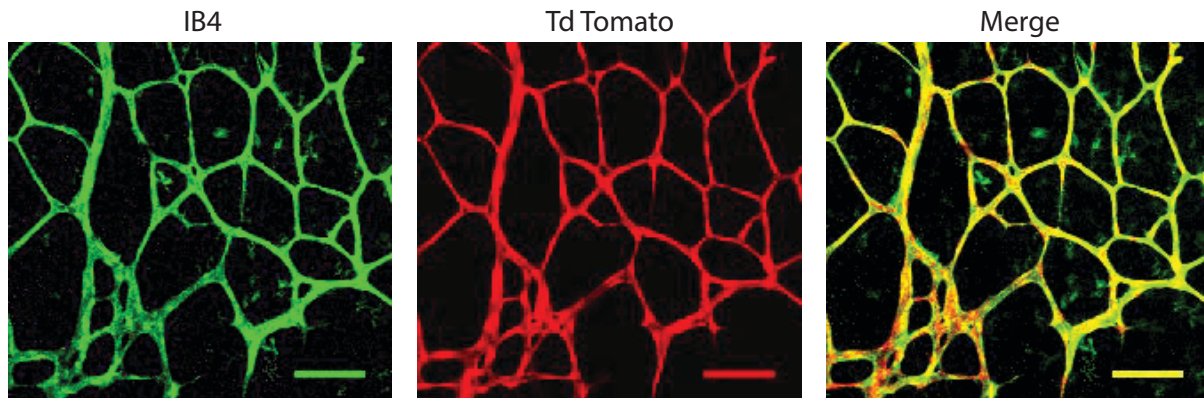


Figure 3.2.4.2 Verification of Cre recombinase activity in QPC KO ECs

Representative images of QPC-KO whole-mounted retinas from P7 pups treated with tamoxifen (P0-P4) harboring a lox-stop-lox TdTomato allele to test for cre recombination. Retinas were stained with isolectin-B4 (IB4) (left panel, green). Middle panel shows expression of TdTomato (red). Right panel shows a merge of IB4 and TdTomato. Images are 10x original magnification and the scale bar represents 100 μ m.

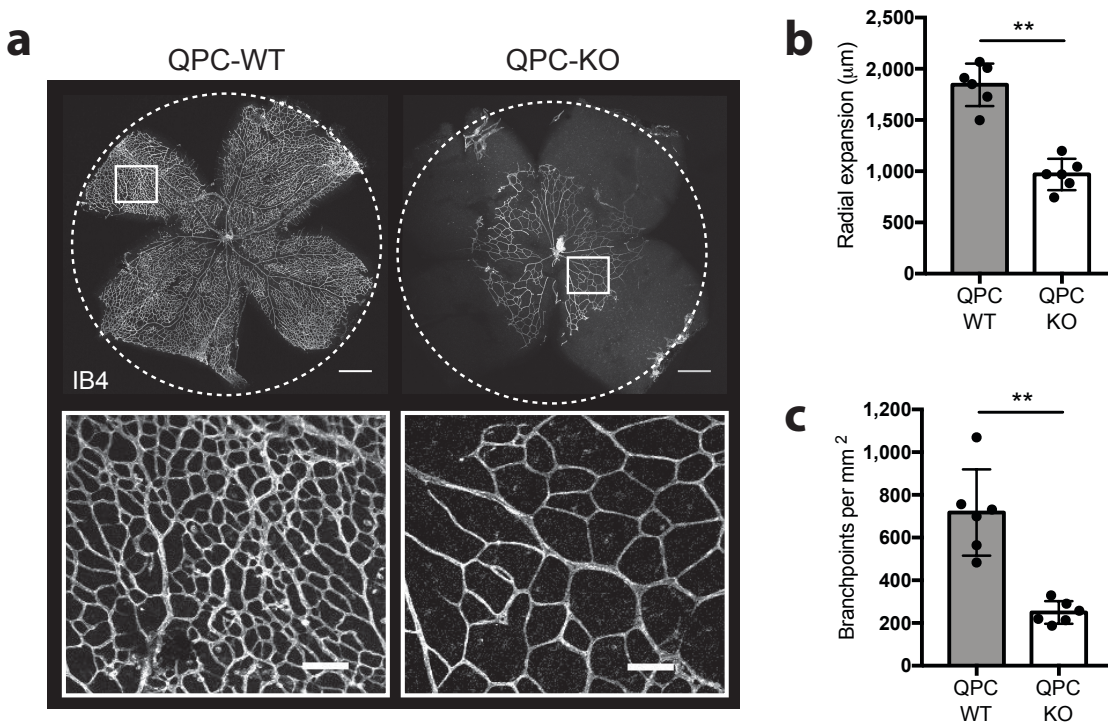


Figure 3.2.4.3 Mitochondrial complex III respiration in ECs is required for post-natal retinal angiogenesis

a. Representative images QPC-WT and -KO retinas stained with isolectin-B4 (IB4) at 10x original magnification. Top panels: Dotted circle represents the QPC-WT radial expansion. Scale bars represent 500 μm . Bottom panels: zoomed image representing white box from top panel. Scale bar represents 100 μm . **b.** Quantification of radial expansion in QPC-WT and -KO retinas (WT: n=6; KO: n=6 mice). **c.** Quantification of the number of branchpoints per mm^2 in QPC-WT and -KO retinas (WT: n=6; KO: n=6 mice). Data represent whole-mounted retinas from QPC-WT and -KO post-natal day 7 (P7) pups treated with tamoxifen (P0-P4). Data represents mean \pm SEM and were analyzed with a two-tailed t-test (* $p < 0.05$, ** $p < 0.01$, NS=not significant).

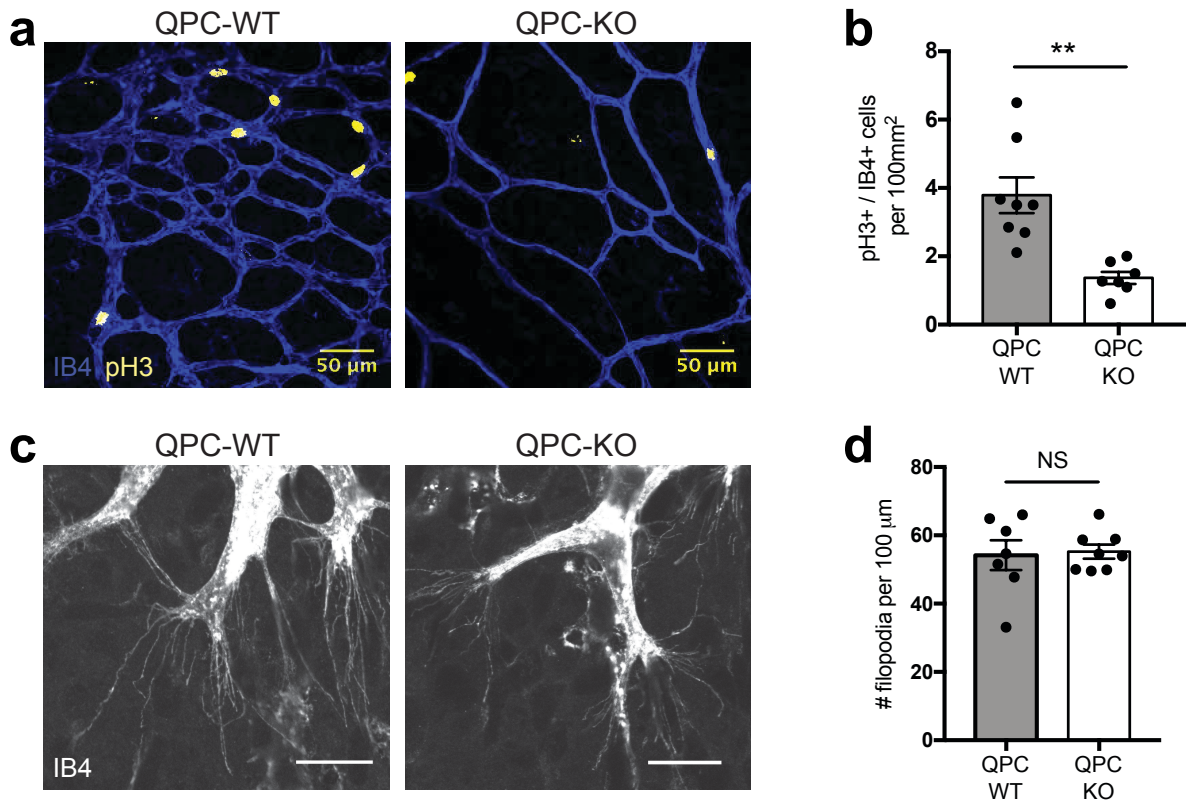


Figure 3.2.4.4 Complex III is required for EC proliferation, but not migration during post natal retinal angiogenesis

a. Representative images of QPC-WT and -KO retinas stained with IB4 (blue) and phospo-histone 3 (pH3) (yellow) taken at 40x magnification. Scale bars represent 50 μ m. **b.** Quantification of pH3+/IB4+ ECs per 100mm² (WT: n=8; KO: n=7 mice). **c.** Representative images of filopodia from QPC-WT and -KO retinas stained with IB4 taken at 100x magnification. Scale bars represent 20 μ m. **d.** Quantification of the number of filopodia per 100 μ m at the outer retinal edge. (WT: n=7; KO: n=8 mice). Data represent whole-mounted retinas from QPC-WT and -KO post-natal day 7 (P7) pups treated with tamoxifen (P0-P4). Data represents mean +/- SEM and were analyzed with a two-tailed t-test (*p<0.05, **p<0.01, NS=not significant).

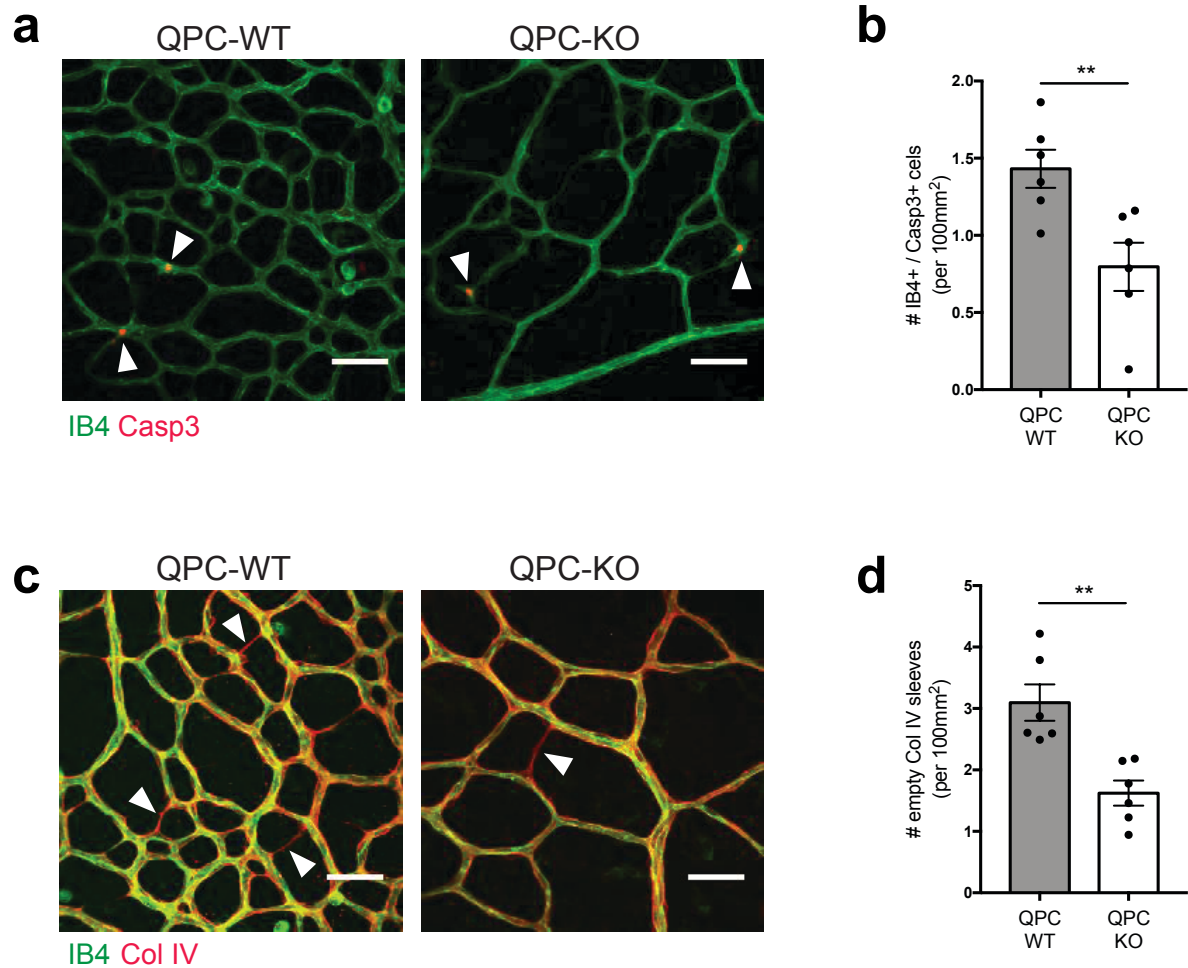


Figure 3.2.4.5 Diminished vascularity in QPC-KO retinas is not due to increased EC death or vessel pruning

a. Representative images of QPC-WT and -KO retinas stained with IB4 (green) and cleaved caspase 3 (Casp3) (red). 20x original magnification, scale bars represent 50 μ m. **b.** Quantification of IB4+/Casp3+ ECs per 100mm² (WT: n=6 mice; KO: n=6 mice). **c.** Representative images of QPC-WT and -KO retinas stained with IB4 (green) and Collagen IV (Col IV) (red). 20x original magnification, scale bars represent 50 μ m. **d.** Quantification of the number of empty Col IV sleeves per 100mm² (WT: n=6 mice; KO: n=6 mice). Data represents mean \pm SEM and were analyzed with a two-tailed t-test (*p<0.05, **p<0.01, NS=not significant).

3.2.5 Mitochondrial complex III function in ECs is necessary for post-natal developmental angiogenesis

Next, we aimed to uncover whether mitochondrial respiration in ECs is necessary for post-natal pup survival. To answer this question, QPC-WT and -KO pups were given 5 doses of tamoxifen (P0-P4) to induce Cre recombination and loss of QPC in ECs. We observed a striking decrease in survival of QPC-KO pups, the majority of which died between P15 and P30 (Figure 3.2.5.1). We observed survival of approximately 25% of QPC-KO pups. It is important to note here that we saw variability in the recombination of cre recombinase in KO pups dosed with tamoxifen. In all other experiments, the recombination efficiency was checked by TdTomato expression, however was not checked in this particular experiment. We surmise that the QPC-KO pups that survived after tamoxifen treatment did not express cre recombinase and therefore did not properly excise QPC.

To further explore vascular defects in this model, lungs were harvested from P15 QPC-WT and -KO pups. We chose to investigate the lung as it contains a large population of ECs, which are actively undergoing angiogenesis at this age, a critical process in post-natal lung alveolarization¹²⁶. QPC-KO lung ECs have diminished expression of QPC mRNA, and displayed decreased OCR and NAD⁺/NADH ratio, indicating a loss of respiratory chain function (Figure 3.2.5.2). QPC-KO pups showed no obvious signs of distress or decline in body weight at P15 (Figure 3.2.5.3 a). However, flow cytometric analysis of homogenized P15 lungs revealed a significant reduction in both the percentage and total number of ECs, consistent with a decrease in lung angiogenesis (Figure 3.2.5.3 b-d and Figure 3.2.5.4). Recall that *in vitro*, as well as in the retina, mitochondrial respiratory chain complex III inhibition caused reduced proliferation

(Figure 3.2.1.5 and Figure 3.2.4.4). Likewise, pH3 staining of P15 lungs revealed a decrease in EC proliferation (Figure 3.2.5.5). Taken together, these data show that loss of mitochondrial complex III leads to a significant defect in lung angiogenesis, likely caused by decreased lung EC proliferation. We speculate that QPC-KO pups may fail to survive to adulthood due to, at least in part, a loss of gas exchange capability during development.

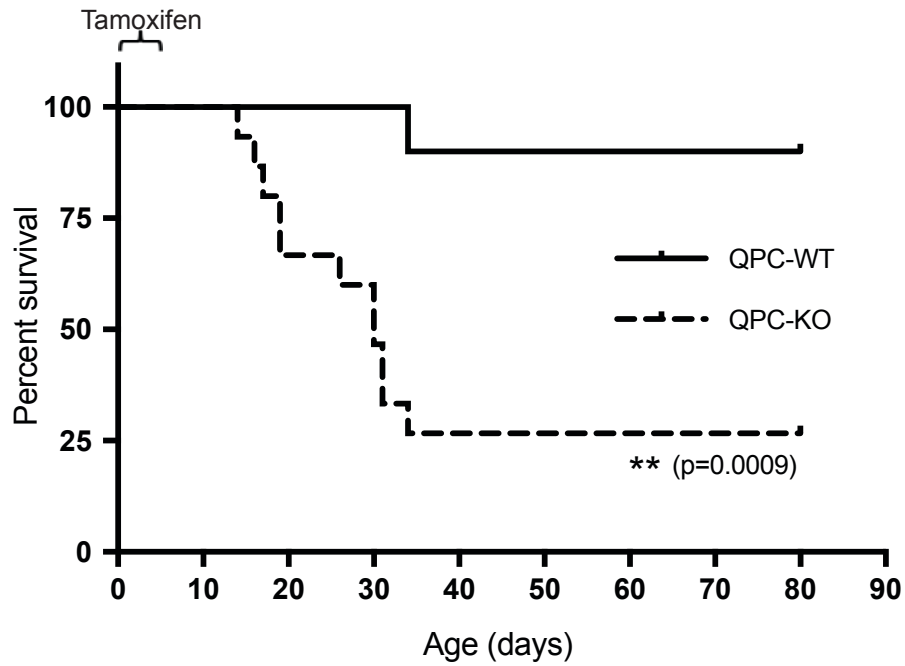


Figure 3.2.5.1 Mitochondrial complex III in ECs is required for survival

Survival curve of QPC-WT and -KO pups treated with tamoxifen (P0-P4) (WT: n=10; KO: n=15). Survival curve was analyzed using a Log-rank (Mantel-Cox) test.

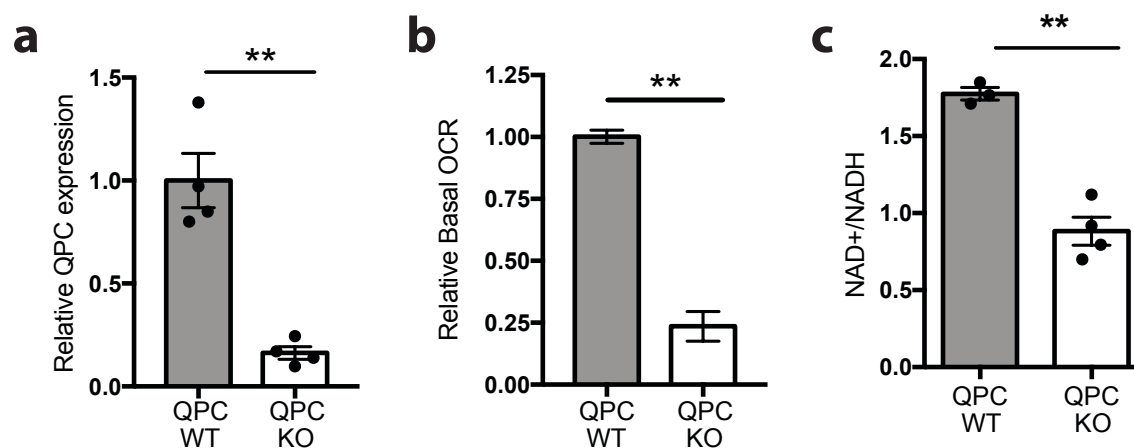


Figure 3.2.5.2 QPC-KO lung ECs lose mitochondrial electron transport chain function

a. qRT-PCR showing relative QPC expression from QPC-WT and –KO P15 lung ECs from P15 pups treated with tamoxifen (P0-P4) (WT: n=4; KO: n=4). **b.** Oxygen consumption in QPC-WT and –KO P7 lung ECs. Representative graph from 3 independent experiments. **c.** Ratio of NAD⁺ to NADH in QPC-WT and –KO P7 lung ECs (WT: n=3; KO: n=4). Data represents mean +/- SEM and were analyzed with a two-tailed t-test (*p<0.05, **p<0.01, NS=not significant).

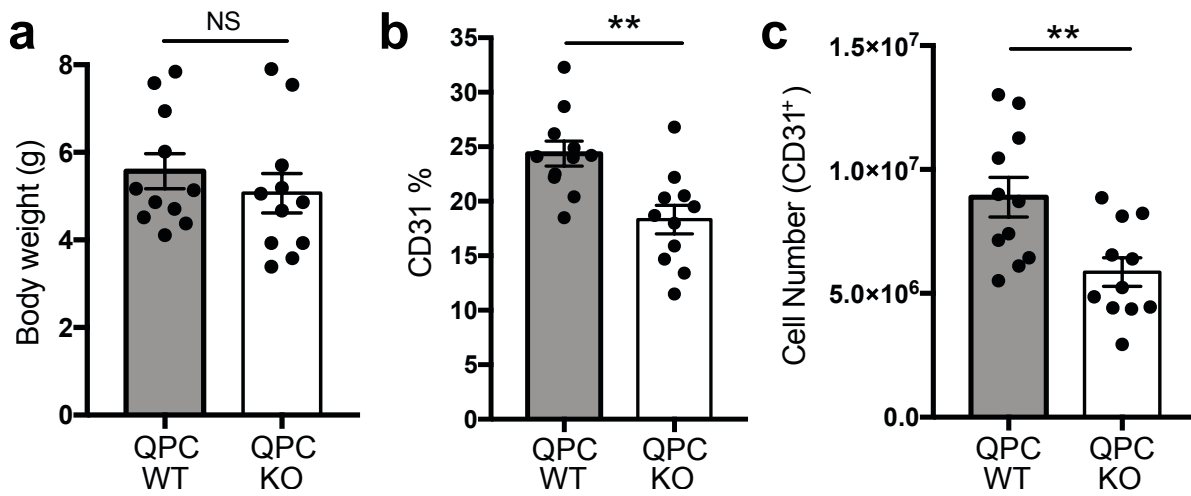


Figure 3.2.5.3 QPC-KO mice have decreased lung EC cellularity

a. Body weight of QPC-WT and -KO P15 pups (WT: n=11; KO: n=11). **b-c.** Percentage of CD31+ cells (b), and total number of CD31+ cells (c) from the lung of QPC-WT and -KO P15 pups (WT: n=11; KO: n=11). Data represent mean \pm SEM and were analyzed with a two-tailed t-test. (* $p < 0.05$, ** $p < 0.01$, NS=not significant).

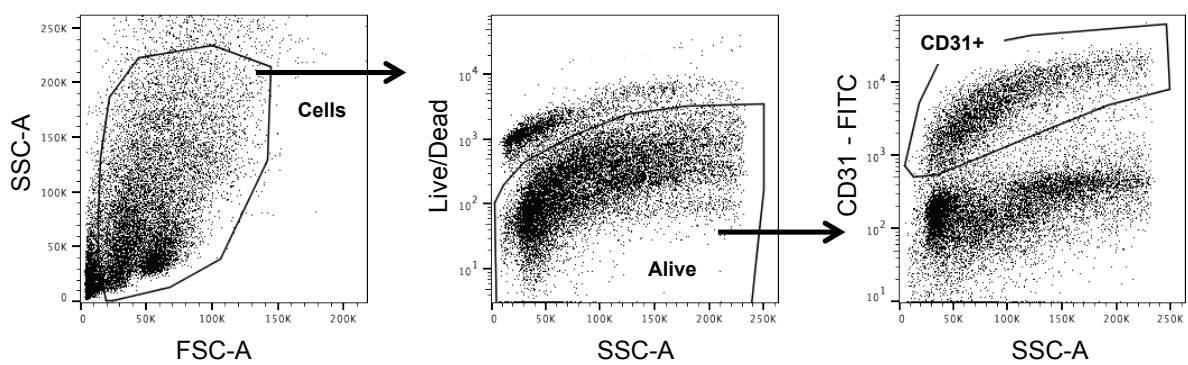


Figure 3.2.5.4 Schematic of flow cytometric gating strategy from homogenized P15 lung tissue

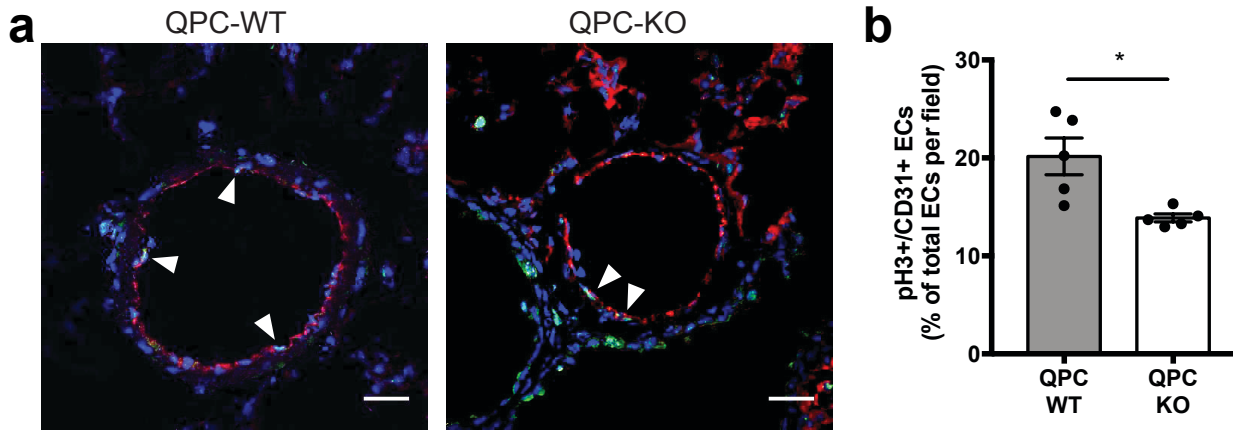


Figure 3.2.5.5 QPC-KO lung ECs have diminished proliferative capacity

a. Representative images of QPC-WT and -KO lung vessels from P15 pups. Vessels stained with CD31 (red), proliferating cells stained with phospho-histone 3 (pH3) (green) and nuclei stained with DAPI (blue), taken at 60x magnification. Scale bars represent 25 μ m. White arrows represent pH3+/CD31+ cells. **b.** Quantification of the number of pH3+/CD31+ cells as a percentage of the total number of CD31+ cells counted per vessel in QPC-WT and -KO lung sections (WT: n=5; KO: n=5). Bar graphs represent mean \pm SEM and were analyzed with a two-tailed t-test (* p <0.05, ** p <0.01, NS=not significant).

3.2.6 Loss of mitochondrial complex III function in ECs increases anabolic-associated gene expression

Although we did not observe profound changes in histone methylation or acetylation in respiration-deficient HUVECs (Figure 3.2.3.2), we wondered whether loss of mitochondrial respiration in ECs would lead to gene deregulation *in vivo*. Thus, we harvested lung ECs from QPC-WT and -KO P15 pups treated with tamoxifen (P0-P4), and performed RNA-sequencing analysis. We observed modest alterations in gene expression, with 237 upregulated and 142 downregulated genes in QPC-KO ECs as compared to QPC-WT ($FDR \leq 0.01$) (Figure 3.2.6.1 a). Surprisingly, gene set enrichment analysis revealed a significant upregulation in pathways associated with anabolism and cellular proliferation, including MYC, MTORC, E2F, and G2M target signaling (Figure 3.2.6.1b). We also observed an increase in the unfolded protein response (UPR), a cellular stress response that has been shown to be activated upon loss of mitochondrial respiratory function¹²⁷ (**Error! Reference source not found.** b). Ribosomal biosynthesis genes are critical targets of cellular pro-growth signaling¹²⁸. Indeed, we found that a substantial percentage (21%) of the significantly upregulated genes in QPC-KO ECs were ribosomal genes, further corroborating intact proliferative signaling (Figure 3.2.6.2 a). QPC-KO ECs show several significantly increased metabolic genes including those regulating glycolysis, one-carbon metabolism, and the urea and TCA cycles (Figure 3.2.6.2 b). Additionally, QPC-KO ECs display a trend toward increased oxidative phosphorylation genes, likely a compensatory mechanism due to massive loss of mitochondrial function (Figure 3.2.6.2 c). These data indicate that although QPC-KO ECs have decreased proliferation, they maintain anabolic gene expression.

Interestingly, RNA-seq revealed a handful of key angiogenic signaling genes that were significantly altered in QPC-KO ECs, however overall, angiogenic signaling genes remained largely unchanged (Figure 3.2.6.3). Specifically, hairy/enhancer-of-split related with YRPW motif protein 1 (Hey1), delta-like 4 (Dll4), and TEK receptor tyrosine kinase (Tek, aka Tie2) were significantly downregulated, while neuropilin-2 (Nrp2), and angiopoitin-2 (Angpt2) were significantly upregulated in QPC-KO ECs (Figure 3.2.6.3). Validation of our RNAseq data at the protein level revealed increased metabolic protein expression, but no change in angiogenic protein expression (Figure 3.2.6.4). Our data suggest that ECs lacking mitochondrial complex III have impaired proliferation and angiogenesis yet retain anabolic gene expression.

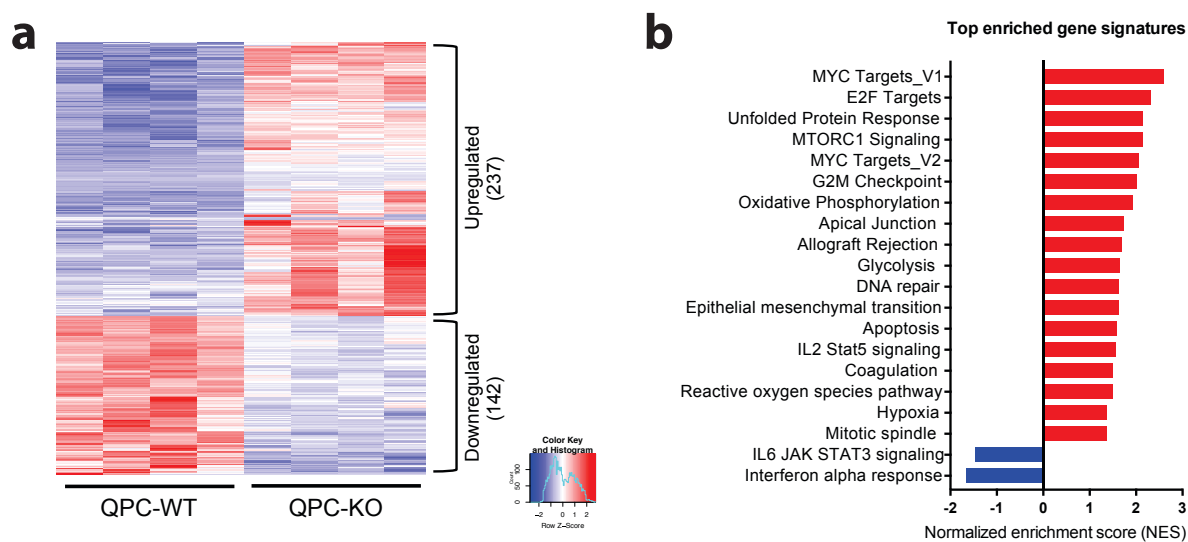


Figure 3.2.6.1 Loss of mitochondrial complex III function in ECs increases anabolic-associated gene expression

a. Heat map of RNA sequencing data representing significantly upregulated (237) and downregulated (142) genes from QPC-WT and -KO P15 lung ECs from pups treated with tamoxifen (P0-P4) ($FDR \leq 0.01$). **b.** Gene set enrichment analysis showing top gene signatures upregulated (red) or downregulated (blue) from QPC-WT and -KO P15 lung ECs (NOM p-value ≤ 0.05). Data shown in heat maps is representative of the z-score. WT: n=4; KO: n=4 mice.

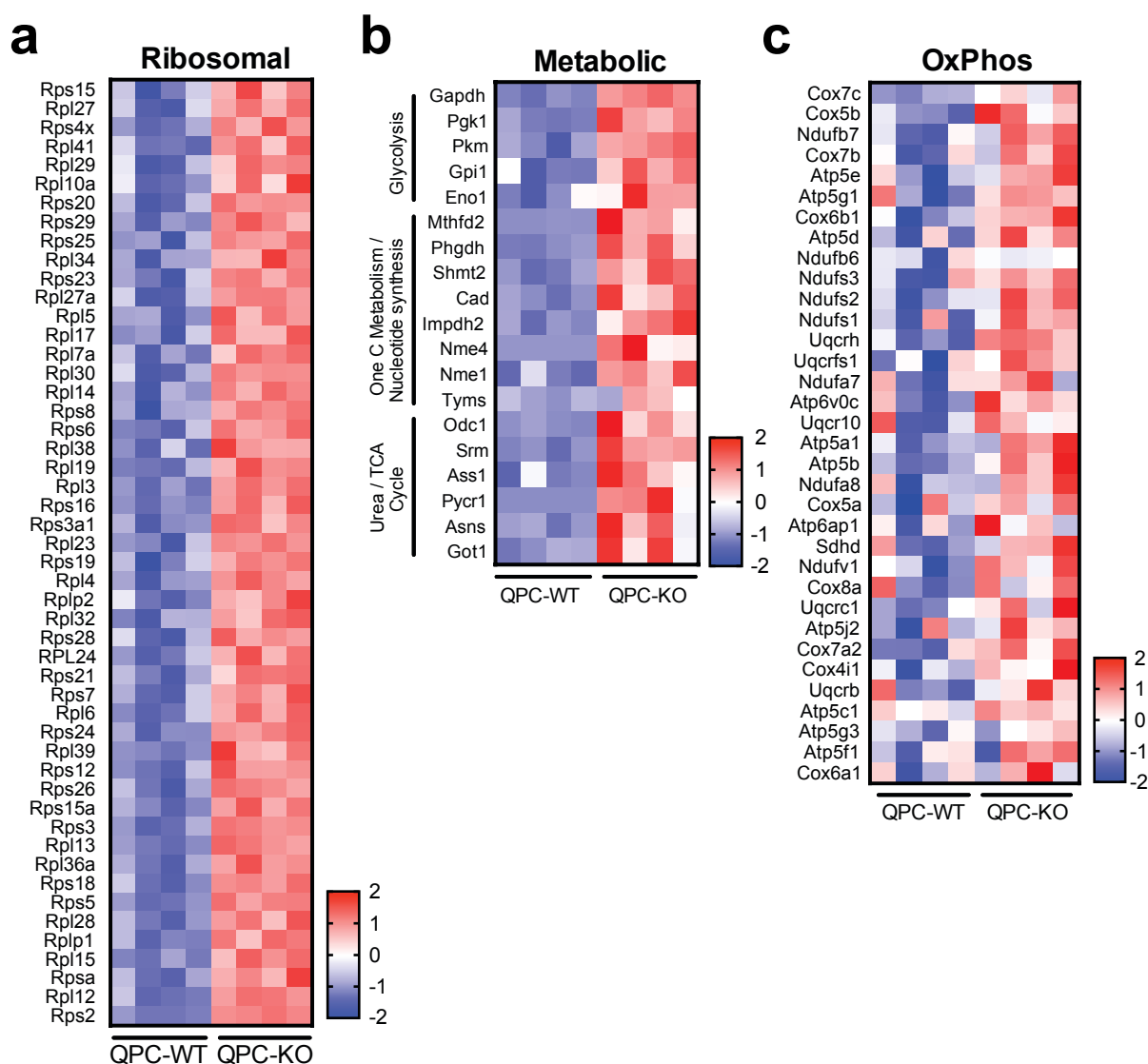


Figure 3.2.6.2 QPC-KO lung ECs display increased expression of ribosomal, metabolic and oxphos genes

c. Heat map of RNA sequencing data showing significantly upregulated ribosomal genes from QPC-KO versus -WT P15 lung ECs ($FDR \leq 0.01$). **d.** Heatmap of RNA sequencing data showing significantly upregulated metabolic genes from QPC-WT and -KO P15 lung ECs ($FDR \leq 0.01$). **e.** Heat map of RNA sequencing data showing oxidative phosphorylation (OxPhos) genes from QPC-WT and -KO P15 lung ECs. Data shown in heat maps is representative of the z-score. WT: n=4; KO: n=4 mice.

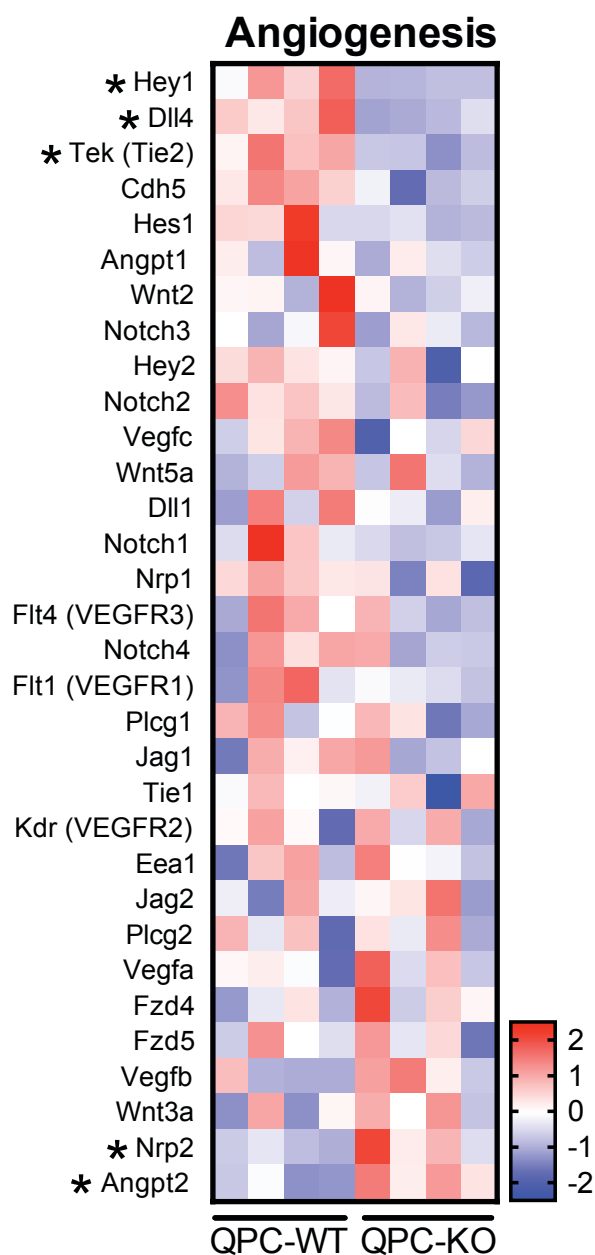


Figure 3.2.6.3 Angiogenic genes are largely unchanged in QPC-KO lung ECs

Heat map of RNA sequencing data showing angiogenic signaling gene expression. * represents genes that are significantly differentially expressed in QPC-KO vs -WT P15 lung ECs (FDR ≤ 0.01). Data shown in heat maps is representative of the z-score. WT: n=4; KO: n=4 mice.

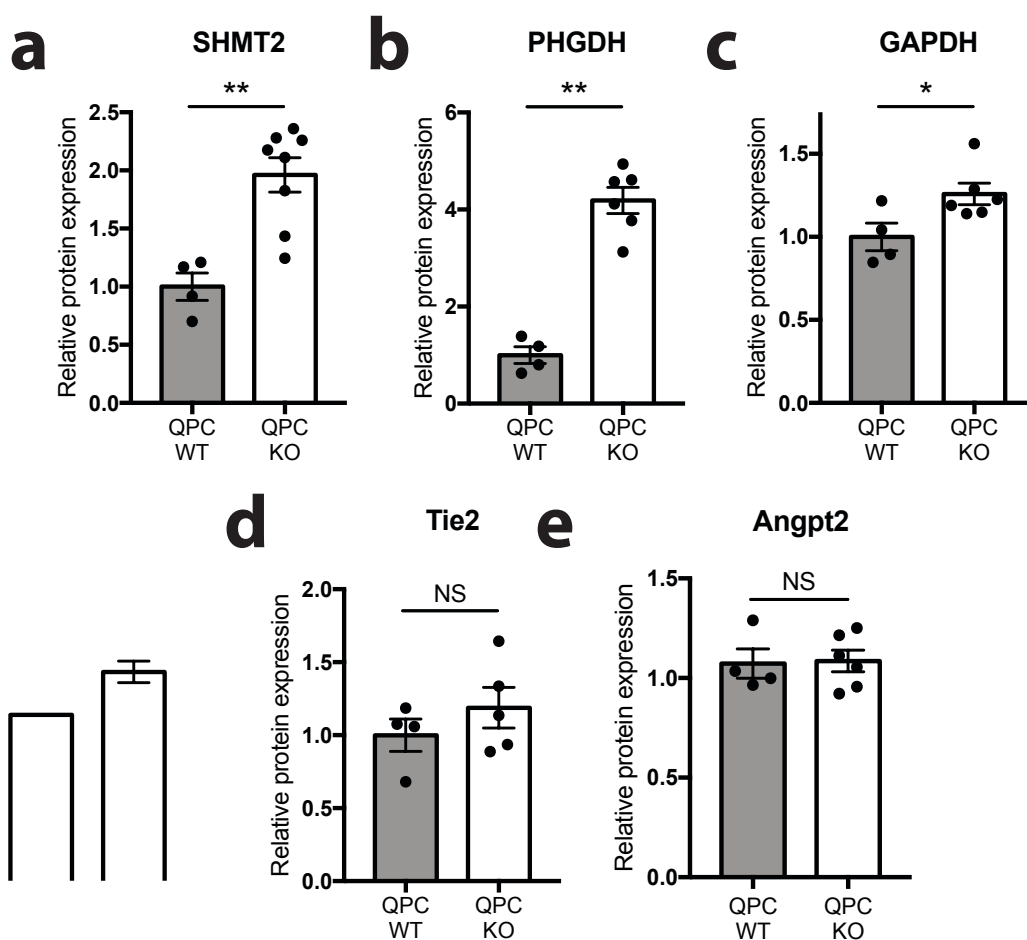


Figure 3.2.6.4 Metabolic, but not angiogenic genes are altered at the protein level in QPC-KO ECs
a-e. Relative protein expression of SHMT2 (a), PHGDH (b), GAPDH (c), Tie2 (d), and Angpt2 (e) from QPC-WT and -KO P15 lung ECs (WT: n=4; KO: n=6 mice). Protein data is representative of mean +/- SEM and was analyzed using a two-tailed t-test (* $p < 0.05$, ** $p < 0.01$, NS=not significant).

3.2.7 Mitochondrial complex III in ECs is necessary to maintain amino acid levels *in vivo*

As anabolic signaling remained intact in QPC-KO ECs, we hypothesized that a metabolic deficiency was preventing proliferation. Metabolite analysis revealed decreased levels of numerous metabolites in the QPC-KO ECs as compared to QPC-WT (Figure 3.2.7.1 a). We did not observe an accumulation of 2HG, however, the TCA cycle metabolites fumarate and malate were significantly lower in QPC-KO ECs, as were several glycolytic intermediates (Figure 3.2.7.1 b and Figure 3.2.7.2). Intriguingly, the majority of the metabolites decreased in QPC-KO ECs were amino acids (Figure 3.2.7.1 a). In contrast to HUVECs *in vitro*, where amino acid levels were maintained with the exception of aspartate, QPC-KO lung ECs displayed significantly diminished levels of nearly all amino acids (Figure 3.2.7.1 a,c). Purine and pyrimidine nucleotide levels, however, remained largely unchanged upon loss of EC respiration (Figure 3.2.7.1 d-e). Together, these results suggest that mitochondrial complex III in ECs is required to maintain amino acid levels, but not nucleotides, which could lead to the impaired proliferation observed in QPC-KO ECs.

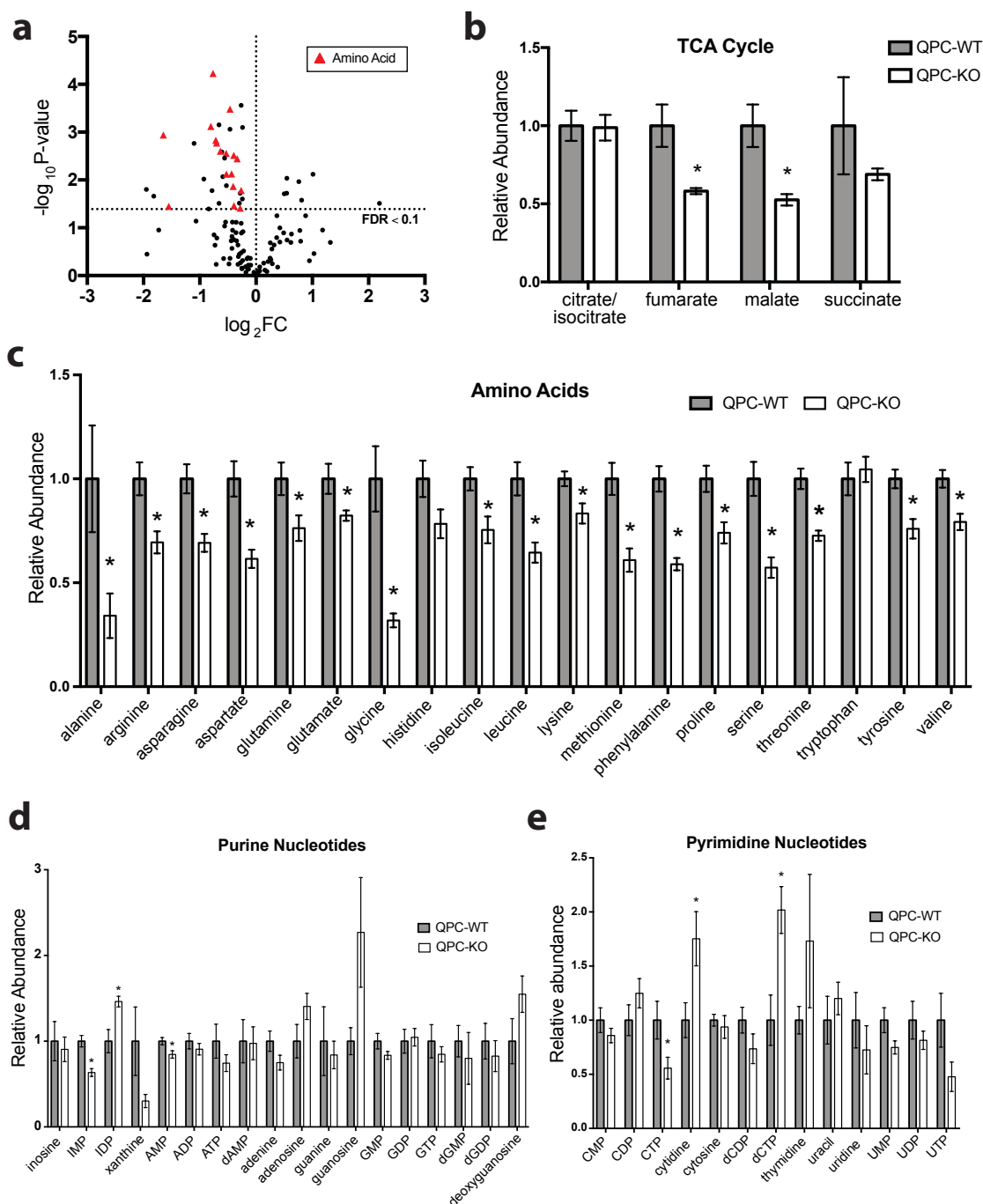


Figure 3.2.7.1 Mitochondrial complex III in ECs is necessary to maintain amino acid levels *in vivo*

a. Volcano plot representing metabolites that are over or under represented in QPC-KO P15 lung ECs versus WT from pups treated with tamoxifen (P0-P4). Red triangles represent amino acid metabolites (WT: n=7; KO: n=7 mice). **b-e.** Relative abundance of TCA cycle (b), amino acid (c), purine nucleotide (d), and pyrimidine nucleotide (e) metabolites from P15 QPC-WT and -KO lung ECs (WT: n=7; KO: n=7 mice). Data are normalized to QPC-WT mean and were analyzed using the Two-stage linear step-up procedure of Benjamini, Krieger and Yekutieli, with $FDR < 0.1$. (* $p < 0.05$, ** $p < 0.01$, NS=not significant).

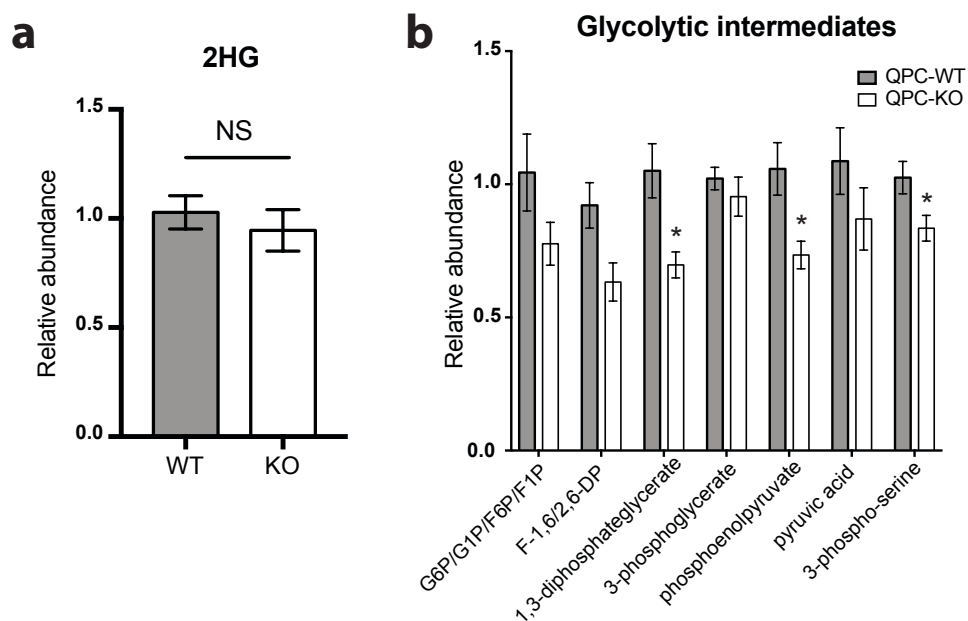


Figure 3.2.7.2 Loss of mitochondrial complex III in ECs does not alter 2HG levels

a-b. Relative abundance of L-2-hydroxyglutarate (2HG) (a), and glycolytic intermediates (b) from P15 QPC-WT and -KO lung ECs (WT: n=7; KO: n=7 mice). Data are normalized to QPC-WT mean and were analyzed using the Two-stage linear step-up procedure of Benjamini, Krieger and Yekutieli, with FDR<0.1. (*p<0.05, **p<0.01, NS=not significant).

3.2.8 Mitochondrial complex III function in ECs is required for tumor angiogenesis

To further investigate the role of EC respiration and determine its requirement in adult mice, we asked whether mitochondrial respiration in ECs is required for tumor angiogenesis. 8-week old adult QPC-WT and QPC-KO mice were fed tamoxifen chow for 2 weeks to induce Cre recombination and loss of QPC mRNA expression and respiration in ECs (Figure 3.2.8.1 a-b). Next, we subcutaneously injected syngeneic B16-F10 melanoma cells into the mice and measured tumor volume over the course of 21 days. QPC-KO mice showed a decrease in tumor growth as compared to QPC-WT, and by days 19 and 21 harbored significantly smaller tumors (Figure 3.2.8.1 c). On day 21, when tumors were harvested, QPC-KO mice also displayed a reduction in tumor weight (Figure 3.2.8.1 d). Histological analysis revealed that QPC-KO tumors had fewer vessels per area, indicating decreased tumor angiogenesis (Figure 3.2.8.2 a-b). Consistent with data from the retina and lung, tumor ECs proliferated less, suggesting that impaired tumor angiogenesis is likely due to reduced EC proliferation (Figure 3.2.8.2 c-d). These data suggest that mitochondrial complex III function is required in adult ECs in order to sustain tumor angiogenesis and tumor growth.

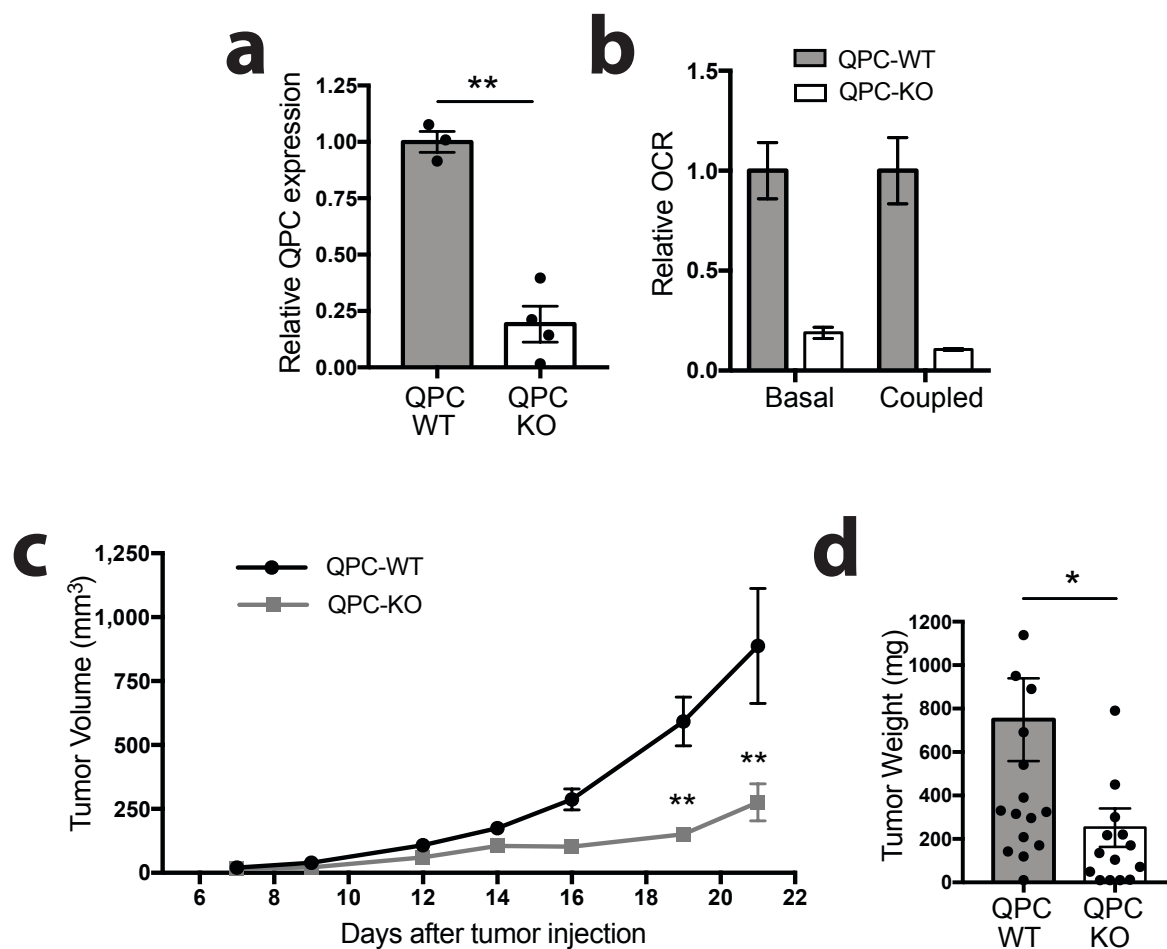


Figure 3.2.8.1 Mitochondrial complex III respiration in ECs is required for tumor angiogenesis
a. qRT-PCR showing relative QPC expression from QPC-WT and -KO lung ECs from adult mice (WT: n=3; KO: n=4). **b.** Relative basal and coupled oxygen consumption (OCR) from QPC-WT and -KO lung ECs (WT: n=2; KO: n=2). **c.** Growth curve of subcutaneous B16-F10 melanoma tumors in QPC-WT and -KO mice (WT: n=20; KO: n=15 mice). **d.** Tumor weight (mg) of subcutaneous B16-F10 melanoma tumors from QPC-WT and -KO mice measured 21 days after injection (WT: n=20; KO: n=15 mice). Mice were fed tamoxifen chow for 2 weeks to induce loss of QPC prior to tumor injections and remained on tamoxifen chow for the duration of the experiment. Data represents mean +/- SEM and were analyzed with a two-tailed t-test (*p<0.05, **p<0.01, NS=not significant).

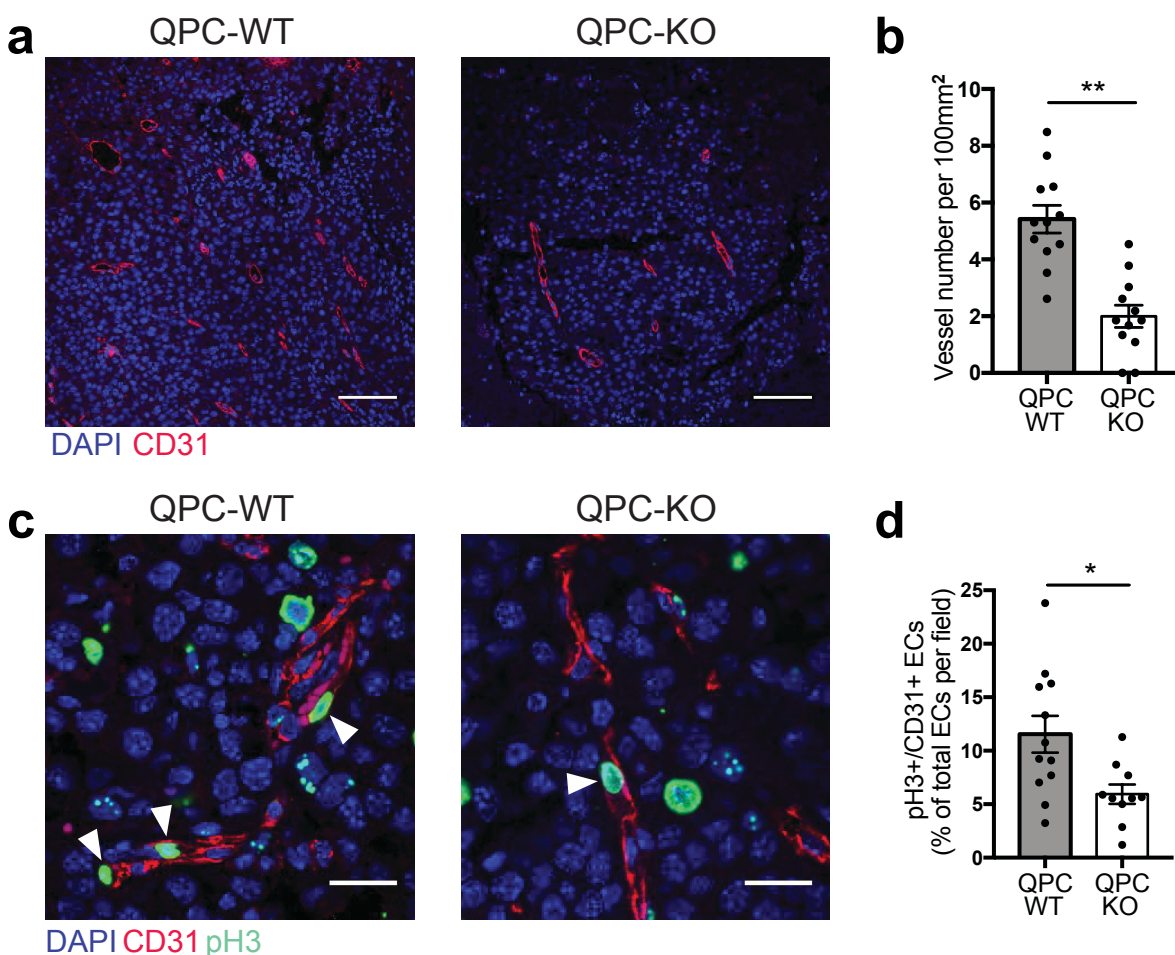


Figure 3.2.8.2 Mitochondrial complex III in ECs is necessary to maintain tumor vascularity and EC proliferation

a. Representative images of QPC-WT and -KO B16-F10 melanoma tumor sections. Vessels stained with CD31 (red) and nuclei stained with DAPI (blue), taken at 20x magnification. Scale bar represents 100 μ m. **b.** Quantification of the number of vessels per 100mm² in QPC-WT and -KO tumor sections (WT: n=12; KO: n=12 mice). **c.** Representative images of QPC-WT and -KO B16-F10 melanoma tumor sections. Vessels stained with CD31 (red), proliferating cells stained with phospho-histone 3 (pH3) (green) and nuclei stained with DAPI (blue), taken at 60x magnification. Scale bars represent 25 μ m. White arrows represent pH3+/CD31+ cells. **d.** Quantification of the number of pH3+/CD31+ cells as a percentage of the total number of CD31+ cells counted per field in QPC-WT and -KO tumor sections (WT: n=12; KO: n=12 mice). Mice were fed tamoxifen chow for 2 weeks to induce loss of QPC prior to tumor injections and remained on tamoxifen chow for the duration of the experiment. Data represents mean +/- SEM and were analyzed with a two-tailed t-test (*p<0.05, **p<0.01, NS=not significant).

3.3 Discussion

Endothelial cells exhibit high levels of flux through glycolysis, only oxidizing a small fraction of glucose-derived carbons in the mitochondria^{74,89}. Accordingly, limiting glycolysis profoundly impairs angiogenesis^{74,112-116}. By contrast, the function of mitochondrial metabolism in ECs is not fully understood. Here we report that pharmacological inhibition of mitochondrial respiratory transport chain complex III in ECs impairs cell proliferation by decreasing NAD⁺/NADH *in vitro*. Conditional loss of respiratory chain complex III in ECs *in vivo* diminished post-natal retinal, lung, and tumor angiogenesis. Our results conclusively demonstrate that mitochondrial respiratory chain complex III is necessary for angiogenesis by controlling EC cell proliferation. These results fill a critical gap in knowledge about the role of the mitochondrial respiratory chain in ECs, a classically glycolytic cell type in which mitochondrial metabolism has largely been underappreciated. Our results indicate that angiogenesis requires coordination of both glycolysis and mitochondrial respiratory chain linked metabolism. It is likely that this coordination in ECs occurs through MYC, since loss of MYC specifically in ECs impairs glycolysis, mitochondrial metabolism and proliferation¹²⁹.

Mitochondria serve three main functions within a cell: (1) they generate ATP via oxidative phosphorylation for cell survival; (2) the TCA cycle generates metabolic intermediates that produce critical macromolecules required for cell growth, including amino acids, nucleotides and lipids; and (3) mitochondria act as signaling organelles, generating reactive oxygen species (ROS) to activate transcriptional networks and produce metabolic intermediates that control epigenetics. The major phenotype we observed due to mitochondrial complex III function impairment is diminished cell proliferation *in vitro* and *in vivo*. This defect is likely not due to

lack of mitochondrial ATP production as it has been suggested that ECs generate up to 85% of their ATP through glycolysis alone⁷⁴. Additionally, complex III loss in ECs did not impair ATP demanding activities such as sprouting and migration in vitro or filopodia formation in vivo, further highlighting that glycolysis can alone provide sufficient ATP for these processes. Our data are consistent with previous studies showing that glycolysis drives filopodia formation and migration in ECs⁷⁴.

The proliferative impairment observed in complex III deficient ECs in vitro and in vivo is likely due to the inability to generate the necessary metabolites for macromolecule synthesis. Previous studies in cancer cells in vitro have demonstrated that loss of complex III decreases NAD⁺ levels, resulting in diminished aspartate, which is necessary for cancer cell proliferation^{24,25}. In cancer cells treated with complex III inhibitors, restoration of NAD⁺ levels, either by supplementation with pyruvate or by genetic expression of NAD⁺ regenerating enzymes, restores aspartate levels and cell proliferation in vitro^{25,104}. Congruently, in vitro, we observed decreased NAD⁺/NADH and diminished aspartate levels in respiration-deficient HUVECs. As previous studies have shown, supplementation with pyruvate restored proliferation after ETC inhibition as well as aspartate levels. Additionally, we found that genetically increasing the ratio of NAD⁺/NADH was sufficient to rescue proliferation and aspartate in antimycin A treated HUVECs, which is again consistent with in vitro cancer cell data¹⁰⁴. Intriguingly, unlike cancer cells, aspartate was not able to restore proliferation in respiration deficient ECs in vitro, perhaps due to distinct metabolic programming between cancer and primary cells. It is important to note that proliferation of not all cancer cell lines is sensitive to aspartate limitation²⁶. Additionally, cancer cells differ in their ability to uptake aspartate, and have varied asparaginase activity²⁷.

We suggest that perhaps aspartate is not sufficient to support proliferation in HUVECs.

However, NAD⁺/NADH ratio, which is linked to other metabolic functions beyond restoring aspartate levels, is sufficient to support HUVEC proliferation.

Additionally, we found that ECs *in vivo* lacking complex III function not only had diminished NAD⁺/NADH and aspartate levels, but also decreased abundance of the majority of amino acids. It is not clear why amino acid levels were markedly diminished from complex III deficient ECs. Gene set enrichment analysis revealed an unexpected increase in anabolic gene expression profiles in QPC-KO ECs, with an increase in genes linked to MYC and mTORC1, including upregulated ribosomal gene expression. This increase in anabolic programs would impose a high demand for amino acids. Thus, in the absence of a functional respiratory chain, the TCA cycle metabolites are not able to maintain amino acid levels to keep up with the increased anabolic demand, resulting in diminished growth. Previously, we observed that gene set enrichment analysis from mitochondrial complex III deficient hematopoietic stem cells (HSCs) similarly displayed upregulation of MYC and mTORC1 linked genes⁵⁰. Going forward it will be important to decipher how loss of mitochondrial complex III function causes an increase in MYC and mTORC1 related genes *in vivo*.

Although our present data on ECs indicate that respiratory chain linked metabolism is necessary for cell proliferation, it is not a universal feature of proliferating cells. For example, fetal mouse HSCs do not require mitochondrial complex III for cell proliferation, but to generate sufficient progenitor populations *in vivo*⁵⁰. Moreover, adult mouse complex III deficient HSCs lose quiescence and undergo stem cell exhaustion; thus, complex III is required for HSCs to function

properly⁵⁰. Mitochondrial complex III deficient HSCs display deregulated expression of approximately 1000 genes, concomitant with histone H3K4, H3K9, and H3K79 hypermethylation⁵⁰. These changes were accompanied by increased levels of succinate, fumarate, and 2HG, metabolites known to inhibit α -KG-dependent dioxygenases including KDMs and TETs^{50,52,53}. We hypothesized that we would see these same trends in ECs, however we did not observe accumulation of succinate, fumarate, or 2HG *in vivo*.

Although, the mitochondrial complex III deficient ECs did not display widespread deregulation of gene expression, there were a few angiogenic associated genes altered, including those involved in the Notch signaling pathway (Dll4 and the two downstream targets Hey1 and Hes1) *in vivo*. Previous studies have shown that Notch signaling is critical for angiogenesis both *in vitro* and *in vivo*^{71,74}. Specifically, decreased Notch signaling in HUVECs accelerated sprouting, while constitutive Notch activation had the opposite effect⁷⁴. In a mouse model, pharmacological inhibition of Notch signaling with the inhibitor DAPT, or genetic ablation through conditional knockout of the Notch ligand Dll4 in ECs, increased branching and tip cell formation in the retina⁷¹. In our *in vivo* model, loss of complex III in ECs lead to decreased Notch signaling, however we observed decreased branching, contrary to what has been observed upon loss of Notch signaling in ECs. As loss of Notch signaling has been found to have the opposite phenotype as diminished respiration in ECs, we conclude that decreased Notch signaling is likely not the dominant factor that leads to impaired angiogenesis in our model. Additionally, mitochondrial complex III deficient ECs display decreased mRNA expression of Tie2, along with overexpression of the Tie2 negative regulator Angpt2, suggesting decreased signaling through Tie2 in QPC-KO ECs. However, we observed no concomitant change in Tie2

or Angpt2 protein levels suggesting no alterations in Tie2 signaling. Overall, we conclude that mitochondrial complex III's dominant function in ECs is to sustain amino acid availability for cell proliferation *in vivo*.

Our observation that complex III linked metabolism in ECs is necessary for cell proliferation is similar to observations in cancer cells. Previously, both others and we have demonstrated that pharmacological inhibition or genetic ablation of the respiratory chain within cancer cells diminishes tumorigenesis in part by decreasing cell proliferation^{13,15,130-137}. This has led to the idea of targeting the respiratory chain for cancer therapy¹³⁸. We observed that inhibition of the respiratory chain, by diminishing complex III in ECs, impaired tumorigenesis. Consequently, administration of respiratory chain inhibitors could work as an anti-cancer therapy through decreasing proliferation of both cancer and endothelial cells. Interestingly, increasing mitochondrial function diminishes prostate tumor vascularization highlighting that mitochondrial homeostasis is crucial for maintaining tumor angiogenesis¹³⁹.

4. CHAPTER 4: CONCLUSIONS AND FUTURE DIRECTIONS

In this thesis work, I have provided novel evidence that mitochondrial complex III is required for EC proliferation during angiogenesis. ECs are highly glycolytic and are often thought to rely little on mitochondrial metabolism. Other recent studies have described how loss of individual mitochondrial pathways can impair EC proliferation and angiogenesis (recall section 1.2.2 above), however, ETC inhibition leads to a more profound angiogenic impairment. This is likely because loss of ETC function not only impairs ATP production, but also diminishes a myriad of other mitochondrial reactions that rely on the reduction of NAD^+ to NADH. For example, a decreased ratio of NAD^+/NADH drastically slows forward TCA cycle function (and consequently reduces the abundance of TCA cycle intermediates for macromolecule biogenesis) and fatty acid oxidation.

While this thesis provides answers to many unknowns regarding EC metabolism, it leaves many questions unanswered, opening the door to future work. First, like respiration deficient cancer cells, antimycin A treated HUVECS require pyruvate to proliferate. The mechanism by which respiration deficient cells are auxotrophic for pyruvate is still up for debate, and may differ depending on cell type. Unlike cancer cells, pyruvate does not restore NAD^+/NADH in HUVECs after loss of ETC function. Although, maintenance of NAD^+/NADH is sufficient in respiration deficient HUVECs to sustain proliferation, pyruvate rescues proliferation by an independent mechanism. Perhaps HUVECs utilize the enzyme pyruvate carboxylase (PC), which directly converts pyruvate to oxaloacetate, which is subsequently utilized for aspartate production, however this mechanism remains unknown. Also unlike cancer cells, aspartate is not sufficient to restore proliferation after ETC inhibition in HUVECs. This was a perplexing

finding, as aspartate was drastically diminished after antimycin A treatment, and aspartate levels were largely restored after pyruvate treatment, AOX expression, and restoration of NAD⁺/NADH with LbNOX expression. Aspartate uptake was not measured in HUVECs, and it is possible that HUVECs inefficiently import aspartate. However, neither cell permeable methyl-aspartate nor asparagine were able to rescue proliferation in respiration deficient HUVECs, however this may be due to methyl-aspartate not properly being metabolized to aspartate within the cells, or lack of asparaginase activity in HUVECs. Another plausible explanation is that, unlike cancer cells, aspartate is simply not sufficient to sustain proliferation in HUVECs, but rather they have a unique metabolism that does not rely heavily on aspartate. Aspartate metabolism has been extensively studied in cancer cells; however, future work will hopefully elucidate the complexities of aspartate utilization in other cell types such as ECs.

A unique feature of this thesis work is the use of *in vivo* metabolic profiling of ECs. Previous studies have exclusively used ECs grown in 2-dimensional monolayers in culture, which does not accurately represent the complex microenvironment of tissues. This work identifies that HUVECs grown in culture lack aspartate, maintaining or increasing levels of all other amino acids, while *in vivo*, loss of complex III in ECs leads to an overall depletion of amino acids. While this particular difference may not be of great significance, this study highlights the likelihood of profound metabolic disparities between culture and *in vivo*. In general, it will be important for future metabolic profiling to be done using cells in (or as close to) their native environment as possible.

Additionally, this thesis work demonstrates that respiration deficient ECs *in vivo* are lacking in amino acids, however they unexpectedly upregulate anabolic signaling genes such as mTOR and MYC. We have previously shown that complex III null HSCs similarly upregulate these pathways⁵⁰. This is surprising, as mTOR signaling is thought to decrease upon intracellular nutrient depletion¹⁴⁰. Why mTOR and other pro-growth signaling pathways are upregulated upon ETC inhibition requires further investigation. Perhaps in mice with respiration-deficient ECs, hypoxic (i.e. under-vascularized) tissues release large amounts of pro-angiogenic signals, which dominantly activate anabolic signaling, even though ECs cannot complete the cell cycle due to lack of macromolecule synthesis. Interestingly, in mice with Leigh syndrome (a complex I deficiency) treatment with the mTOR inhibitor rapamycin, improves survival and attenuates disease progression¹⁴¹. This suggests that perhaps hyperactive anabolic signaling may be exacerbating mitochondrial disease. To test this theory in ECs, we plan to treat QPC-WT and –KO mouse pups with tamoxifen (to induce cre recombination) and rapamycin to determine if inhibition of mTOR is able to rescue retinal angiogenesis and survival in QPC-KO mice. This result would be surprising since respiration deficient ECs would likely still lack sufficient macromolecule biosynthesis for proliferation, however it would provide important insight into the mechanism by which QPC-KO mice fail to properly vascularize tissues. Furthermore, the lab will be obtaining an AOX mouse, which will allow for conditional expression of AOX in cre-expressing tissues, which we plan to cross to QPC-WT and –KO mice. As observed in HUVECs *in vitro*, AOX should rescue OCR, TCA cycle function, as well as macromolecule biosynthesis in KO ECs. We expect that AOX expression will rescue angiogenic phenotypes observed in QPC-KO mice.

Finally, this thesis describes the necessity for mitochondrial complex III respiration in ECs during angiogenesis, however we did not explore its requirement beyond vessel sprouting. Endothelial cells not actively undergoing angiogenesis are largely quiescent, however they are not inert, and play an important role in mediating inflammation¹⁴². During the inflammatory response, ECs become activated, secrete cytokines, express adhesion molecules to bind immune cells, and control vascular permeability¹⁴². Initial experiments in the lab indicate that respiration in ECs is not required for normal maintenance of ECs, as adult mice on tamoxifen chow show no signs of disease after nearly 6 months. However, whether complex III in ECs is necessary during inflammation remains unknown. To this end, we plan to perform sepsis experiments with QPC-WT and -KO mice to determine whether mice with respiration deficient ECs show decreased survival during sepsis. As previous experiments suggest that mitochondria primarily serve as biosynthetic organelles and are required for EC proliferation, it is likely that ECs will be able to perform non-proliferative tasks in the absence of mitochondrial respiration. Ultimately, an important next step following this thesis work is to elucidate the complex role of mitochondrial metabolism in ECs during inflammation.

5. CHAPTER 5: REFERENCES

1. Pagliarini, D. J. & Rutter, J. Hallmarks of a new era in mitochondrial biochemistry. *Genes Dev.* **27**, 2615–2627 (2013).
2. Gray, M. W. Mitochondrial Evolution. *Cold Spring Harb. Perspect. Biol.* **4**, a011403–a011403 (2012).
3. Chandel, N. S. Evolution of Mitochondria as Signaling Organelles. *Cell Metab.* **22**, 204–206 (2015).
4. Chaban, Y., Boekema, E. J. & Dudkina, N. V. Structures of mitochondrial oxidative phosphorylation supercomplexes and mechanisms for their stabilisation. *Biochim. Biophys. Acta BBA - Bioenerg.* **1837**, 418–426 (2014).
5. Hüttemann, M., Lee, I., Samavati, L., Yu, H. & Doan, J. W. Regulation of mitochondrial oxidative phosphorylation through cell signaling. *Biochim. Biophys. Acta BBA - Mol. Cell Res.* **1773**, 1701–1720 (2007).
6. Gautheron, D. C. Mitochondrial oxidative phosphorylation and respiratory chain: Review. *J. Inherit. Metab. Dis.* **7**, 57–61 (1984).
7. Mookerjee, S. A., Goncalves, R. L. S., Gerencser, A. A., Nicholls, D. G. & Brand, M. D. The contributions of respiration and glycolysis to extracellular acid production. *Biochim. Biophys. Acta BBA - Bioenerg.* **1847**, 171–181 (2015).
8. Hanahan, D. & Weinberg, R. A. Hallmarks of Cancer: The Next Generation. *Cell* **144**, 646–674 (2011).
9. Pavlova, N. N. & Thompson, C. B. The Emerging Hallmarks of Cancer Metabolism. *Cell Metab.* **23**, 27–47 (2016).
10. Koppenol, W. H., Bounds, P. L. & Dang, C. V. Otto Warburg's contributions to current concepts of cancer metabolism. *Nat. Rev. Cancer* **11**, 325–337 (2011).
11. DeBerardinis, R. J. & Chandel, N. S. Fundamentals of cancer metabolism. *Sci. Adv.* **2**, e1600200 (2016).
12. Joshi, S. *et al.* The Genomic Landscape of Renal Oncocytoma Identifies a Metabolic Barrier to Tumorigenesis. *Cell Rep.* **13**, 1895–1908 (2015).
13. Weinberg, F. *et al.* Mitochondrial metabolism and ROS generation are essential for Kras-mediated tumorigenicity. *Proc. Natl. Acad. Sci.* **107**, 8788–8793 (2010).
14. Martínez-Reyes, I. *et al.* TCA Cycle and Mitochondrial Membrane Potential Are Necessary for Diverse Biological Functions. *Mol. Cell* **61**, 199–209 (2016).

15. Wheaton, W. W. *et al.* Metformin inhibits mitochondrial complex I of cancer cells to reduce tumorigenesis. *eLife* **3**, (2014).
16. Ahn, C. S. & Metallo, C. M. Mitochondria as biosynthetic factories for cancer proliferation. *Cancer Metab.* **3**, 1 (2015).
17. Currie, E., Schulze, A., Zechner, R., Walther, T. C. & Farese, R. V. Cellular Fatty Acid Metabolism and Cancer. *Cell Metab.* **18**, 153–161 (2013).
18. Kuhajda, F. P. Fatty-acid synthase and human cancer: new perspectives on its role in tumor biology. *Nutr. Burbank Los Angel. Cty. Calif* **16**, 202–208 (2000).
19. Pizer, E. S. *et al.* Inhibition of fatty acid synthesis delays disease progression in a xenograft model of ovarian cancer. *Cancer Res.* **56**, 1189–1193 (1996).
20. Pizer, E. S. *et al.* Malonyl-coenzyme-A is a potential mediator of cytotoxicity induced by fatty-acid synthase inhibition in human breast cancer cells and xenografts. *Cancer Res.* **60**, 213–218 (2000).
21. Gabrielson, E. W., Pinn, M. L., Testa, J. R. & Kuhajda, F. P. Increased fatty acid synthase is a therapeutic target in mesothelioma. *Clin. Cancer Res. Off. J. Am. Assoc. Cancer Res.* **7**, 153–157 (2001).
22. Berg, J. M., Tymoczko, J. L., Stryer, L. & Stryer, L. *Biochemistry: Section 24.2 Amino Acids Are Made from Intermediates of the Citric Acid Cycle and Other Major Pathways.* (W.H. Freeman, 2002).
23. Chandel, N. S. *Navigating metabolism.* (Cold Spring Harbor Laboratory Press, 2015).
24. Birsoy, K. *et al.* An Essential Role of the Mitochondrial Electron Transport Chain in Cell Proliferation Is to Enable Aspartate Synthesis. *Cell* **162**, 540–551 (2015).
25. Sullivan, L. B. *et al.* Supporting Aspartate Biosynthesis Is an Essential Function of Respiration in Proliferating Cells. *Cell* **162**, 552–563 (2015).
26. Garcia-Bermudez, J. *et al.* Aspartate is a limiting metabolite for cancer cell proliferation under hypoxia and in tumours. *Nat. Cell Biol.* **20**, 775–781 (2018).
27. Sullivan, L. B. *et al.* Aspartate is an endogenous metabolic limitation for tumour growth. *Nat. Cell Biol.* **20**, 782–788 (2018).
28. Grégoire, M., Morais, R., Quilliam, M. A. & Gravel, D. On auxotrophy for pyrimidines of respiration-deficient chick embryo cells. *Eur. J. Biochem.* **142**, 49–55 (1984).
29. Capps, G. J., Samuels, D. C. & Chinnery, P. F. A Model of the Nuclear Control of Mitochondrial DNA Replication. *J. Theor. Biol.* **221**, 565–583 (2003).

30. Griffiths, E. J. & Rutter, G. A. Mitochondrial calcium as a key regulator of mitochondrial ATP production in mammalian cells. *Biochim. Biophys. Acta BBA - Bioenerg.* **1787**, 1324–1333 (2009).
31. Cai, J., Yang, J. & Jones, D. Mitochondrial control of apoptosis: the role of cytochrome c. *Biochim. Biophys. Acta BBA - Bioenerg.* **1366**, 139–149 (1998).
32. Glasauer, A. & Chandel, N. S. ROS. *Curr. Biol.* **23**, R100–R102 (2013).
33. Weinberg, F. & Chandel, N. S. Reactive oxygen species-dependent signaling regulates cancer. *Cell. Mol. Life Sci.* **66**, 3663–3673 (2009).
34. Rhee, S. G. H₂O₂, a Necessary Evil for Cell Signaling. *Science* **312**, 1882–1883 (2006).
35. Murphy, M. P. How mitochondria produce reactive oxygen species. *Biochem. J.* **417**, 1–13 (2009).
36. Quinlan, C. L., Pervoshchikova, I. V., Hey-Mogensen, M., Orr, A. L. & Brand, M. D. Sites of reactive oxygen species generation by mitochondria oxidizing different substrates. *Redox Biol.* **1**, 304–312 (2013).
37. Nickel, A., Kohlhaas, M. & Maack, C. Mitochondrial reactive oxygen species production and elimination. *J. Mol. Cell. Cardiol.* **73**, 26–33 (2014).
38. Turrens, J. F. Mitochondrial formation of reactive oxygen species. *J. Physiol.* **552**, 335–344 (2003).
39. Muller, F. L., Liu, Y. & Van Remmen, H. Complex III Releases Superoxide to Both Sides of the Inner Mitochondrial Membrane. *J. Biol. Chem.* **279**, 49064–49073 (2004).
40. Fridovich, I. Superoxide anion radical (O₂⁻), superoxide dismutases, and related matters. *J. Biol. Chem.* **272**, 18515–18517 (1997).
41. Han, D., Antunes, F., Canali, R., Rettori, D. & Cadenas, E. Voltage-dependent Anion Channels Control the Release of the Superoxide Anion from Mitochondria to Cytosol. *J. Biol. Chem.* **278**, 5557–5563 (2003).
42. Orr, A. L. *et al.* Suppressors of superoxide production from mitochondrial complex III. *Nat. Chem. Biol.* **11**, 834–836 (2015).
43. Janssen-Heininger, Y. M. W. *et al.* Redox-based regulation of signal transduction: Principles, pitfalls, and promises. *Free Radic. Biol. Med.* **45**, 1–17 (2008).
44. D'Autréaux, B. & Toledano, M. B. ROS as signalling molecules: mechanisms that generate specificity in ROS homeostasis. *Nat. Rev. Mol. Cell Biol.* **8**, 813–824 (2007).
45. Brandes, N., Schmitt, S. & Jakob, U. Thiol-Based Redox Switches in Eukaryotic Proteins. *Antioxid. Redox Signal.* **11**, 997–1014 (2009).

46. Finkel, T. From Sulfenylation to Sulfhydration: What a Thiolate Needs to Tolerate. *Sci. Signal.* **5**, pe10-pe10 (2012).
47. Hamanaka, R. B. & Chandel, N. S. Mitochondrial reactive oxygen species regulate cellular signaling and dictate biological outcomes. *Trends Biochem. Sci.* **35**, 505–513 (2010).
48. Wellen, K. E. *et al.* ATP-Citrate Lyase Links Cellular Metabolism to Histone Acetylation. *Science* **324**, 1076–1080 (2009).
49. Kaelin, W. G. & McKnight, S. L. Influence of Metabolism on Epigenetics and Disease. *Cell* **153**, 56–69 (2013).
50. Ansó, E. *et al.* The mitochondrial respiratory chain is essential for haematopoietic stem cell function. *Nat. Cell Biol.* **19**, 614–625 (2017).
51. Loenarz, C. & Schofield, C. J. Physiological and biochemical aspects of hydroxylations and demethylations catalyzed by human 2-oxoglutarate oxygenases. *Trends Biochem. Sci.* **36**, 7–18 (2011).
52. Xiao, M. *et al.* Inhibition of α -KG-dependent histone and DNA demethylases by fumarate and succinate that are accumulated in mutations of FH and SDH tumor suppressors. *Genes Dev.* **26**, 1326–1338 (2012).
53. Xu, W. *et al.* Oncometabolite 2-hydroxyglutarate is a competitive inhibitor of α -ketoglutarate-dependent dioxygenases. *Cancer Cell* **19**, 17–30 (2011).
54. Dang, L. *et al.* Cancer-associated IDH1 mutations produce 2-hydroxyglutarate. *Nature* **462**, 739–744 (2009).
55. Gross, S. *et al.* Cancer-associated metabolite 2-hydroxyglutarate accumulates in acute myelogenous leukemia with isocitrate dehydrogenase 1 and 2 mutations. *J. Exp. Med.* **207**, 339–344 (2010).
56. Ward, P. S. *et al.* The Common Feature of Leukemia-Associated IDH1 and IDH2 Mutations Is a Neomorphic Enzyme Activity Converting α -Ketoglutarate to 2-Hydroxyglutarate. *Cancer Cell* **17**, 225–234 (2010).
57. Intlekofer, A. M. *et al.* Hypoxia Induces Production of L-2-Hydroxyglutarate. *Cell Metab.* **22**, 304–311 (2015).
58. Oldham, W. M., Clish, C. B., Yang, Y. & Loscalzo, J. Hypoxia-Mediated Increases in l-2-hydroxyglutarate Coordinate the Metabolic Response to Reductive Stress. *Cell Metab.* **22**, 291–303 (2015).
59. Ye, D., Guan, K.-L. & Xiong, Y. Metabolism, Activity, and Targeting of D- and L-2-Hydroxyglutarates. *Trends Cancer* **4**, 151–165 (2018).
60. Eelen, G. *et al.* Endothelial Cell Metabolism. *Physiol. Rev.* **98**, 3–58 (2018).

61. Potente, M. & Carmeliet, P. The Link Between Angiogenesis and Endothelial Metabolism. *Annu. Rev. Physiol.* **79**, 43–66 (2017).
62. Carmeliet, P. & Jain, R. K. Molecular mechanisms and clinical applications of angiogenesis. *Nature* **473**, 298–307 (2011).
63. Potente, M., Gerhardt, H. & Carmeliet, P. Basic and Therapeutic Aspects of Angiogenesis. *Cell* **146**, 873–887 (2011).
64. Gerhardt, H. *et al.* VEGF guides angiogenic sprouting utilizing endothelial tip cell filopodia. *J. Cell Biol.* **161**, 1163–1177 (2003).
65. Geudens, I. & Gerhardt, H. Coordinating cell behaviour during blood vessel formation. *Development* **138**, 4569–4583 (2011).
66. Fantin, A. *et al.* Tissue macrophages act as cellular chaperones for vascular anastomosis downstream of VEGF-mediated endothelial tip cell induction. *Blood* **116**, 829–840 (2010).
67. Ruhrberg, C. Spatially restricted patterning cues provided by heparin-binding VEGF-A control blood vessel branching morphogenesis. *Genes Dev.* **16**, 2684–2698 (2002).
68. Blanco, R. & Gerhardt, H. VEGF and Notch in Tip and Stalk Cell Selection. *Cold Spring Harb. Perspect. Med.* **3**, a006569–a006569 (2013).
69. Phng, L.-K. & Gerhardt, H. Angiogenesis: A Team Effort Coordinated by Notch. *Dev. Cell* **16**, 196–208 (2009).
70. Jakobsson, L. *et al.* Endothelial cells dynamically compete for the tip cell position during angiogenic sprouting. *Nat. Cell Biol.* **12**, 943–953 (2010).
71. Hellström, M. *et al.* Dll4 signalling through Notch1 regulates formation of tip cells during angiogenesis. *Nature* **445**, 776–780 (2007).
72. Lobov, I. B. *et al.* Delta-like ligand 4 (Dll4) is induced by VEGF as a negative regulator of angiogenic sprouting. *Proc. Natl. Acad. Sci.* **104**, 3219–3224 (2007).
73. Suchting, S. *et al.* The Notch ligand Delta-like 4 negatively regulates endothelial tip cell formation and vessel branching. *Proc. Natl. Acad. Sci.* **104**, 3225–3230 (2007).
74. De Bock, K. *et al.* Role of PFKFB3-driven glycolysis in vessel sprouting. *Cell* **154**, 651–663 (2013).
75. Ucuzian, A. A., Gassman, A. A., East, A. T. & Greisler, H. P. Molecular Mediators of Angiogenesis: *J. Burn Care Res.* **31**, 158–175 (2010).
76. Davidson, S. M. *et al.* Environment Impacts the Metabolic Dependencies of Ras-Driven Non-Small Cell Lung Cancer. *Cell Metab.* **23**, 517–528 (2016).
77. Cantor, J. R. *et al.* Physiologic Medium Rewires Cellular Metabolism and Reveals Uric Acid as an Endogenous Inhibitor of UMP Synthase. *Cell* **169**, 258–272.e17 (2017).

78. Culic, O., Gruwel, M. L. & Schrader, J. Energy turnover of vascular endothelial cells. *Am. J. Physiol.-Cell Physiol.* **273**, C205–C213 (1997).
79. Krützfeldt, A., Spahr, R., Mertens, S., Siegmund, B. & Piper, H. M. Metabolism of exogenous substrates by coronary endothelial cells in culture. *J. Mol. Cell. Cardiol.* **22**, 1393–1404 (1990).
80. Peters, K. *et al.* Changes in Human Endothelial Cell Energy Metabolic Capacities during in vitro Cultivation. The Role of ‘Aerobic Glycolysis’ and Proliferation. *Cell. Physiol. Biochem.* **24**, 483–492 (2009).
81. Parra-Bonilla, G., Alvarez, D. F., Al-Mehdi, A.-B., Alexeyev, M. & Stevens, T. Critical role for lactate dehydrogenase A in aerobic glycolysis that sustains pulmonary microvascular endothelial cell proliferation. *Am. J. Physiol. Lung Cell. Mol. Physiol.* **299**, L513-522 (2010).
82. Yeh, W.-L., Lin, C.-J. & Fu, W.-M. Enhancement of glucose transporter expression of brain endothelial cells by vascular endothelial growth factor derived from glioma exposed to hypoxia. *Mol. Pharmacol.* **73**, 170–177 (2008).
83. Paik, J.-Y., Jung, K.-H., Lee, J.-H., Park, J.-W. & Lee, K.-H. Reactive oxygen species-driven HIF1 α triggers accelerated glycolysis in endothelial cells exposed to low oxygen tension. *Nucl. Med. Biol.* **45**, 8–14 (2017).
84. Chung, S.-J. *et al.* Pyruvate protection against endothelial cytotoxicity induced by blockade of glucose uptake. *J. Biochem. Mol. Biol.* **37**, 239–245 (2004).
85. Merchan, J. R. *et al.* Antiangiogenic Activity of 2-Deoxy-D-Glucose. *PLoS ONE* **5**, e13699 (2010).
86. Wang, Q., Liang, B., Shirwany, N. A. & Zou, M.-H. 2-Deoxy-D-Glucose Treatment of Endothelial Cells Induces Autophagy by Reactive Oxygen Species-Mediated Activation of the AMP-Activated Protein Kinase. *PLoS ONE* **6**, e17234 (2011).
87. Blouin, A., Bolender, R. P. & Weibel, E. R. Distribution of organelles and membranes between hepatocytes and nonhepatocytes in the rat liver parenchyma. A stereological study. *J. Cell Biol.* **72**, 441–455 (1977).
88. Schoors, S. *et al.* Fatty acid carbon is essential for dNTP synthesis in endothelial cells. *Nature* **520**, 192–197 (2015).
89. Kim, B., Li, J., Jang, C. & Arany, Z. Glutamine fuels proliferation but not migration of endothelial cells. *EMBO J.* **36**, 2321–2333 (2017).
90. Browne, C. D., Hindmarsh, E. J. & Smith, J. W. Inhibition of endothelial cell proliferation and angiogenesis by orlistat, a fatty acid synthase inhibitor. *FASEB J.* **20**, 2027–2035 (2006).
91. Seguin, F. *et al.* The fatty acid synthase inhibitor orlistat reduces experimental metastases and angiogenesis in B16-F10 melanomas. *Br. J. Cancer* **107**, 977–987 (2012).

92. Glatz, J. F. C., Luiken, J. J. F. P. & Bonen, A. Membrane Fatty Acid Transporters as Regulators of Lipid Metabolism: Implications for Metabolic Disease. *Physiol. Rev.* **90**, 367–417 (2010).
93. Harjes, U., Bridges, E., McIntyre, A., Fielding, B. A. & Harris, A. L. Fatty Acid-binding Protein 4, a Point of Convergence for Angiogenic and Metabolic Signaling Pathways in Endothelial Cells. *J. Biol. Chem.* **289**, 23168–23176 (2014).
94. Elmasri, H. *et al.* Endothelial cell-fatty acid binding protein 4 promotes angiogenesis: role of stem cell factor/c-kit pathway. *Angiogenesis* **15**, 457–468 (2012).
95. Elmasri, H. *et al.* Fatty acid binding protein 4 is a target of VEGF and a regulator of cell proliferation in endothelial cells. *FASEB J. Off. Publ. Fed. Am. Soc. Exp. Biol.* **23**, 3865–3873 (2009).
96. Stein, W. H. & Moore, S. The free amino acids of human blood plasma. *J. Biol. Chem.* **211**, 915–926 (1954).
97. Jain, M. *et al.* Metabolite Profiling Identifies a Key Role for Glycine in Rapid Cancer Cell Proliferation. *Science* **336**, 1040–1044 (2012).
98. Wu, G., Haynes, T. E., Li, H. & Meininger, C. J. Glutamine metabolism in endothelial cells: ornithine synthesis from glutamine via pyrroline-5-carboxylate synthase. *Comp. Biochem. Physiol. A. Mol. Integr. Physiol.* **126**, 115–123 (2000).
99. Leighton, B., Curi, R., Hussein, A. & Newsholme, E. A. Maximum activities of some key enzymes of glycolysis, glutaminolysis, Krebs cycle and fatty acid utilization in bovine pulmonary endothelial cells. *FEBS Lett.* **225**, 93–96 (1987).
100. Lohmann, R., Souba, W. W. & Bode, B. P. Rat liver endothelial cell glutamine transporter and glutaminase expression contrast with parenchymal cells. *Am. J. Physiol.* **276**, G743–750 (1999).
101. Unterluggauer, H. *et al.* Premature senescence of human endothelial cells induced by inhibition of glutaminase. *Biogerontology* **9**, 247–259 (2008).
102. Huang, H. *et al.* Role of glutamine and interlinked asparagine metabolism in vessel formation. *EMBO J.* **36**, 2334–2352 (2017).
103. Cannino, G. *et al.* Glucose Modulates Respiratory Complex I Activity in Response to Acute Mitochondrial Dysfunction. *J. Biol. Chem.* **287**, 38729–38740 (2012).
104. Titov, D. V. *et al.* Complementation of mitochondrial electron transport chain by manipulation of the NAD⁺/NADH ratio. *Science* **352**, 231–235 (2016).
105. Benedito, R. *et al.* The notch ligands Dll4 and Jagged1 have opposing effects on angiogenesis. *Cell* **137**, 1124–1135 (2009).

106. Pitulescu, M. E., Schmidt, I., Benedito, R. & Adams, R. H. Inducible gene targeting in the neonatal vasculature and analysis of retinal angiogenesis in mice. *Nat. Protoc.* **5**, 1518–1534 (2010).
107. Garcia, B. A. *et al.* Chemical derivatization of histones for facilitated analysis by mass spectrometry. *Nat. Protoc.* **2**, 933–938 (2007).
108. Zheng, Y., Thomas, P. M. & Kelleher, N. L. Measurement of acetylation turnover at distinct lysines in human histones identifies long-lived acetylation sites. *Nat. Commun.* **4**, 2203 (2013).
109. Zheng, Y., Tipton, J. D., Thomas, P. M., Kelleher, N. L. & Sweet, S. M. M. Site-specific human histone H3 methylation stability: fast K4me3 turnover. *Proteomics* **14**, 2190–2199 (2014).
110. MacLean, B. *et al.* Skyline: an open source document editor for creating and analyzing targeted proteomics experiments. *Bioinforma. Oxf. Engl.* **26**, 966–968 (2010).
111. Teuwen, L.-A., Geldhof, V. & Carmeliet, P. How glucose, glutamine and fatty acid metabolism shape blood and lymph vessel development. *Dev. Biol.* (2017). doi:10.1016/j.ydbio.2017.12.001
112. Cantelmo, A. R. *et al.* Inhibition of the Glycolytic Activator PFKFB3 in Endothelium Induces Tumor Vessel Normalization, Impairs Metastasis, and Improves Chemotherapy. *Cancer Cell* **30**, 968–985 (2016).
113. Schoors, S. *et al.* Partial and transient reduction of glycolysis by PFKFB3 blockade reduces pathological angiogenesis. *Cell Metab.* **19**, 37–48 (2014).
114. Boeckel, J.-N. *et al.* JMJD8 Regulates Angiogenic Sprouting and Cellular Metabolism by Interacting With Pyruvate Kinase M2 in Endothelial Cells. *Arterioscler. Thromb. Vasc. Biol.* **36**, 1425–1433 (2016).
115. Tang, M. *et al.* Brain microvasculature defects and Glut1 deficiency syndrome averted by early repletion of the glucose transporter-1 protein. *Nat. Commun.* **8**, 14152 (2017).
116. Yu, P. *et al.* FGF-dependent metabolic control of vascular development. *Nature* **545**, 224–228 (2017).
117. Houten, S. M. & Wanders, R. J. A. A general introduction to the biochemistry of mitochondrial fatty acid β -oxidation. *J. Inherit. Metab. Dis.* **33**, 469–477 (2010).
118. Huang, L., Cobessi, D., Tung, E. Y. & Berry, E. A. Binding of the Respiratory Chain Inhibitor Antimycin to the Mitochondrial bc1 Complex: A New Crystal Structure Reveals an Altered Intramolecular Hydrogen-bonding Pattern. *J. Mol. Biol.* **351**, 573–597 (2005).

119. De Smet, F., Segura, I., De Bock, K., Hohensinner, P. J. & Carmeliet, P. Mechanisms of vessel branching: filopodia on endothelial tip cells lead the way. *Arterioscler. Thromb. Vasc. Biol.* **29**, 639–649 (2009).
120. Hakkaart, G. A. J., Dassa, E. P., Jacobs, H. T. & Rustin, P. Allotopic expression of a mitochondrial alternative oxidase confers cyanide resistance to human cell respiration. *EMBO Rep.* **7**, 341–345 (2006).
121. Perales-Clemente, E. *et al.* Restoration of electron transport without proton pumping in mammalian mitochondria. *Proc. Natl. Acad. Sci. U. S. A.* **105**, 18735–18739 (2008).
122. King, M. P. & Attardi, G. Human cells lacking mtDNA: repopulation with exogenous mitochondria by complementation. *Science* **246**, 500–503 (1989).
123. Sellers, K. *et al.* Pyruvate carboxylase is critical for non–small-cell lung cancer proliferation. *J. Clin. Invest.* **125**, 687–698 (2015).
124. Wong, B. W. *et al.* The role of fatty acid β -oxidation in lymphangiogenesis. *Nature* **542**, 49–54 (2017).
125. Korn, C. & Augustin, H. G. Mechanisms of Vessel Pruning and Regression. *Dev. Cell* **34**, 5–17 (2015).
126. Amaya, C. N. & Bryan, B. A. Differential Expression of Angiogenic Gene Networks during Post-natal Lung Alveolarization. *Angiol. Open Access* **4**, (2016).
127. Jovaisaite, V., Mouchiroud, L. & Auwerx, J. The mitochondrial unfolded protein response, a conserved stress response pathway with implications in health and disease. *J. Exp. Biol.* **217**, 137–143 (2014).
128. Warner, J. R., Vilardell, J. & Sohn, J. H. Economics of Ribosome Biosynthesis. *Cold Spring Harb. Symp. Quant. Biol.* **66**, 567–574 (2001).
129. Wilhelm, K. *et al.* FOXO1 couples metabolic activity and growth state in the vascular endothelium. *Nature* **529**, 216–220 (2016).
130. Tan, A. S. *et al.* Mitochondrial Genome Acquisition Restores Respiratory Function and Tumorigenic Potential of Cancer Cells without Mitochondrial DNA. *Cell Metab.* **21**, 81–94 (2015).
131. Liu, X., Romero, I. L., Litchfield, L. M., Lengyel, E. & Locasale, J. W. Metformin Targets Central Carbon Metabolism and Reveals Mitochondrial Requirements in Human Cancers. *Cell Metab.* **24**, 728–739 (2016).
132. Naguib, A. *et al.* Mitochondrial Complex I Inhibitors Expose a Vulnerability for Selective Killing of Pten-Null Cells. *Cell Rep.* **23**, 58–67 (2018).

133. Birsoy, K. *et al.* Metabolic determinants of cancer cell sensitivity to glucose limitation and biguanides. *Nature* **508**, 108–112 (2014).
134. Shackelford, D. B. *et al.* LKB1 Inactivation Dictates Therapeutic Response of Non-Small Cell Lung Cancer to the Metabolism Drug Phenformin. *Cancer Cell* **23**, 143–158 (2013).
135. Guo, J. Y. *et al.* Activated Ras requires autophagy to maintain oxidative metabolism and tumorigenesis. *Genes Dev.* **25**, 460–470 (2011).
136. Romero, R. *et al.* Keap1 loss promotes Kras-driven lung cancer and results in dependence on glutaminolysis. *Nat. Med.* (2017). doi:10.1038/nm.4407
137. Molina, J. R. *et al.* An inhibitor of oxidative phosphorylation exploits cancer vulnerability. *Nat. Med.* **24**, 1036–1046 (2018).
138. Weinberg, S. E. & Chandel, N. S. Targeting mitochondria metabolism for cancer therapy. *Nat. Chem. Biol.* **11**, 9–15 (2015).
139. Zahalka, A. H. *et al.* Adrenergic nerves activate an angio-metabolic switch in prostate cancer. *Science* **358**, 321–326 (2017).
140. Yoon, M.-S. & Choi, C. S. The role of amino acid-induced mammalian target of rapamycin complex 1(mTORC1) signaling in insulin resistance. *Exp. Mol. Med.* **48**, e201–e201 (2016).
141. Johnson, S. C. *et al.* mTOR Inhibition Alleviates Mitochondrial Disease in a Mouse Model of Leigh Syndrome. *Science* **342**, 1524–1528 (2013).
142. Pate, M., Damarla, V., Chi, D. S., Negi, S. & Krishnaswamy, G. Endothelial Cell Biology: Role in the Inflammatory Response. in *Advances in Clinical Chemistry* **52**, 109–130 (Elsevier, 2010).

6. CURRICULUM VIATE

Lauren Diebold

Driskill Graduate Program | Feinberg School of Medicine | Northwestern University
 Laurendiebold2012@u.northwestern.edu

EDUCATION

Northwestern University 2012 - Nov. 2018
Driskill Graduate Program – Feinberg School of Medicine
PhD.

University of Illinois at Urbana-Champaign 2005-2009
Bachelors of Science in Molecular and Cellular Biology
 GPA: 3.5

RESEARCH EXPERIENCE

Ph.D. 2012 - Nov. 2018
Northwestern University
Driskill Graduate Program – Feinberg School of Medicine
Laboratory of Dr. Navdeep Chandel

Research Technologist I 2009-2012
Northwestern University
Laboratory of Dr. John Crispino

Undergraduate Research Assistant 2008-2009
University of Illinois at Urbana-Champaign
Laboratory of Dr. Monday Alhonsi

Undergraduate Research Assistant May 2008-Nov. 2008
University of Illinois at Urbana-Champaign
Laboratory of Dr. Andrew Miller

Undergraduate Research Assistant 2006-2007
University of Illinois at Urbana-Champaign
Laboratory of Dr. Ray Ming

PUBLICATIONS

1. **Lauren P. Diebold**, Hyea Jin Gil, Peng Gao, Carlos A. Martinez, Samuel E. Weinberg, and Navdeep S. Chandel. (2018). Mitochondrial respiratory chain complex III is necessary for endothelial cell proliferation during angiogenesis. Nat Metab. In Press.
2. Juncheng Wei, Yanzhi Yuan, Lu Chen, Yuanming Xu, Yuehui Zhang, Yajun Wang, Yanjie Yang, Clara Bien Peek, **Lauren Diebold**, Yi Yang, Beixue Gao, Chaozhi Jin, Johanna Melo-Cardenas, Navdeep S. Chandel, Donna D. Zhang, Hui Pan, Kezhong Zhang, Jian Wang, Fuchu He & Deyu Fang. (2018). ER-associated ubiquitin ligase HRD1 programs liver metabolism by targeting multiple metabolic enzymes. Nat Commun. 10;9(1):3659.
3. Elena Ansó, Samuel E. Weinberg, **Lauren P. Diebold**, Benjamin J. Thompson, Sébastien Malinge, Paul T. Schumacker, Xin Liu, Yuannyu Zhang, Zhen Shao, Mya Steadman, Kelly M. Marsh, Jian Xu, John D. Crispino and Navdeep S. Chandel. (2017). The mitochondrial respiratory chain is essential for haematopoietic stem cell function. Nat Cell Biol. 9(6):614-625.
4. **Diebold, Lauren**, Chandel NS. (2016). Mitochondrial ROS regulation of proliferating cells. Free Radic Biol Med. 100:86-93.
5. **Diebold, Lauren P**, Chandel NS. (2016). HSC fate is tethered to Mitochondria. Cell Stem Cell. 18(3):303-4
6. Inmaculada Martínez-Reyes, **Lauren P. Diebold**, Hyewon Kong, Michael Schieber, He Huang, Christopher T. Hensley, Manan M. Mehta, Tianyuan Wang, Janine H. Santos, Richard Woychik, Eric Dufour, Johannes N. Spelbrink, Samuel E. Weinberg, Yingming Zhao, Ralph J. DeBerardinis and Navdeep S. Chandel. (2015). The mitochondrial membrane potential and TCA cycle regulate divergent biological functions. Mol Cell. 61(2):199-209.
7. Thompson BJ, Bhansali R, **Diebold L**, Cook DE, Stolzenburg L, Casagrande AS, Besson T, Leblond B, Désiré L, Malinge S, Crispino JD. (2015). DYRK1A controls the transition from proliferation to quiescence during lymphoid development by destabilizing Cyclin D3. J Exp Med. 212(6):953-70.
8. Glasauer A, Sena LA, **Diebold LP**, Mazar AP, Chandel NS. (2014). Targeting SOD1 reduces experimental non-small-cell lung cancer. J Clin Invest. 124(1):117-28.
9. Malinge S, Thiollier C, Chlon TM, Doré LC, **Diebold L**, Bluteau O, Mabialah V, Vainchenker W, Dessen P, Winandy S, Mercher T, Crispino JD. (2013). Ikaros inhibits megakaryopoiesis through functional interaction with GATA-1 and NOTCH signaling. Blood. 121(13):2440-51.

10. Wen Q, Goldenson B, Silver SJ, Schenone M, Dancik V, Huang Z, Wang LZ, Lewis TA, An WF, Li X, Bray MA, Thiollier C, **Diebold L**, Gilles L, Vokes MS, Moore CB, Bliss-Moreau M, Verplank L, Tolliday NJ, Mishra R, Vemula S, Shi J, Wei L, Kapur R, Lopez CK, Gerby B, Ballerini P, Pflumio F, Gilliland DG, Goldberg L, Birger Y, Izraeli S, Gamis AS, Smith FO, Woods WG, Taub J, Scherer CA, Bradner JE, Goh BC, Mercher T, Carpenter AE, Gould RJ, Clemons PA, Carr SA, Root DE, Schreiber SL, Stern AM, Crispino JD. (2012). Identification of regulators of polyploidization presents therapeutic targets for treatment of AMKL. *Cell*. 150(3):575-89
11. Malinge S, Bliss-Moreau M, Kirsammer G, **Diebold L**, Chlon T, Gurbuxani S, Crispino JD. (2012). Increased dosage of the chromosome 21 ortholog Dyrk1a promotes megakaryoblastic leukemia in a murine model of Down syndrome. *J Clin Invest*. 122(3):948-62
12. Chen C, Yu Q, Hou S, Li Y, Eustice M, Skelton RL, Veatch O, Herdes RE, **Diebold L**, Saw J, Feng Y, Qian W, Bynum L, Wang L, Moore PH, Paull RE, Alam M, Ming R. (2007). Construction of a sequence-tagged high-density genetic map of papaya for comparative structural and evolutionary genomics in brassicales. *Genetics*. 177(4):2481-91.

GRANT SUPPORT

National Institutes of Health (T32-GM008061-33) 2013-2016
Cellular and Molecular Basis of Disease (CMBD) training grant

TEACHING EXPERIENCE

Teaching Assistant (Tumor Cell Biology) Spring 2015
Northwestern University Driskill Graduate Program

PRESENTATIONS AND CONFERENCES

Nutrient Signaling Symposium. October 25-28, 2018. Cold Spring Harbor Laboratory, Cold Spring Harbor, NY. Poster Presentation. "Mitochondrial respiratory chain complex III is necessary for endothelial cell proliferation during angiogenesis".

2017 Annual Lung Symposium. June 20, 2017. Northwestern University, Chicago, IL. Oral Presentation. "Mitochondrial respiration is necessary for angiogenesis".

Pulmonary and Critical Care research in progress conference. July 10, 2017. Northwestern University, Chicago, IL. Oral Presentation. "Mitochondrial respiration is necessary for angiogenesis".

Metallomes, Mito-tones and Chromosomes Workshop. May 8-9, 2017. Northwestern University, Evanston, IL. Poster Presentation. "Respiration is required for angiogenesis".

13th Annual Lewis Landsberg Research Day. April 6, 2017. Northwestern University, Chicago, IL. Poster Presentation. "Respiration is essential for hematopoietic stem cell function".

Keystone Symposia. Tumor Metabolism: Mechanisms and Targets. March 5-9, 2017. Whistler, British Columbia, Canada. Poster Presentation. "Respiration is required for angiogenesis".

Cellular and Molecular Basis of Disease research-in-progress meeting. November 19, 2015. Evanston, IL. Oral Presentation. "The role of mitochondria in endothelial cell function and angiogenesis".

Multifaceted Mitochondria Cell Symposia, July 19-21, 2015, Chicago, IL.

Cellular and Molecular Basis of Disease research-in-progress meeting. December 16, 2014. Evanston, IL. Oral Presentation. "The role of mitochondrial reactive oxygen species in angiogenesis".